Heinrich Pette Institute
Leibniz Institute of Experimental Virology

Herpesvirus use of protein aggregation and selective autophagy as immune evasion mechanism

Dissertation
Submitted to the
Department of Chemistry
Faculty of Mathematics, Informatics and Natural Sciences
University of Hamburg
In fulfillment of the requirements
For the degree of
Doctor of Natural Sciences (Dr. rer. nat.)

By
Elena Muscolino
(born in Messina, Italy)

Hamburg, December 2019

Prof. Dr. Wolfram Brune (First Reviewer)

Prof. Dr. Nicole Fischer (Second Reviewer)

Date of oral defense: 13.03.2020

This study was conducted between April 2015 and December 2019 at the Heinrich Pette Institute, Leibniz Institute for Experimental Virology under the supervision of Prof. Dr. Wolfram Brune and Prof. Dr. Thomas Dobner.

Ai miei nonni,
Maria e Nino,
Elena e Nino.

Publications, presentations and awards

Publication

The study presented in this thesis was published in:

Herpesviruses induce aggregation and selective autophagy of host signalling proteins NEMO and RIPK1 as an immune-evasion mechanism.

E. Muscolino, R. Schmitz, S. Loroch, E. Caragliano, C. Schneider, M. Rizzato, Y.H Kim, E. Krause, V. Juranic Lisnić, A. Sickmann, R. Reimer, E. Ostermann and W. Brune. Nature Microbiology, December 2019.

Presentations

The author presented part of this study at the following conferences:

March 2016	25th Annual Meeting of the Society for Virology (GfV)	Poster presentation
October 2016	6th European Conference of Virology (ECV)	Oral presentation
December 2016	Keystone Symposia on *Cellular Stress Responses and Infectious Agents*	Oral and poster presentation
March 2017	26th Annual Meeting of the Society for Virology (GfV)	Poster presentation
June 2017	4th International Symposium on "Protein Trafficking in Health and Disease (GRK1459)	Oral and poster presentation
July 2017	42nd International Herpesvirus Workshop (IHW)	Oral and poster presentation
November 2017	7th Scientific days on Autophagy (CFATG7)	Oral presentation
March 2018	27th Annual Meeting of the Society for Virology (GfV)	Poster presentation

July 2018	43nd International Herpesvirus Workshop (IHW)	Oral and poster presentation
November 2018	7th International Workshop on CMV and Immunosenescence	Oral presentation
March 2019	28th Annual Meeting of the Society for Virology (GfV)	Poster presentation

Awards

June 2017	4th International Symposium on “Protein Trafficking in Health and Disease (GRK1459)	Travel award
November 2017	7th Scientific days on Autophagy (CFATG7)	Travel award
November 2018	7th International Workshop on CMV and Immunosenescence	Best presentation award

Contents

1 **Abstract** 17

2 **Zusammenfassung** 19

3 **Introduction** 21

3.1 Herpesvirus 21

3.1.1 Cytomegalovirus: pathogenesis and treatment 21

3.1.2 Cytomegalovirus: structure and replication cycle 22

3.2 Cellular antiviral responses 25

3.2.1 NF-κB activation by Toll-like Receptors 25

3.2.2 Programmed cell death 29

3.3 Autophagy 32

3.3.1 Selective autophagy 35

3.3.2 TBC1D5 and the retromer complex 36

3.3.3 Aggrephagy and protein quality control machinery 37

3.3.4 Autophagy and herpesviruses 39

3.4 Modulation of the cellular antiviral response and autophagy by MCMV M45 40

3.4.1 Functions of M45 homologs in other herpesviruses 43

4 **Aims of the study** 45

5 **Results** 47

5.1 M45 mediates NEMO and RIPK1 accumulation in the insoluble fraction 47

5.2 MCMV induces the formation of aggregates 50

5.3 A sequence motif within the C-terminal part of M45 mediates NEMO and RIPK1 aggregation 54

5.4 M45 aggregates co-localize with LC3BII but not with HSP70 or Caveolin-1. 58

5.5 The IPAM is required for M45 interactions with RIPK1, NEMO, and itself... 60

5.6 The IPAM is required for inhibition of necroptosis and viral dissemination *in vivo* 61

5.7 M45 interacts with the retromer component VPS26B 63

5.8 M45 benefits from VPS26B to promote NEMO degradation 66
5.9 TBC1D5 is required as an autophagy adaptor to redirect NEMO to autophagosomes 67
5.10 Induced protein aggregation and selective autophagy are conserved in HSV-1 ICP6 70
6 **Discussion** 77
6.1 Implication aggregate formation and autophagy during MCMV infection ... 77
6.2 Characterization of M45 aggresomes 79
6.3 Mechanism and implication of aggregate formation........................... 80
6.4 Potential inactivation of RIPK3 and DAI through aggregate formation...... 81
6.5 M45 uses autophagy adaptors to tether aggregates to LC3BII................ 82
6.6 Possible implication of cellular chaperones in aggregate disposal 84
6.7 Aggregate formation is a conserved mechanism among herpesviruses 85
6.8 Short summary and conclusions 87
6.9 Graphical Summary 88
7 **Material** 89
7.1 Cells.. 89
7.2 Viruses 89
7.3 Bacteria 91
7.4 Plasmids 91
7.5 Primers 93
7.5.1 Molecular cloning primers... 93
7.5.2 *En passant* BAC mutagenesis primers 94
7.5.3 CRISPR/Cas9 mutagenesis primers 95
7.6 Antibodies.. 96
7.6.1 Primary antibodies 96
7.6.2 Secondary antibodies 97
7.7 Chemical and reagents 97

7.7.1 Antibiotics 97
7.7.2 Enzymes 98
7.7.3 Receptor agonists 98
7.7.4 Other reagents and chemicals 98
7.8 Media 99
7.8.1 Cell culture media 99
7.8.2 Bacterial media 99
7.9 Buffers 100
7.9.1 Agarose gel electrophoresis 100
7.9.2 SDS polyacrylamide gel electrophoresis (SDS-Page) and Western Blot 100
7.9.3 Immunoprecipitation 101
7.9.4 Immunofluorescence 101
7.9.5 DNA preparation from bacteria (“Mini Scale”) 102
7.10 Kits 102
7.11 Devices and equipment 102
7.12 Bioinformatics tools 103
8 **Methods** 104
8.1 Molecular biology methods 104
8.1.1 Production of electrocompetent bacteria 104
8.1.2 Bacterial transformation 104
8.1.3 DNA isolation from bacteria 105
8.1.4 Polymerase chain reaction (PCR) 105
8.1.5 Restiction digestion of DNA 106
8.1.6 Agarose gel electrophoresis 106
8.1.7 Purification of DNA fragments 106
8.1.8 DNA ligation 106
8.1.9 DNA sequencing 107
8.1.10 *En Passant* BAC mutagenesis 107

8.1.11 Gibson assembly 107
8.2 Cell biology and virology methods 108
8.2.1 Cell culture 108
8.2.2 Transfection of plasmid DNA 108
8.2.3 Transfection of BAC DNA 109
8.2.4 MCMV stock production and titration 109
8.2.5 HSV-1 stock production and titration 111
8.2.6 Viral infections 112
8.2.7 Viral kinetics 112
8.2.8 Viral DNA extraction 112
8.2.9 Cell viability assay 112
8.2.10 CRISPR/Cas9 mutagenesis 113
8.3 Biochemistry methods 113
8.3.1 Cell lysis for immunoblotting and immunoprecipitation 113
8.3.2 SDS polyacrylamide gel electrophoresis (SDS-Page) and immunoblot . 114
8.3.3 (Co-) Immunoprecipitation 114
8.4 Microscopy methods 115
8.4.1 Live cell imaging and fluorescence recovery after photo bleaching (FRAP) 115
8.4.2 Immunofluorescence 116
8.4.3 Correlative light and electron microscopy (CLEM) 117
8.5 Animal experiment 117
9 **References** 119
10 **Appendix** 129
10.1 Curriculum Vitae 129
10.2 List of abbreviation 130
10.3 Toxicity of chemicals 133
10.4 Acknowledgments 137

10.5 Statement of Authorship 139

1 Abstract

A viral infection induces a broad spectrum of innate and adaptive immune responses including the production of cytokines, the induction of cell death, and the activation and proliferation of T- and B-lymphocytes. Pattern recognition receptors (PRRs) serve as first-line sentinels for innate immune detection of pathogenic infections. After recognizing various conserved molecular motifs called "pathogen-associated-molecular patterns" (PAMPs), PRRs activate defense mechanisms that are important to restrict viral replication such as the nuclear factor kappa beta (NF-κB) pathway and programmed necrosis. Viruses have evolved strategies to prevent cellular detection by inducing the degradation of restriction factors. For example, it has been extensively reported that viral proteins can induce the ubiquitination and proteasomal degradation of cellular target proteins. However, many novel pathways are still being discovered. Recently, our laboratory has shown that the murine cytomegalovirus (MCMV) protein M45 redirects the NF-κB essential modulator (NEMO) to autophagosomes for degradation in order to block pro-inflammatory NF-κB signaling.

The aim of this study was to investigate how M45 promotes the degradation of NEMO by autophagy. Indeed, M45 induces NEMO degradation by a two-step process: first by inducing its sequestration as an insoluble protein aggregate and second by facilitating its degradation by autophagy. Moreover, the same strategy is adopted for the degradation of the receptor interacting protein 1 (RIPK1). Aggregation of target proteins requires a characteristic sequence motif that I mapped within the C-terminal part of M45. The motif is conserved in homologous proteins of other herpesviruses and has been named Induced Protein Aggregation Motif (IPAM).

The IPAM is not only required for M45 dimerization/oligomerization but is also necessary for inhibition of viral induced necroptosis and for effective viral dissemination *in vivo*. In the second step, M45 recruits the retromer component VPS26B and the LC3-interacting adaptor protein TBC1D5 to facilitate autophagic degradation of aggregates. Finally, the ICP6 protein of human herpes simplex virus type 1 (HSV-1) utilizes a similar mechanism as M45. Altogether, this study shows that protein aggregation and selective autophagy degradation represent a novel and conserved viral strategy to overcome innate cellular immune defenses.

2 Zusammenfassung

Eine virale Infektion induziert ein breites Spektrum an angeborenen und adaptiven Immunantworten, einschließlich der Produktion von Zytokinen, der Induktion des Zelltods und der Aktivierung und Proliferation von T- und B-Lymphozyten. Pattern Recognition Receptors (PRRs, dt. etwa ‚Mustererkennungsrezeptoren‘) dienen als Wächter des angeborenen Immunnachweises pathogener Infektionen. Nach der Erkennung verschiedener konservierter molekularer Motive, so genannter „pathogen-assoziierter molekularer Muster“ (PAMPs), aktivieren PRRs Abwehrmechanismen, die wichtig sind, um die Virusreplikation einschränken, beispielsweise mittels dem Nuclear Factor Kappa Beta (NF-κB) Pfad und die programmierte Nekroptose. Durch den Abbau von Restriktionsfaktoren haben Viren Strategien entwickelt, um den zellulären Erkennungsmechanismus zu unterbinden. So wurde beispielsweise ausführlich berichtet, dass virale Proteine die Ubiquitierung und den proteasomalen Abbau von zellulären Zielproteinen induzieren können. Jedoch werden noch immer viele neue Signalwege entdeckt. Jüngst hat unser Labor gezeigt, dass das Murine Cytomegalievirus (MCMV)-Protein M45 den NF-κB essenziellen Modulator (NEMO) zu den Autophagosomen für den Abbau umleitet, und so die pro-inflammatorische NF-κB-Signalisierung blockiert.

Ziel dieser Studie war es, zu untersuchen, wie M45 den Abbau von NEMO durch Autophagie induziert. M45 induziert den NEMO-Abbau in zwei Schritten: erstens durch die Induktion von Sequestrierung als unlösliches Proteinaggregat und zweitens durch den Abbau durch Autophagie. Darüber hinaus wird die gleiche Strategie für den Abbau des rezeptorinteragierenden Proteins 1 (RIPK1) verfolgt.

Die Aggregation von Zielproteinen erfordert ein charakteristisches Sequenzmotiv, das ich im C-terminalen Teil von M45 identifiziert habe. Dieses Motiv ist in homologen Proteinen anderer Herpesviren konserviert und wurde als Induced Protein Aggregation Motif (IPAM) bezeichnet.

Das IPAM wird nicht nur für die M45-Dimerisierung/Oligomerisierung benötigt, sondern auch zur Hemmung der viral induzierten Nekroptose und zur effektiven viralen Ausbreitung in vivo. Im zweiten Schritt rekrutiert M45 die Retromerkomponente VPS26B und das LC3-interagierende Adapterprotein TBC1D5, um den autophagischen Abbau von Aggregaten zu ermöglichen. Die biologische Relevanz dieser Ergebnisse wird durch die Tatsache gestützt, dass das Protein ICP6

des humanen Herpes-simplex-Virus 1 (HSV-1) einen ähnlichen Mechanismus nutzt wie M45. Zusammenfassend zeigt diese Studie, dass Proteinaggregation und selektiver Autophagieabbau eine neuartige und konservierte virale Strategie zur Überwindung der angeborenen zellulären Immunabwehr darstellen.

3 Introduction

3.1 Herpesvirus

Herpesviruses have a linear dsDNA genome and are members of the family *Herpesviridae* within the order *Herpesvirales* [1]. Herpesviruses are extremely well adapted pathogens with their respective host and are widely distributed in nature. In fact, most animal species have at least one herpesvirus. Nine members of this family can infect humans and are classified into three subfamilies. Herpes simplex virus 1 (HSV-1), HSV-2, and Varicella zoster virus (VZV) belong to the subfamily *Alphaherpesvirinae*. Human cytomegalovirus (HCMV), human herpesvirus 6A and 6B (HHV6-A/B) and human herpesvirus 7 (HHV-7) belong to the subfamily *Betaherpesvirinae*. Epstein-Barr virus (EBV) and Kaposi-associated sarcoma herpesvirus (KSHV) belong to the *Gammaherpesvirinae* subfamily [2].

All families share significant biological properties and are morphologically distinct from all other viruses. They have several genes encoding for enzymes involved in DNA synthesis, in the processing of proteins, and in nucleic acid metabolism (e.g. all herpesviruses carry a homologue of the cellular ribonucleotide reductase (RNR)). The synthesis of viral DNA and capsid assembly occurs in the nucleus while the final processing of the virion takes place in the cytoplasm. Their morphogenesis includes different budding steps. The virus persists lifelong in its host [2].

Herpesviruses are widespread in the human population. For instance, HCMV infections are among the most prevalent viral infections worldwide with high incidence in both developed and developing countries with seroprevalence ranging from 35% to 95% [3].

3.1.1 Cytomegalovirus: pathogenesis and treatment

Cytomegalovirus-infected cells were first observed in 1881 by the pathologist Hugo Ribbert who described large inclusion-bearing cells in the kidney of a stillborn infant with syphilis. In the following years, more clinical cases of inclusion-bearing cells were documented, and in 1950, Smith and Vellios described this condition as “cytomegalic inclusion disease”[4].

HCMV enters the host via the epithelium of the genitourinary, upper alimentary or respiratory tracts. However, the virus can also be acquired through a blood transfusion, organ transplant, or vertically. The virus is acquired from an infected person through direct contact of the mucosae with body fluids like saliva, urine, blood, semen and milk [5, 6].

In immunocompetent adults, HCMV infection is often sub-clinical, but in some cases produces acute illness with a mononucleosis syndrome [7]. The most common and severe HCMV manifestations occur in immunocompromised hosts and transplant recipients [8, 9]. The infection can occur as primary infection, reactivation of a latent virus, as well as superinfection. The most severe infections are seen in recipients of allogenic bone marrow or solid organ transplants [10, 11].

Importantly, HCMV can be transmitted from mother to fetus or newborns through three main routes: transplacental, peripartum, and via human milk [12-16]. Congenital HCMV infections can be severe, depending on the gestational time at which the virus is acquired [17]. Symptoms include microcephaly, hearing loss, neurological abnormalities, rash, hypotonia, and hepatosplenomegaly. Approximately 13.5 % of newborns with congenital HCMV infection are symptomatic at birth [12].

Several drugs have been approved for HCMV treatment. They include ganciclovir (GCV), the GCV derivative valganciclovir (VGCV), foscarnet (FOS), cidofovir and derivates (CDV), and letermovir [18, 19]. These drugs target viral replication and packaging; hence, resistance can develop with extended use. Moreover they are far from ideal because of poor oral bioavailability or associated toxicities (e.g. myelosuppression, nephrotoxicity, retinal detachment, neutropenia, anaemia) [20]. Indeed, there are still many challenges that have to be resolved for the development of new therapeutic agents.

3.1.2 Cytomegalovirus: structure and replication cycle

Cytomegaloviruses have the largest genome amongst the herpesviruses. The CMV virions are between 150 – 200 nm in diameter [21]. Their structural architecture includes an icosahedral nucleocapsid which contains the 235 kbp viral linear genome encoding for 160-200 viral proteins [22, 23] (Figure 1).

The capsid is surrounded by the tegument that contains several viral proteins, as well as cellular and viral RNA [24]. Tegument proteins are released into the cytoplasm upon viral entry and play a crucial role in the regulation of viral gene expression and immune evasion [25-28]. Furthermore, proteins present in the tegument mediate capsid migration from the cytoplasm to the nuclear pore and the delivery of the genome to the nucleus [29] (Figure 1).

The tegument is in turn surrounded by the envelope which derives from host membranes. The envelope is a lipid bilayer and contains numerous viral glycoproteins that are important for the entry of the virus into its target cells. Different glycoprotein complexes mediate the steps of initial attachment and fusion that occur between the viral envelope and host cell membrane [30-32].

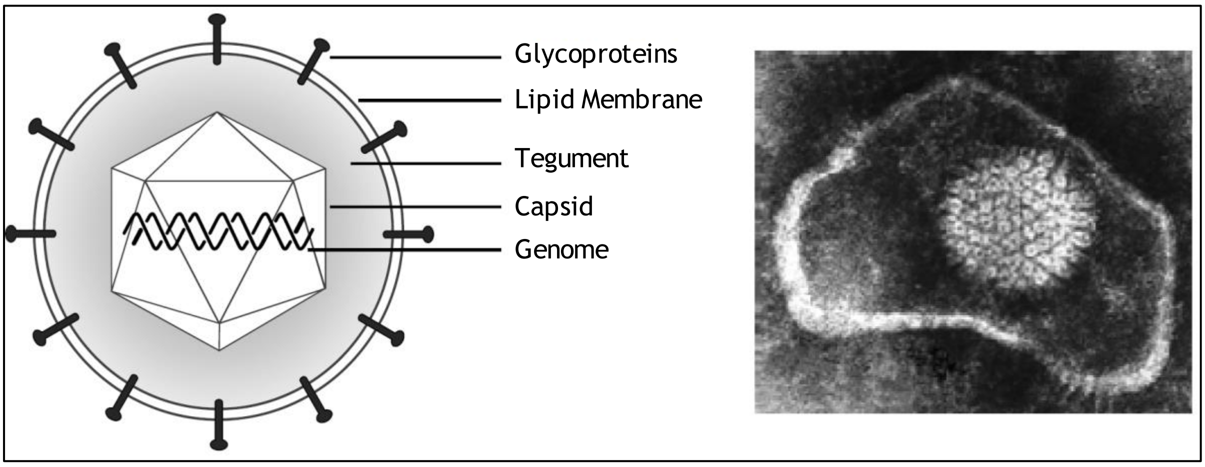

Figure 1. Structure of HCMV virion
A schematic (left) and electron micrograph (right) image of an HCMV virion are shown with the corresponding layers. Source: L. Stannard, University of Cape Town.

One peculiarity of CMVs is the highly restricted host range, which results in its capability to replicate only in cells of the natural host or very closely related species [33]. Due to this limitation, Murine Cytomegalovirus (MCMV) is commonly used as an animal model for HCMV [34-36].

Within its host, CMV has a broad tropism and infects many cell types. Leukocytes and vascular endothelial cells are important for the systemic spread of the virus after primary infection [37, 38]. In an immunocompetent individual, primary infection is usually controlled by a combination of innate and adaptive immune responses. The virus is eliminated from the majority of sites and is forced to enter a latent state in certain cells (e.g., hematopoietic stem cells), allowing the virus to persist lifelong in its host [39, 40]. In lytically infected permissive cells, the initial step of the replication cycle is the attachment and penetration at the cell surface, which depends on the presences of cellular receptors and is mediated by viral glycoproteins [41]. Entry into fibroblasts involves direct fusion with the plasma

membrane while entry into epithelial and endothelial cells involves macropinocytosis and fusion within endosomes [31, 42].
Once the capsid is released in the cytosol, it is transported along the microtubular network and reaches the nuclear membrane where the genome is injected through the nuclear pores (Figure 2).

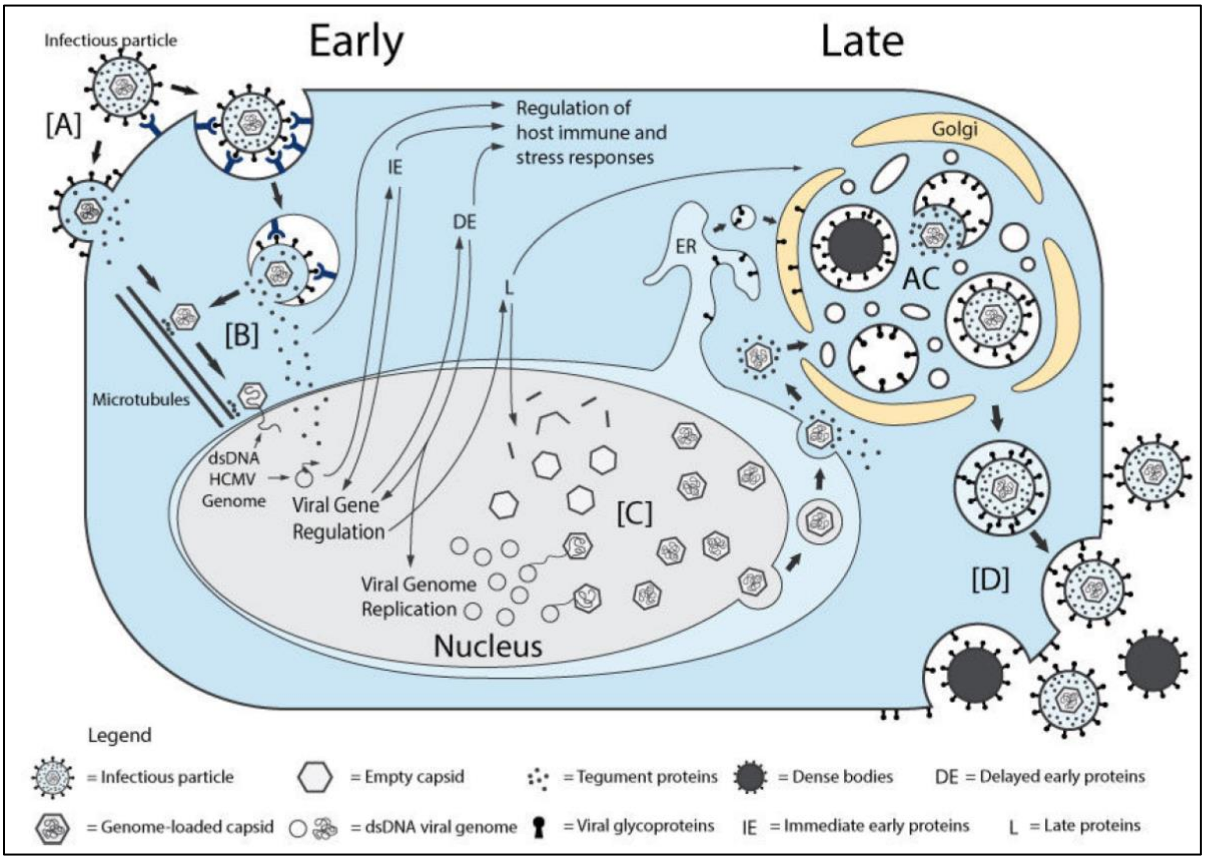
Infectious particle
Early
Late
[A]
Regulation of host immune and stress responses
Golgi
IE
DE
L
ER
AC
[B]
Microtubules
dsDNA HCMV Genome
Viral Gene Regulation
[C]
Viral Genome Replication
Nucleus
[D]
Legend
= Infectious particle
= Empty capsid
= Tegument proteins
= Dense bodies
DE = Delayed early proteins
= Genome-loaded capsid
= dsDNA viral genome
= Viral glycoproteins
IE = Immediate early proteins
L = Late proteins

Figure 2. CMV replication cycle.
Infectious particles enter the cell and the capsid and tegument proteins are delivered to the cytosol. The capsid travels to the nucleus where the genome is delivered and circularized. IE, E, and L genes are expressed, followed by nuclear egress of newly synthesized capsids to the cytosol. Capsids move to viral assembly compartment where they finally become infectious enveloped particles and are released along with NIEPs and DBs. Modified from: Pierre M. Jean Beltran and Ileana M. Cristea, Expert Rev Proteomics., 2014.

Tegument proteins regulate host cell responses and initiate the expression of immediate early (IE) genes, the first to be transcribed, which occurs a few hours after viral entry. The products of these genes modify the cellular environment and drive the expression of early genes (E). The products of early genes mediate replication of the viral genome through a rolling cycle mechanism and encode for proteins that are essential for counteracting cellular defense mechanisms.

Moreover, they promote expression of late (L) genes, which encode for the structural components of the viral particle. New capsids are formed in the nucleus and after nuclear egress, are transported to the viral assembly compartments. The capsid undergoes tegumentation, and secondary envelopment occurs at membranes derived from the Endoplasmic Reticulum (ER) and Golgi. Finally the infectious particles, together with non-infectious enveloped particles (NIEPs) and dense bodies (DBs), which lack viral DNA or the nucleocapsid entirely, respectively, are released from the cell [43-46] (Figure 2).

3.2 Cellular antiviral responses

Cells are armed with an elaborate immune response that allows defending themselves against invading viruses. At the same time, viruses have co-evolved with their hosts, and this has led to them developing mechanisms to evade the innate cellular immune response.

Immediately after entry, the host can recognize the virus and trigger the cellular immune responses as a first line of defense. This includes the production of inflammatory cytokines, type I interferon (IFN), and the upregulation of molecules that activate the adaptive immune response or trigger several mechanisms that restrict viral replication, such as blocking host and viral translation, degradation of the pathogens in lysosomes, or cell death [47].

3.2.1 NF-κB activation by Toll-like Receptors

The activation of the cellular immune response begins with the detection of the pathogen. This is mediated by Pattern Recognition Receptors (PRRs) that do not recognize specific antigens but molecular structures called Pathogens Associated Molecular Patterns (PAMPs [48]). The Toll-like receptors (TLRs) are the best characterized PRRs and together with the Interleukin-1 receptors form a receptor superfamily known as the "interleukin-1 receptor/toll-like receptor superfamily” that contains a so-called toll-IL-1 receptor (TIR) domain. Thirteen TLRs have been identified in humans and mice and are localized either on the plasma membrane or in endosomes [49]. Depending to their localization, they can either recognize structural patterns or sense nucleic acids. The microbial components that they recognize include bacterial lipopolysaccharide (LPS; TLR4 ligand), lipoproteins (TLR2 ligand), flagellin (TLR5 ligand), bacterial CpG DNA (TLR9 ligand), viral single-stranded RNA (TLR7 ligand), and viral double-stranded RNA (TLR3 ligand) [50]. TLRs transduce their signal by interacting with several adaptor proteins that contain TIR domains. These interactions triggers downstream signals that activate transcription factors like the nuclear factor kappa B (NF-κB), the activator protein-1 (AP-1), and the interferon regulating factors (IRFs) [51] (Figure 3).

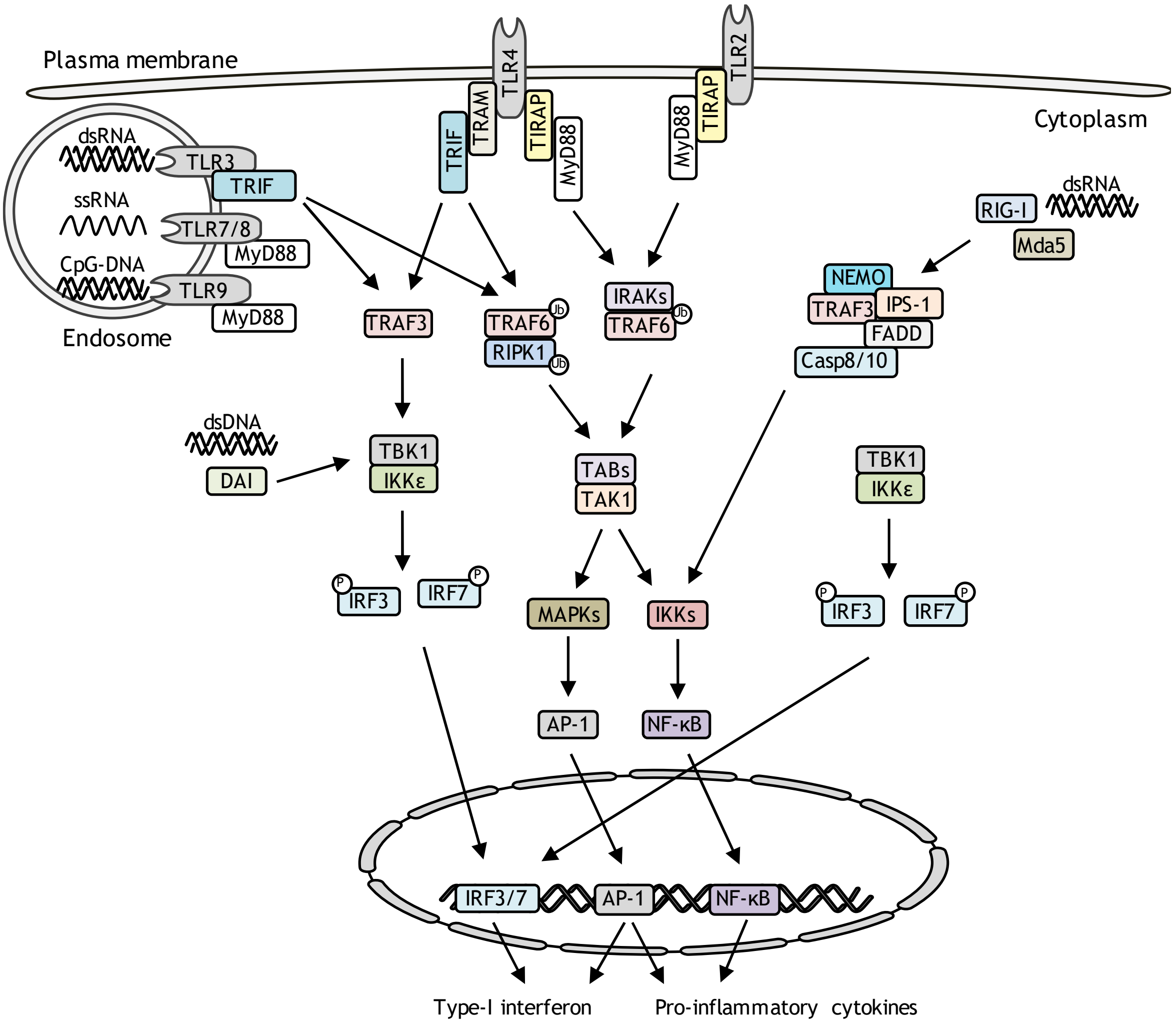
Plasma membrane
Cytoplasm
TLR4
TLR2
TRAM
TRIF
TIRAP
MyD88
dsRNA
TLR3
TRIF
ssRNA
TLR7/8
MyD88
CpG-DNA
TLR9
MyD88
Endosome
RIG-I
Mda5
NEMO
TRAF3
IPS-1
FADD
Casp8/10
TRAF3
TRAF6
RIPK1
Ub
IRAKs
TRAF6
dsDNA
DAI
TBK1
IKKε
TABs
TAK1
IRF3
IRF7
P
MAPKs
IKKs
AP-1
NF-κB
IRF3/7
Type-I interferon
Pro-inflammatory cytokines

Figure 3. Toll-like Receptors signaling.
Schematic representation of TLR mediated signaling that leads to the nuclear translocation of NF-κB, IRF3/7, and AP-1.

NF-κB represents a family of transcription factors that contain a Rel-homology domain (RHDs) that bind to DNA sequences known as κB sites. In mammalian cells, there are five members of the NF-κB family: p65 (RelA), RelB, C-Rel, p105 (NF-κB1) and p100 (NF-κB2). These factors are normally kept inactive in the cytosol by the inhibitory molecules of the IκB family [52, 53].

In response to inflammatory cytokines, viral infection, or other type of stress, the IκB molecules are phosphorylated on two critical serine residues, ubiquitinated, and degraded by the proteasomal system. In this way, NF-κB is free to enter the nucleus and activate the transcription of over 100 target genes, including those that participate in the immune and inflammatory response.

There are two well characterized pathways leading to the activation of NF-κB: the canonical and non-canonical (or alternative) pathway. The canonical form of NF-κB is a heterodimer composed of p65 and p50, and the pathway is triggered by numerous signals, is rapid, and independent of protein synthesis. The non-canonical pathway is triggered by a subset of receptors, is slow and persistent, and depends on protein synthesis [52, 53]. This thesis will focus on the canonical NF-κB activation pathway.

TLRs can activate NF-κB through the myeloid differentiation primary response gene 88 (MyD88) receptor or the TIR-domain-containing adapter-inducing interferon-ß (TRIF) receptor and might require other adaptor proteins [48, 54-57].

MyD88, which contains a TIR domain and a death domain (DD), signals to NF-κB via the interleukin receptor associated kinase 1 and 4 (IRAK1 and IRAK4) [58]. IRAK4 is initially activated by the DD of MyD88 and in turn phosphorylates IRAK1. Then, they dissociate from MyD88 and interact with the TNF receptor-associated factor 6 (TRAF6). In contrast, TRIF contains the RIP homotypic interacting motif (RHIM) at the C-terminus, which binds to the polyubiquitinated receptor interacting protein 1 (RIPK1), while its N-terminus binds to TRAF6 [59].

TRAF6 is an E3 ubiquitin ligase that acts together with the E2 ligases Ubc13/Uev1A to catalyze Lysin-63 polyubiquitination of target proteins, including the NF-κB essential modulator (NEMO) and TRAF6 itself [60]. This event leads to the recruitment of a protein kinase complex formed by the transforming growth factor ß-activated kinase 1 (TAK1) and the TAK1 binding proteins (TAB1, TAB2 and TAB3), which leads to NF-κB activation through the inhibitor of nuclear factor kappa-B kinases (IKK) complex or to the mitogen-activated protein kinase (MAPK) pathway signaling [61-64].

It is important to note that NF-κB can be activated in a TLR-independent manner. RNA viruses are sensed by the retinoic acid-inducible gene-I (RIG-I) and the melanoma differentiation-associated gene 5 (MDA5). RIG-I and MDA5 recruit a caspase recruitment domain (CARD) containing adaptor protein called IFN-β promoter stimulator 1 (IPS-1), which interacts with NEMO or TRAF3. In this way, they activate either the production of type-I interferon or of NF-κB. The production of type-I interferon is mediated by the TRAF family member-associated NF-κB activator binding kinase-1 (TBK1) and the inducible IκB kinase ε (IKKε) that promotes the translocation of interferon-regulating factor 3 and 7 (IRF3 and IRF7) to the nucleus. The association of TBK1 with caspase8/10 and FAS-associated death domain-containing protein (FADD) leads instead to NF-κB activation [65].

Moreover, the DNA-dependent activator of IRFs/Z-DNA binding protein-1 (DAI/ZBP1), initially identified as a cytoplasmic DNA sensor and now described as a sensor of Z-form dsRNA, activates IRF3 via TBK1 and induces NF-κB activation (Figure 3) [66].

The final activator of the canonical NF-κB activation is IKK complex (Figure 4). This complex consists of two catalytic subunits, IKKα and IKKβ, and the regulatory subunit IKKγ, also known as NEMO [67, 68]. By contrast, the non-canonical pathway proceeds through an IKK complex that contains two IKKα subunits but does not contain NEMO.

TAK1 mediates the activation of IKKα and IKKβ by phosphorylation of two serine residues located in an activation loop [69, 70]. It has been reported that the phosphorylation of IKKβ is required for canonical NF-κB activation while the phosphorylation of IKKα is not. The third subunit of the IKK complex, NEMO, is devoid of catalytic activity, but its presence is absolute necessary for the canonical NF-κB activation. The N-terminus of NEMO binds to IKKβ while the C-terminus recognizes Lys63 polyubiquitin chains. The polyubiquitin chains serve as a scaffold to recruit the IKK complex through NEMO, facilitating the phosphorylation of IKKβ by TAK1. Once the IKK complex is activated, it phosphorylates the IκB proteins, which are subsequently ubiquitinated and degraded by the proteasome. In this way, NF-κB is free to enter the nucleus and promote the transcription of target genes (Figure 4) [71].

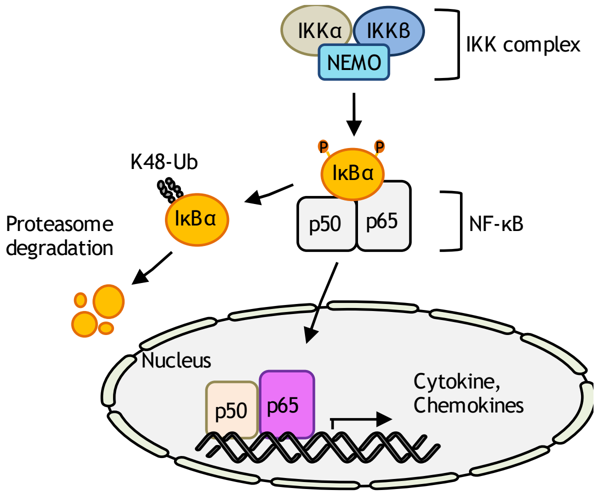

Figure 4. The IKK complex mediates the canonical NF-κB activation.
After the receptor senses stimuli, the IKK complex mediates the phosphorylation of the IκBα inhibitor that is subsequently ubiquitinated and degraded by the proteasome. This releases NF-κB to enter the nucleus and activate transcription of chemokines and cytokines.

3.2.2 Programmed cell death

Programmed cell death (PCD) is an important cellular mechanism involved in a variety of physiological process including development, preservation of homeostasis, and elimination of damaged cells, and pathophysiological conditions like cancer and infection.

In the context of viral infection, PCD is a host defense used to eliminate virally infected cells in order to restrict viral propagation to neighboring cells [72]. Several forms of PCD have been described in the last few decades. One of the most characterized is apoptosis, which can be initiated by intrinsic or extrinsic signals such as oxidative stress or TNF ligands, respectively. Apoptosis, from the Greek “falling off”, is regulated by a group of proteins called caspases and is characterized by cell shrinkage, nuclear condensation, DNA fragmentation, and the formation of apoptotic bodies [73]. In addition to apoptosis, alternative types of PCD have been characterized; this includes pyroptosis and necroptosis. Similar to apoptosis, the pyroptosis signaling pathway is driven by caspases, mainly caspase-1, 4, 5, and 11. Pyroptosis differs from apoptosis in that it is lytic and characterized by cell swelling and formation of pores at the plasma membrane [74].

Programmed necrosis (necroptosis), on the other hand, is a regulated form of PCD that is independent of caspases and is characterized by an increase in cell volume, swelling of organelles, perforation of the plasma membrane, cellular collapse, and release of cellular contents [75].

Necroptosis is induced either by ligands binding to tumor necrosis factor (TNF) family death death domain-containing receptors, like the TNF receptor (TNFR) and the Fas cell surface death receptor (Fas), or by PRRs or by virus sensors [76].

Key players in the necroptosis pathway are the receptor interacting protein kinase 1 (RIPK1) and RIPK3. Both contain a RIP homotypic interaction motif (RHIM) that allows their association [77].

RIPK1 is a serine-threonine protein kinase (PK) that, depending on the cellular context, can form three different complexes that are involved in NF-κB activation, apoptosis, or programmed necrosis. Ubiquitinated RIPK1 promotes NF-κB transcriptional activity and signals through NEMO (TNFR1 complex I), otherwise RIPK1 forms the Ripoptosome, a cytosolic complex, with FADD and caspase-8, which activates apoptotic cell death (TNFR1 complex IIa). When apoptosis is inhibited, RIPK1 forms the necrosome with RIPK3 to initiate programmed necrosis (TNFR1 complex IIb) (Figure 5) [78].

RIPK1 has a C-terminal death domain (DD), which allows its association with other DD-containing proteins, and a central domain involved in NF-κB activation and RHIM dependent signaling. RIPK3 lacks the DD domain but contains the RHIM domain that is required for interacting with RIPK1 upon death domain-containing receptors or PRR activation. RIPK1 and RIPK3 associate to form the necrosome and mediate the phosphorylation of the mixed lineage kinase domain like pseudokinase (MLKL), which oligomerizes and translocates to the cellular surface where it causes an influx of ions and disrupts the cellular membrane [79]. Interestingly, in recent years it has become evident that the RIPK1/RIPK3 necrosome is a functional amyloid signaling complex [80].

RIPK1-independent but RIPK3-dependent necroptosis has also been described. It has been shown that the intracellular nucleotide sensor DAI/ZBP1 triggers RIPK3 dependent necroptosis. DAI/ZBP1 contains a RHIM domain and together with RIPK3 can form a RHIM dependent complex that contributes to MLKL translocation to the plasma membrane[81]. In addition, TLR3 and TLR4 can induce necroptosis by TRIF, which contains a RHIM domain and associates with RIPK3 [82](Figure 5).

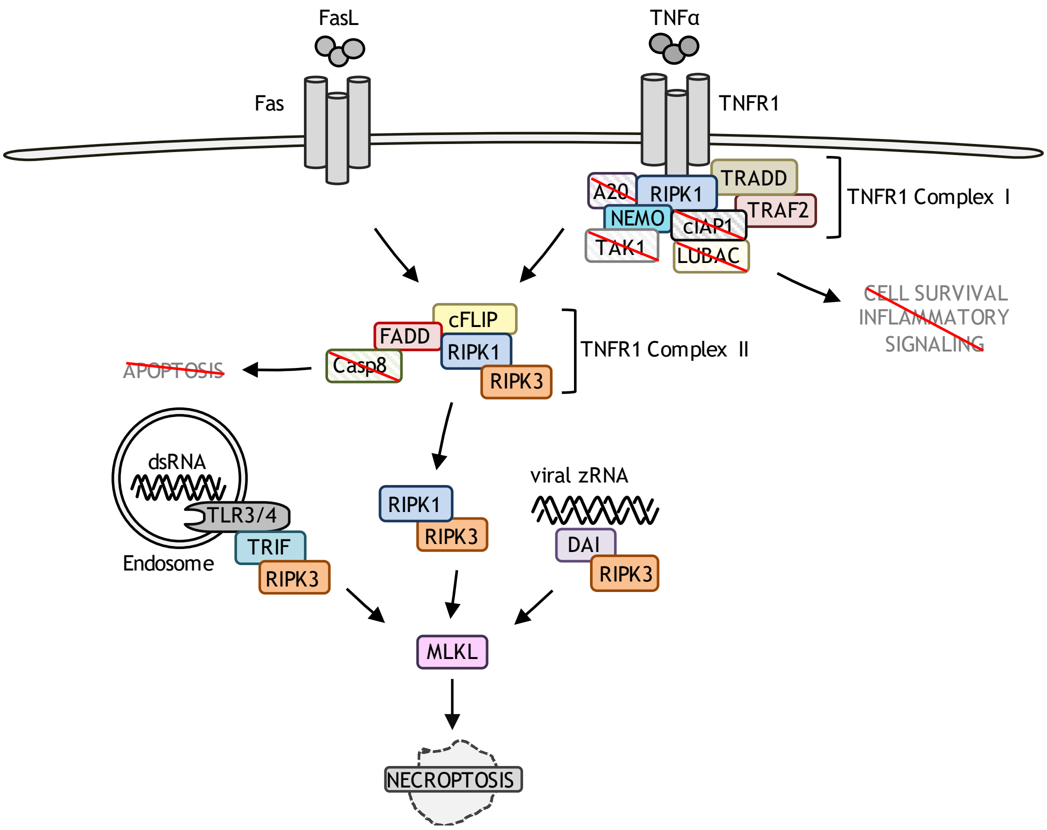
FasL
TNFα
Fas
TNFR1
~~A20~~
RIPK1
TRADD
TRAF2
NEMO
~~cIAP1~~
~~TAK1~~
~~LUBAC~~
TNFR1 Complex I
~~CELL SURVIVAL INFLAMMATORY SIGNALING~~
cFLIP
FADD
RIPK1
~~Casp8~~
RIPK3
TNFR1 Complex II
~~APOPTOSIS~~
dsRNA
TLR3/4
TRIF
RIPK3
Endosome
RIPK1
RIPK3
viral zRNA
DAI
RIPK3
MLKL
NECROPTOSIS

Figure 5. Induction of necroptosis.
Upon TNFα stimulation, TNFR1 complex I is formed at the plasma membrane and initiates cell survival inflammatory signaling. If it is blocked, as shown in this image, TNFR1 complex I transit to TNFR1 complex II. The composition of TNFR1 complex II determines the cell death outcome: apoptosis or necroptosis if casp8 is blocked. Necroptosis is also activated by DAI and TRIF, which carries a RHIM capable of engaging RIPK3. Induction of necroptosis involves the activation of RIPK1, RIPK3, DAI, and MLKL. Adapted from Vanlangenakker et al., Cell Death & Differentiation, 2011 and Brune and Andoniou, Viruses, 2017.

3.3 Autophagy

Autophagy is an adaptive process that occurs in response to different forms of stress, such as nutrient deprivation, hypoxia, physical stress or infection, and plays a crucial role in assuring cellular homeostasis [83]. Even though autophagy has been initially described as a non-selective process occurring upon nutrient deprivation, it has become clear that it plays a crucial role in the clearance of toxic metabolites, protein aggregates, and bacterial or viral components.

Autophagy also plays a key role in the innate and adaptive immune responses by limiting inflammasome activation, inhibiting production of type I interferons, and regulating NF-κB activation. Moreover, peptides generated from proteins degraded by autophagy can also be used for antigen presentation by T-cells on the major histocompatibility complexes (MHC) class I and II for regulation of adaptive immunity [84, 85].

Three main types of autophagy have been described in mammalian cells: macroautophagy, microautophagy, and chaperone mediated autophagy.

Macroautophagy, often referred to as simply autophagy, is the best characterized process and will be the focus of this thesis. Characteristic of the pathway is the formation of a double-membraned structure called the autophagosome, which engulfs cytoplasmic components, referred to as cargo. Autophagosomes use dynein motors to travel along the microtubule network towards the microtubule organizing centre (MTOC), where they fuse with endosomes (to form amphisomes) or lysosomes (to form autolysosomes). Depending on the stimuli that initiates the process, the sequestered components are either recycled or degraded [86].

Microautophagy is instead a non-selective lysosomal degradation process that is necessary for nutrient recycling under starvation conditions and involves direct uptake of cellular constituents into lysosomes [87].

Proteins subjected to chaperone-mediated autophagy (CMA) are instead targeted from the cytosol to the lysosome without the formation of additional vesicles. CMA targets only single proteins, and the key molecules involved in the process are the heat shock chaperone protein 70 (HSP70) and the chaperone heat shock cognate 70 (HSC70). The specificity of CMA is given by the fact that the HSP70/HSC70 complex recognizes proteins containing either a KFERQ or a KFERQ-like motif and then binds

to the lysosome-associated membrane protein 2 (LAMP2A), which transfers both the chaperone complex and the targeted protein into the lysosomal lumen [88].
The sophisticate mechanism of macroautophagy is characterized by several key steps and regulated by several AuTophaGy (ATG) proteins (Figure 6). The initial step of autophagy requires the formation of an isolation membrane in proximity of the ER in the so called phagophore assembly sites (PAS) [89].

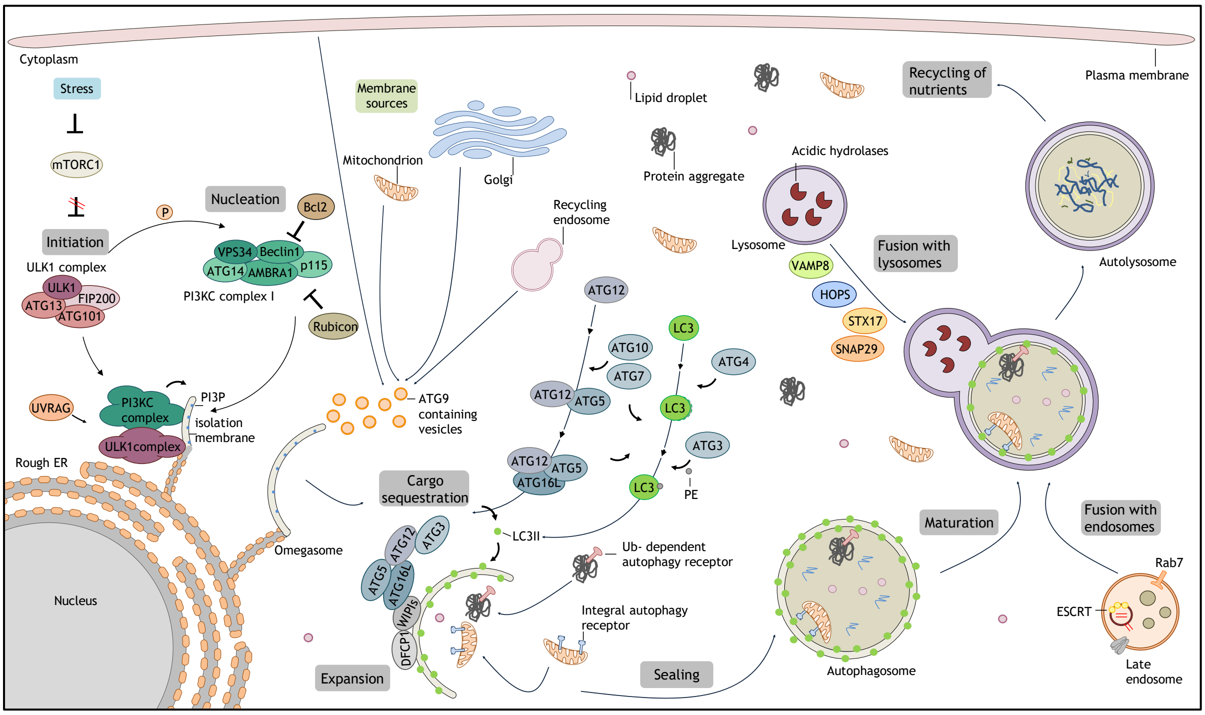
Cytoplasm
Stress
mTORC1
Initiation
ULK1 complex
ULK1
FIP200
ATG13
ATG101
P
Nucleation
Bcl2
VPS34
Beclin1
ATG14
AMBRA1
p115
PI3KC complex I
Rubicon
UVRAG
PI3KC complex
ULK1complex
PI3P
isolation membrane
Rough ER
Nucleus
Membrane sources
Mitochondrion
Golgi
ATG9 containing vesicles
Omegasome
Cargo sequestration
Recycling endosome
ATG12
ATG10
ATG7
ATG12
ATG5
ATG12
ATG5
ATG16L
LC3
ATG4
LC3
ATG3
LC3
PE
LC3II
ATG12
ATG3
ATG5
ATG16L
WIPI2
DFCP1
Expansion
Ub- dependent autophagy receptor
Integral autophagy receptor
Sealing
Lipid droplet
Protein aggregate
Acidic hydrolases
Lysosome
Recycling of nutrients
Plasma membrane
Autolysosome
Fusion with lysosomes
VAMP8
HOPS
STX17
SNAP29
Maturation
Autophagosome
Fusion with endosomes
Rab7
ESCRT
Late endosome

Figure 6. Overview of the autophagy process.
Schematic representation of the steps of the autophagy pathway: Initiation, nucleation, cargo sequestration, expansion, sealing, maturation, fusion with lysosomes/endosomes, and recycling of components. Adapted from I. Dikic and Z. Elazar, Nat Rev Mol Cell Biol 2018.

This step requires the interaction of several proteins with the Unc-51 like autophagy activating kinases 1 and 2 (ULK1/2) and the formation of the ULK complex. Under physiological conditions, the master cell growth regulator, the mammalian target of rapamycin complex 1 (mTORC1), blocks autophagy by phosphorylating the ULK complex and preventing its association with other components [90]. Upon cell starvation, mTORC1 is dephosphorylated and dissociates from the ULK1 complex, which in turn can interact with Beclin1 (known also as BECN1), additional adapters, and the vacuolar protein sorting 34 (VPS34) which form the phosphatidylinositol 3-kinase catalytic subunit type 3 (PI3KC3) complex. Stable association of the PI3KC3 and ULK1 complexes at the ER triggers the isolation of the nascent membrane and the completion of the omegasome [91-93]. This step is negatively regulated by the B-cell lymphoma 2 (Bcl-2) proteins such as Bcl-2, Bcl-xL, and Bcl-w [94].

The formation of the omegasome induces the recruitment of several proteins, like the PI3P effector proteins WD repeat domain phosphoinositide-interacting proteins (WIPIs) and the zinc-finger FYVE domain-containing protein 1 (DFCP1), which in turn promotes the recruitment of the ATG5-ATG12-ATG16L multimeric complex [95]. Moreover, several cellular membranes are involved in the elongation of the autophagosomes, and part of these lipid bilayers is delivered by ATG9 containing vesicles [96, 97].

The ATG5-ATG12-ATG16L multimeric complex and the lipidation of the microtubule associated protein light chain 3 (LC3) (or the γ-aminobutyric acid receptor-associated protein (GABARAP)) are required for the phagophore expansion. They depend on two ubiquitin-like conjugation systems. In the first conjugation system, ATG7, an E1-like enzyme, activates ATG12, which is then conjugated to ATG5 by ATG10, E2-like enzyme. Afterwards, ATG5-ATG12 binds in a non-covalent manner ATG16L to form the ATG5-ATG12-ATG16L complex. The second conjugation system involves ATG4, a protease, that cleaves LC3 leaving a glycine residue at the C-terminus which is then conjugated to the polar head of phosphatidylethanolamine (PE), a component of cellular membranes, through a reaction that requires ATG7, ATG3 (E2-like), and the ATG12-ATG5-ATG16L (E3 like) complex [98-100].

Once the phagophore has surrounded the cargo and given rise to a closed vesicle called the autophagosome, the autophagosome undergoes maturation by fusing with an endosome or a lysosome. While stress induces perinuclear clustering of lysosomes, the autophagosomes are generated randomly in the cell periphery, and the dynein motor assures their centripetal movement and promotes their fusion [101-103].

Rubicon and UVRAG are two important regulators of autophagosome maturation. Rubicon downregulates the trafficking events by interacting with Beclin1 while UVRAG is a positive regulator of autophagosome maturation and endocytic trafficking and associates to the Beclin1-hVPS34 complex [104-106]. Other regulators are the GTPase protein RAB7, which is required for the fusion of autophagosomes with late endosomes or lysosomes, the endosomal sorting complexes required for transport (ESCRT) and the hepatocyte growth factor-regulated tyrosine kinase substrate (Hrs), which are important for endosomal sorting, and finally microtubules, which are exploited by autophagosomes for their trafficking and fusion with lysosomes [107, 108]. The fusion with lysosomes depend from the soluble N-ethylmaleimide-sensitive factor attachment protein receptors (SNAREs) and requires syntaxin 17 (STX17) and synaptosomal-associated protein 29 (SNAP29) on the autophagosome and vesicle-associated protein 8 (VAMP8) on the lysosome. Membrane tethering is supported by the homotypic fusion and protein sorting (HOPS) complex. After fusion, the newly generated autophagolysosomes undergo acidification, a process that is regulated by ATPases, and subsequent degradation of their contents [109].

3.3.1 Selective autophagy

Whereas upon starvation the autophagosomes engulf cytoplasmic components in a non-selective manner to mediate their recycling and to accelerate global turnover, invading pathogens and protein aggregates can stimulate a highly selective autophagy that targets these distinct structures.

The selectivity is conferred by the labeling of the cargo with signals, often ubiquitin (Ub) chains, which can be recognized by autophagy receptors that link the cargo to LC3 present on the autophagy membrane via their LC3-interacting regions (LIR). The five well-known autophagy receptors are the sequestosome 1 (p62/SQSTM1), neighbor of BRCA1 gene 1 (NBR1), calcium-binding and coiled coil containing protein 2 (NDP52), optineurin (OPTN), and Bcl2/adenovirus E1B 19kDa protein-interacting preotein-3 like (NIX). Most of them harbor both LC3-interacting region (LIR) and ubiquitin-binding domain (UBD) [110, 111]. The best characterized of these autophagy receptors is p62, which is a multifunctional protein that plays a crucial role in the oligomerization of important signaling molecules in cytosolic speckles to control cell survival, apoptosis, and autophagy. Moreover, it is implicated in the clearance of ubiquitinated protein aggregates [112]. p62, along with its partner, NBR1, regulates the packing and delivery of polyubiquitinated, misfolded, or aggregated proteins and dysfunctional organelles for their clearance through autophagy.

3.3.2 TBC1D5 and the retromer complex

It has been recently suggested that proteins known to accelerate hydrolysis of GTP on small Rab GTPases (RabGAP) act as autophagic adaptors that regulate autophagy via direct interaction with the autophagy key marker LC3 [97, 113].

Among several identified Tre-2/Bub2/Cdc16 (TBC) domain-containing Rab GAP proteins, TBC1D5 is particularly interesting since it contains two LIR motifs which are both required for LC3 binding upon autophagy induction [113] (Figure 7A).

TBC1D5 is involved in the retrograde transport from endosome to Golgi by co-operating with the vacuolar protein associated VPS35-VPS29-VPS26A/B retromer sub-complex. The retromer complex is a vital element of the endosomal sorting machinery that operates by the recognition of specific cargos, like the cation independent mannose 6 phosphate receptor (CI-M6PR), on the cellular membranes and transports them from the endosomes to the trans-Golgi network (TGN).

The retromer is characterized by two distinct sub-complexes: a trimer composed of VPS35-VPS29-VPS26A or B that mediates the cargo selection, and a dimer formed by the sorting nexin proteins 1 (SNX1) and SNX2 (also called VPS5 and VPS17, respectively) that have the function to mediate tubule or vesicle formation from the endosomal membrane [114, 115] (Figure 7B).

The retromer subunit VPS35 is the central scaffold of the complex and it associates with VPS29 and one of the two paralogues VPS26A or VPS26B. VPS29 is the smallest subunit of the trimer, and its role is still poorly understood. VPS26A and VPS26B compete for the binding to VPS35, and they define two distinct retromer complexes. VPS26A is involved in CI-M6PR trafficking and is associated with Rab5 positive early endosomes. VPS26B is not involved in CI-M6PR trafficking and localizes mainly with RAB7 and RAB9 positive late endosomes [116].

Both VPS26A and VPS26B retromers bind to TBC1D5. It has been described that the binding of TBC1D5 to the retromer complex occurs through VPS29 [113, 117].

In contrast, Bugaric *et al.* have shown that TBC1D5 co-precipitates with VPS26A or VPS26B in co-transfected cells [116].

It has been reported that upon starvation induced autophagy, TBC1D5 employs two different LIR motifs to switch from binding to the VPS retromer sub-complex to binding to LC3B for being localized on the autophagosomes. Both LIR domains seems to be required for the efficient transport of TBC1D5 to the lipidated LC3BII, suggesting that TBC1D5 must be localize in the endosomal compartment before transport to the autophagosomes [113].

Moreover, TBC1D5 also associates with the ATG9 and the adaptor protein 2 (AP2) complex upon autophagy and TBC1D5 depletion leads to mis-sorting of ATG9 to late endosomes. Inhibition of clathrin-mediated endocytosis or AP2 depletion alters ATG9 trafficking and its association with TBC1D5 [97].

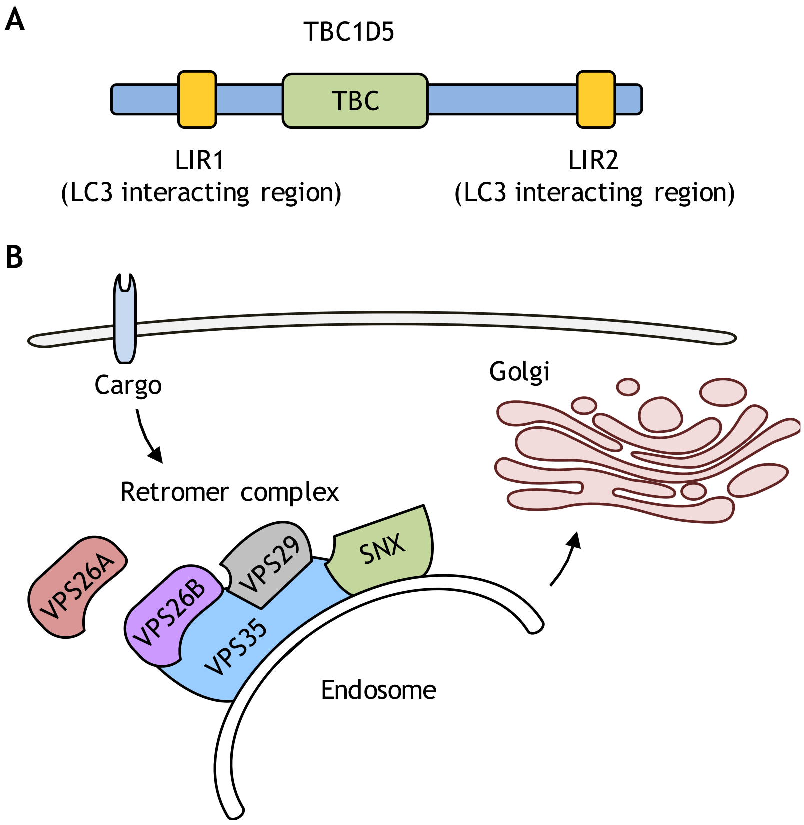
A
TBC1D5
TBC
LIR1
(LC3 interacting region)
LIR2
(LC3 interacting region)
B
Cargo
Golgi
Retromer complex
VPS26A
VPS26B
VPS29
SNX
VPS35
Endosome

Figure 7. TBC1D5 and the retromer complex.
A) Schematic representation of the TBC1D structure illustrating the LIR domains and the TBC domain; **B)** Representation of the retromer complex components.

3.3.3 Aggrephagy and protein quality control machinery

The term aggrephagy was introduced by Per Seglen to describe the selective sequestration and degradation of protein aggregates by autophagy [118]. Protein aggregation is a phenomenon that constantly occurs in cells. Some proteins polymerize in a regulated way to perform cellular functions, like the RIPK1/RIPK3 necrosome, but in most cases, aggregates are the result of the accumulation of misfolded proteins [119]. Aggregates can interfere with cellular functions and be potentially cytotoxic. Indeed, several neurodegenerative diseases are characterized by the accumulation of protein aggregates, like Alzheimer's, Parkinson's, and Huntington's diseases [120, 121].

Cells regulate the accumulation of aggregation-prone proteins and preserve the protein homeostasis through molecular chaperones (e.g., HSP70, HSP40, and HSP90) and several co-chaperones (e.g., CDC37 and the Bcl-2 associated athanogene 3 (BAG3)), that recognize misfolded proteins. The newly synthetized functional proteins are delivered to the HSP90 chaperone complex while misfolded proteins are degraded via the ubiquitin-proteasome pathway. HSP90 has the role of maintaining the protein folds while HSP70 associates with misfolded proteins and transports them for degradation. This can occur in three different manners: the ubiquitin-proteasome system (UPS), chaperone-mediate autophagy (CMA), and autophagy (in this context often referred as aggrephagy) [122].

UPS and CMA are only capable of degrading one extended polypeptide at a time, making autophagy the only process capable of mediating the lysosomal degradation of larger structures such as organelles or protein aggregates [123].

The aggresome is formed in response to an over expression of an aggregation prone protein when the proteasome dependent degradation fails. It is located at the microtubule-organizing center (MTOC) close to the nuclear membrane; it is insoluble and metabolically stable and the proteins of an aggresome are normally ubiquitinated and enclosed by intermediate filaments like vimentin and keratin [123, 124]. p62, NBR1, and autophagy-linked FYVE protein (ALFY) are present in almost all aggregates and can be involved in their formation and autophagy-mediated degradation [125, 126].

The two pathways described for the formation of an aggresome are regulated by the histone deacetylase 6 (HDAC6) and BAG3. HDAC6 facilitates the dynein motor to transport ubiquitinated substrates to the aggresome, and it has an active role in the fusion between autophagosomes and lysosomes. As a consequence, it facilitates the removal of aggregates by autophagy [127-129]. BAG3 co-operates with CHIP to target HSP70 substrates to the aggresome. This transport, which is dynein dependent, does not require ubiquitination of the substrates.

Finally, a study described aggresome-like structures that do not localize at the MTOC but required microtubular transport for their formation. They were defined as insoluble protein deposit (IPOD) and juxtanuclear quality control (JUNQ). The IPOD is located at the cell periphery and does not contain ubiquitinated proteins, but JUNQ contains ubiquitinated proteins and is located close to the nucleus. However, the relationship between them and the aggresomes has not been fully elucidated [130].

3.3.4 Autophagy and herpesviruses

In addition to its role as guardian of cellular homeostasis, autophagy has evolved to combat infection by a number of intracellular pathogens. At the same time, viruses have evolved mechanisms to evade autophagy. Indeed, it is not surprising that several anti-autophagic proteins have been described in the herpesviridae family. Moreover, some herpesviruses can exploit autophagy for their own benefit [131].

For instance, EBV and KSHV encode homologues of the B-cell lymphoma 2 protein (Bcl-2) that have both anti-apoptotic and anti-autophagic functions. EBV encodes two vBcl-2 proteins, which negatively regulate autophagy by binding to Beclin-1 and preventing the formation of the phagophore [132]. By contrast, the proteins expressed during latency seem to induce rather than inhibit autophagy. Indeed, it has been reported that LMP1 and LMP2A stimulate autophagy to promote cell survival [133, 134].

KSHV encodes for several proteins that mimic the cellular orthologues and regulate the pathways at several steps. In addition to preventing apoptosis, KSHV viral (v) Bcl-2 and viral Fas-associated death domain-like interleukin-1ß (IL-1ß)-converting enzyme-like inhibitory protein (vFLIP) regulate LC3 lipidation by blocking ATG3. In this way, vFLIP also blocks KSHV vCyclin induced autophagy and senescence. Moreover, the KSHV-encoded lytic protein K7 has been reported to block autophagosome maturation by interacting with Rubicon [135-137].

Among α-herpesviruses, autophagy plays a crucial role in restricting HSV-1 in a cell type-dependent manner. It has been reported that *in vitro* it restricts viral replication in primary neurons while it is dispensable in fibroblasts. Even though the majority of the studies agree on the fact that autophagy has a detrimental role on HSV-1 replication, it has been suggested that autophagy might be beneficial in viral entry [138]. HSV-1 blocks autophagy via the infected cell protein 34.5 (ICP34.5), which interacts with Beclin-1 and inhibits autophagosome biogenesis in fibroblasts, in neurons, and in epithelial cells [139, 140]. Indeed, a virus lacking ICP34.5 genes triggers autophagy by activating the eukaryotic translation initiation factor 2-kinase 2 (EIF2AK2)/double-stranded RNA-dependent host protein kinase (PKR) pathway. Moreover, ICP34.5 plays a role in escaping the immune response by blocking the maturation of autophagosomes in dendritic cells (DC) and as a consequence reducing viral antigen presentation [141]. In addition, HSV-1 US11 protein has been recently described to block autophagy by interacting with PKR [142, 143]. In contrast, VZV and Duck Enteritis virus (DEV) activate autophagy at late time points post-infection, and this step is necessary for viral glycoprotein processing [144].

Among ß-herpesviruses, HCMV stimulates autophagy during the early stages of infection and components of the viral particles are sufficient to trigger this mechanism. Inhibition of autophagy reduces HCMV titers, indicating that the pathway might be beneficial for viral replication. At later times post-infection, HCMV blocks autophagy through a US11 homologue, *i.e.* RS1, that is able to bind Beclin-1 [145, 146]. However, this protein is not essential for viral replication, a mutant virus lacking only the ability to block autophagy does not show any replication defects [147]. Interestingly, MCMV employs autophagy in order to inhibit the activation of innate cellular immunity. This mechanism is mediated by the *de novo* synthesized M45 that selectively targets NEMO to autophagosomes for degradation and impedes NF-κB activation [148].

3.4 Modulation of the cellular antiviral response and autophagy by MCMV M45

CMVs have incorporated several cell signaling inhibitors into their genomes in order to provide a cellular environment suitable to sustain their long replication cycles. The M45 gene of MCMV, also known as viral inhibitor of RIP activation (vIRA), encodes a potent inhibitor of NF-κB and necroptosis activation, and it was the first cell death inhibitor identified in MCMV [149].

M45 is a tegument protein of 1174 amino acids. It is expressed in infected cells with early kinetics and accumulates in the cytoplasm. It was initially identified as a homolog of the eukaryotic ribonucleotide reductases (RNR) large (R1) subunit, which is present in other herpesviruses, but M45 lacks catalytic activity [150]. However, screening of a random transposon library identified M45 as being important for MCMV replication. Indeed, a virus lacking M45 rapidly induces PCD in infected endothelial cells, such as SVEC4-10, and macrophages thereby precluding viral spread [149]. Importantly, M45 expression is necessary for viral dissemination *in vivo* [150]. M45 carries a RHIM domain at the N-terminus and the RNR R1 homology region at the C-terminus (Figure 8).

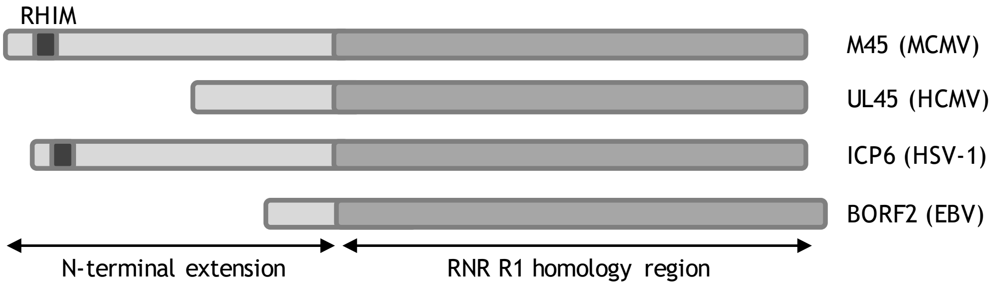
RHIM
M45 (MCMV)
UL45 (HCMV)
ICP6 (HSV-1)
BORF2 (EBV)
N-terminal extension
RNR R1 homology region

Figure 8. Herpesviruses R1 proteins.
Schematic representation of viral ribonucleotide reductase of murine cytomegalovirus (MCMV), human cytomegalovirus (HCMV), herpes simplex virus 1 (HSV-1) and Epstein-Barr virus (EBV). Adapted from Lembo and Brune, Trends in Biochemical Science, 2009.

The RHIM domain is required for inhibition of RIPK1-RIPK3 complex formation and TNFR1 necroptosis (Figure 9) [151].

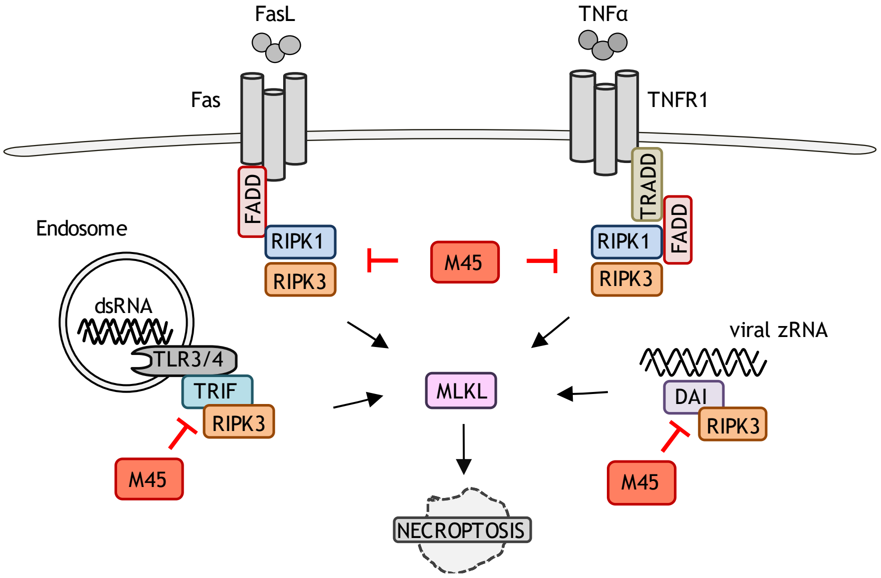
FasL
TNFα
Fas
TNFR1
FADD
TRADD
FADD
Endosome
RIPK1
RIPK3
M45
RIPK1
RIPK3
dsRNA
TLR3/4
TRIF
RIPK3
M45
MLKL
viral zRNA
DAI
RIPK3
M45
NECROPTOSIS

Figure 9. M45 inhibition of necroptosis.
The viral inhibitor of RIP activation (vIRA), encoded by the MCMV M45 gene, inhibits RHIM-dependent activation of RIPK3 by RIPK1, DAI/ZBP1, or TRIF due to its RIP homotypic interaction motif (RHIM). Adapted from Brune and Andoniou, Viruses, 2017.

The same domain is involved in the inhibition of viral induced necroptosis that signals through TRIF, RIPK3, and DAI. Indeed, elevated expression levels of RIPK3 and DAI confer sensitivity to MCMV induced necroptosis while RIPK1 was proved to be dispensable, indicating that death receptor- and virus-induced necroptosis do not rely on an identical set of cellular proteins [152, 153] (Figure 9).

Moreover, M45 inhibits RIPK1-dependent activation of MAPKs and the transcription factor NF-κB [154]. The C-terminus of M45 is involved in NF-κB regulation, but it also plays a role in viral necroptosis inhibition. Due to its importance as a transcription factor, the NF-κB pathway is an attractive target for viruses. In fact, it has been described that M45 has a dual role regarding NF-κB regulation. M45 present in the virion that is released into target cells during entry is important for the activation of NF-κB at very early times post-infection [155]. It has been postulated that MCMV might activate NF-κB to stimulate the Major Immediate Early Promoter (MIEP) and thus promote the transcription of viral genes. However, the contribution of this rapid and transient NF-κB activation to CMV replication and pathogenesis still remains to be fully elucidated. By contrast, newly synthetized M45 in the infected cell blocks NF-κB activation by targeting NEMO to autophagosomes for subsequent degradation in lysosomes [148]. In this way, the irreversible NEMO degradation allows the virus to efficiently block the production of pro-inflammatory cytokines (Figure 10).

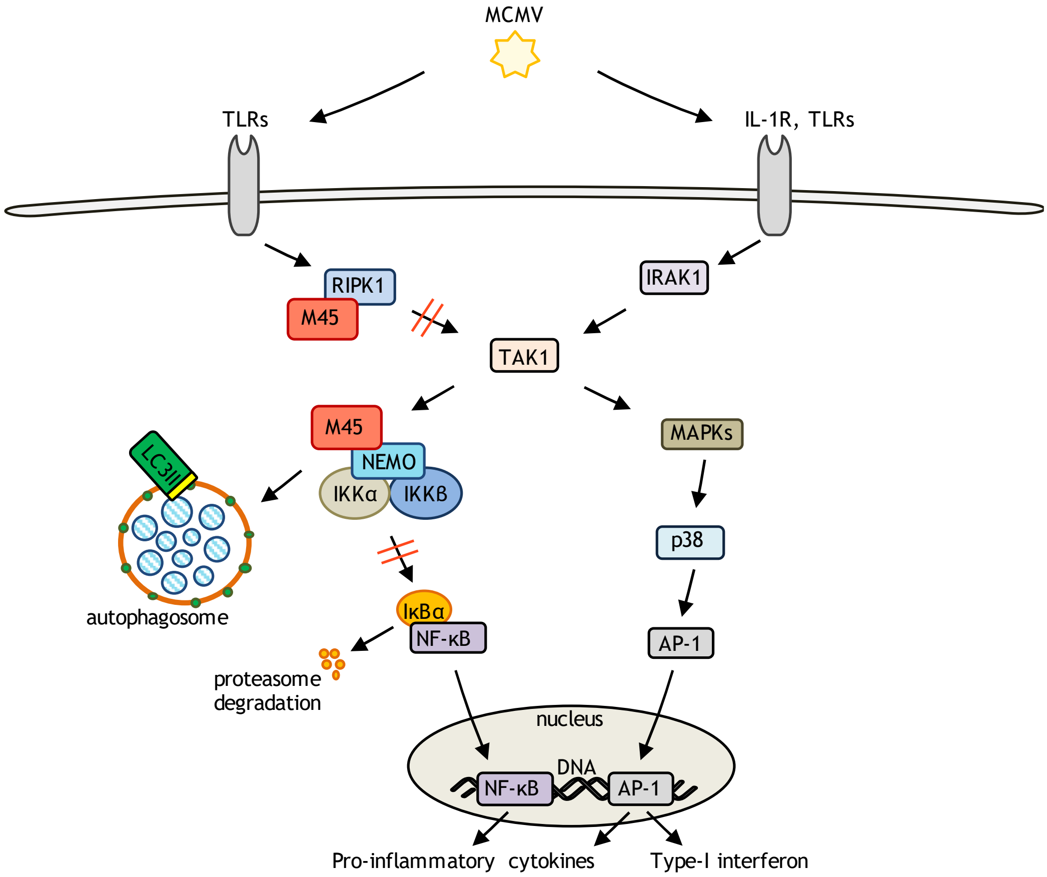
MCMV
TLRs
IL-1R, TLRs
RIPK1
M45
IRAK1
TAK1
M45
NEMO
IKKα
IKKβ
LC3II
autophagosome
MAPKs
p38
IκBα
NF-κB
proteasome degradation
AP-1
nucleus
DNA
NF-κB
AP-1
Pro-inflammatory cytokines
Type-I interferon

Figure 10. M45 inhibition of NF-κB
M45 blocks NF-κB activation by interacting with RIPK1 and NEMO. NEMO is targeted to autophagosomes for degradation. Adapted from P. Fliss et al., PlosPathogen, 2012.

3.4.1 Functions of M45 homologs in other herpesviruses

Amongst the M45 homologs encoded by other herpesviruses, ICP6 of HSV-1 is the best characterized.

HSV-1 ICP6, encoded by UL39, is an early protein that unlike M45 has a catalytically-active R1 domain. ICP6 can suppress apoptosis by binding and blocking caspase 8 and is also required for protecting human cells from induction of necroptosis [156-158]. It has been reported that the RHIM domain of ICP6 is required for the RIPK1-RIPK3 binding while the C-terminal region is necessary for self-oligomerization [159]. ICP6 dimers or oligomers initiate the RIPK1-RIPK3 hetero- and RIPK3-RIPK3 homo-interaction in murine cells independently of the RHIM domain. The finding that virus-host RHIM interaction can be either anti- or pro-necroptotic suggests that necroptosis has a complex interplay with herpesviruses and plays a crucial role in the restriction of certain viruses. By contrast, the HCMV homolog UL45 differs from M45 in that it does not contain a

RHIM and is dispensable for growth in endothelial cells, suggesting that these viruses developed different strategies to antagonize necroptosis [160]. However, it has been recently reported that UL45 interacts with UL48, a deubiquitinating protease, to inhibit NF-κB activation [161].

4 Aims of the study

The MCMV M45 protein inhibits innate antiviral defenses by blocking necroptosis [151-153]. It also inhibits NF-kB activation by redirecting NEMO to autophagosomes for degradation through the autophagosome-lysosome pathway [148]. Similar to NEMO, RIPK1 is also downregulated upon MCMV infection in an M45 dependent manner, suggesting that it can be targeted to autophagosomes as well [154, 155]. However, the molecular mechanism responsible for selective NEMO and RIPK1 degradation was not known.

The aim of this study was to elucidate the specific mechanisms of selective NEMO and RIPK1 degradation exerted by M45 with emphasis on analyzing how exactly the viral protein targets them to autophagosomes and whether autophagy adaptors or other cellular proteins are involved in this process.
Finally, since M45 is conserved across the herpesvirus families, this study aimed to elucidate whether the mechanism is unique to MCMV or shared by other members of the *Herpesvirales* order.

Taken together these findings provide new insights on the strategies used by herpesviruses to dispose of cell signaling proteins with antiviral functions. Current and further analysis of the investigated mechanism will allow a better understanding of virus-host-interaction and viral pathogenesis.

5 Results

5.1 M45 mediates NEMO and RIPK1 accumulation in the insoluble fraction

Previous work performed in our laboratory has shown that MCMV M45 binds NEMO and induces its degradation via the canonical autophagy pathway [148]. This was particularly evident in autophagy-deficient (*Atg5*$^{-/-}$) cells where NEMO levels were unaltered upon MCMV infection. However, when infected cells were harvested with a mild lysis buffer (1% NP-40), an M45-depended NEMO loss was also observed in *Atg5*$^{-/-}$ cells, thus suggesting that an addition mechanism to autophagy was activated by M45 to assure NEMO removal. Intriguingly, the accumulation of aggregate-like structures was observed in proximity of autophagosomes in M45 expressing cells, thus indicating that M45 mediates their formation [148]. Altogether these findings suggested that autophagy induction either involved or followed the formation of insoluble protein aggregates. In order to test this hypothesis, WT and *Atg5*$^{-/-}$ MEFs were infected with MCMV-M45HA as well as with a control MCMV lacking the entire M45 gene (MCMV-ΔM45) [148, 155]. Cells were lysed at different times post infection with 1% NP-40 lysis buffer. After centrifugation, the detergent-soluble and -insoluble fractions were collected, denatured in Lämmli buffer, and analyzed by immunoblot analysis (Figure 11).

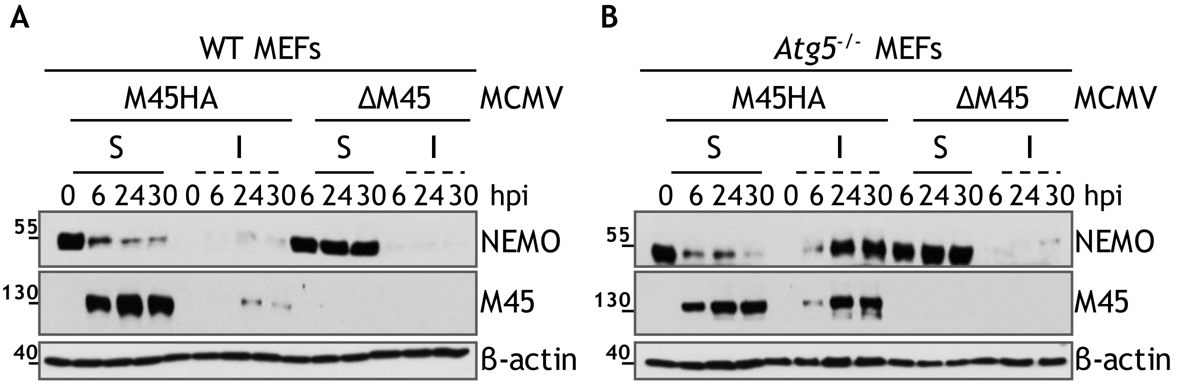

Figure 11. Accumulation of NEMO in the detergent insoluble fraction of MCMV infected MEFs.
(A) Soluble (S) and insoluble (I) fractions of WT MEFs infected with MCMV-M45HA or MCMV-ΔM45 (MOI 5 TCID$_{50}$) harvested over the indicated time course. NEMO, M45 and ß-actin expression were analyzed by immunoblot; **(B)** S and I fractions of *Atg5*$^{-/-}$ MEFs infected with MCMV-M45HA or MCMV-ΔM45 (MOI 5 TCID$_{50}$) harvested over the indicated time course. NEMO, M45, and ß-actin expressions were analyzed by immunoblot.

Supporting previous data, in autophagy competent WT fibroblasts soluble NEMO was degraded upon MCMV-M45HA infection but not by MCMV-ΔM45 mutant infection (Figure 11A). By contrast, large amounts of NEMO and M45 accumulated in the insoluble fraction of autophagy incompetent *Atg5*-/- MEFs infected with MCMV-M45HA (Figure 11B). These data indicate that M45 induces first the accumulation of proteins in the insoluble fraction and afterwards exploit autophagy to degrade them. In order to verify whether M45 co-localizes with NEMO in the absence of autophagy, WT and *Atg5*-/- MEFs were co-transfected with plasmids encoding M45-HA and Flag-NEMO prior to immunofluorescence analysis (Figure 12A).

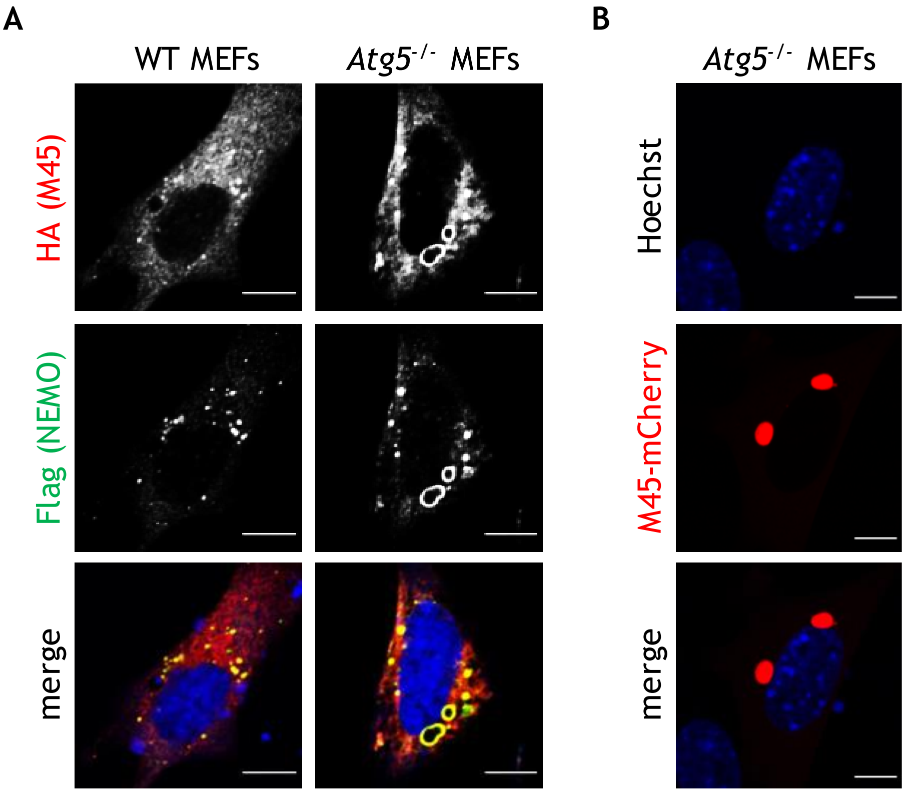

Figure 12. M45 and NEMO localization in WT and *Atg5*-/- MEFs.
(A) WT and *Atg5*-/- MEFs co-transfected with M45-HA (red) and Flag-NEMO (green) expression plasmids. Staining was performed 24 hours post transfection; **(B)** *Atg5*-/- MEFs co-transfected with an M45-mCherry (red) expression plasmid. Staining performed 24 hours post transfection.
Nuclei were stained with Hoechst 33342 (blue). Scale bar, 10 µm.

While in WT MEFs, M45 and NEMO co-localized in small dots, in *Atg5*-/- MEFs the two proteins co-localized but formed bigger structures, in some cases exhibiting an empty central core. A likely explanation for the ring appearance of the M45 and NEMO containing structures is that they are dense aggregates in which the antibodies are not able to penetrate the dense core and only stained the proteins accessible from the external side of the structure (Figure 12A). In order to confirm this hypothesis, *Atg5*$_{-/-}$ MEFs were transfected with an M45-mCherry expression plasmid. Indeed, unstained cores were not observed when an M45-mCherry plasmids was used (Figure 12B).

It has been shown previously that the MCMV M45 protein binds to RIPK1, inhibits its activation by ubiquitination, and blocks the TNFα-induced activation of NF-κB and caspase-independent programmed cell death (PCD), thus making RIPK1 a converging point of two pathways that are both regulated by M45 [154]. An M45-dependent downregulation of RIPK1 levels at late times post infection has also been observed. However, RIPK1 downregulation was MOI-dependent and not as pronounced as the downregulation of NEMO [154, 155].

To test whether M45 affects RIPK1 in a similar fashion as it affects NEMO, WT and *Atg5*$_{-/-}$ MEFs were infected with either MCMV-M45HA or MCMV-ΔM45. Cells were harvested at different time points post-infection, and the soluble and insoluble fractions were analyzed by immunoblot (Figure 13A). At 7 and 24 hours post infection (hpi), WT cells infected with MCMV-M45HA but not with the MCMV-ΔM45 showed an accumulation of RIPK1 in the insoluble fractions. RIPK1 accumulation in the insoluble fraction was even more evident in MCMV-M45HA infected *Atg5*$_{-/-}$ MEFs (Figure 13A).

In order to assess whether RIPK1 is degraded in a lysosome-dependent manner, MCMV-M45HA infected NIH-3T3 cells, treated or not with the lysosomal acidification inhibitor NH_4Cl, were collected at different times post infection and analyzed by immunoblot (Figure 13B). MCMV-ΔM45 was used as control. While RIPK1 was degraded in untreated MCMV-M45HA infected cells, the degradation of RIPK1 was blocked when the cells were incubated with NH_4Cl, similar to those infected with MCMV-ΔM45.

Altogether, these data indicate that M45 renders RIPK1 and NEMO insoluble, most likely as protein aggregates, and then redirects them to autophagosomes for degradation.

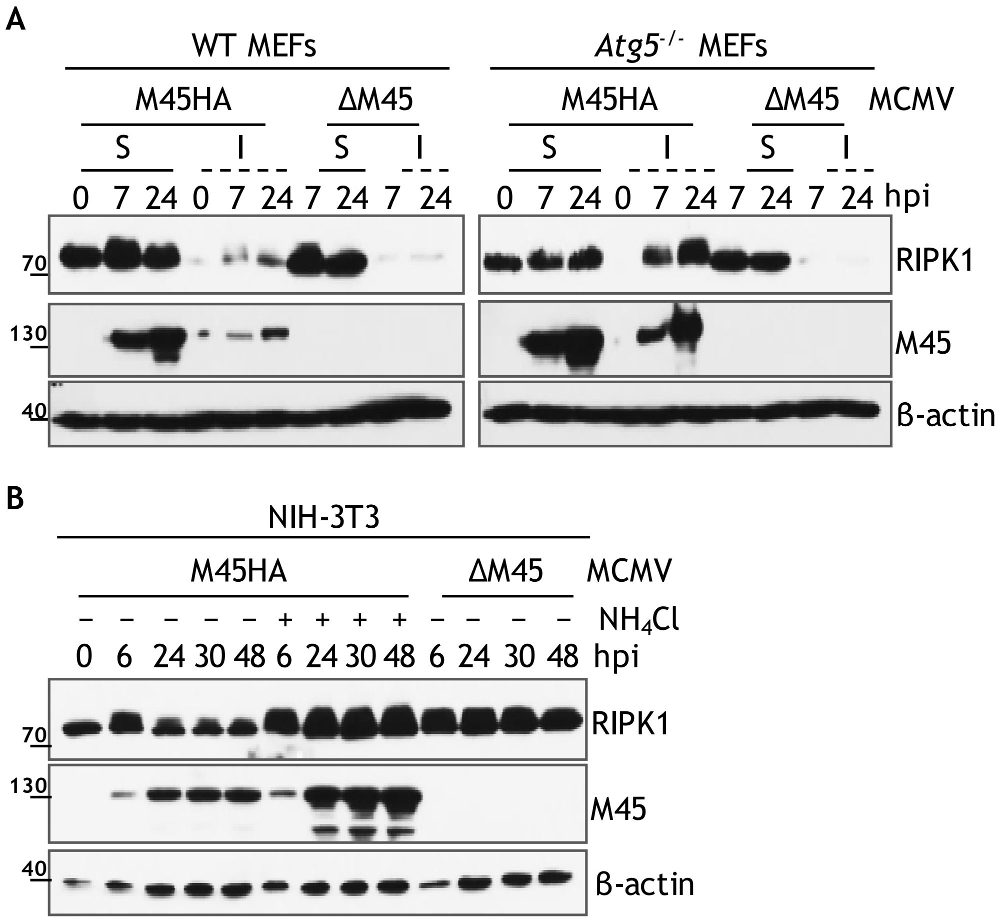
A
WT MEFs
Atg5-/- MEFs
M45HA
ΔM45
MCMV
S
I
0 7 24 0 7 24 7 24 7 24 hpi
70
130
40
RIPK1
M45
ß-actin
B
NIH-3T3
M45HA
ΔM45
MCMV
– – – – – + + + + – – – – NH4Cl
0 6 24 30 48 6 24 30 48 6 24 30 48 hpi

Figure 13. RIPK1 accumulation in the insoluble fraction upon MCMV-M45HA infection. **(A)** Soluble (S) and insoluble (I) fractions of WT and *Atg5*$_{-/-}$ MEFs infected with MCMV-M45HA or MCMV-ΔM45 (MOI 5 TCID$_{50}$) harvested at the indicated times post infection. RIPK1, M45 and ß-actin expression was analyzed by immunoblot; **(B)** NIH-3T3 cells were infected with MCMV-M45HA and MCMV-ΔM45 (MOI 5 TCID$_{50}$). 30 min post infection cells were treated with NH_4Cl (10 mM) or left untreated. Whole cell lysates were collected at the indicated times post infection and RIPK1, M45 and ß-actin expression was analyzed by immunoblot.

5.2 MCMV induces the formation of aggregates

To test whether M45 induces the formation of aggregates, several approaches were used. Firstly, cells were infected with MCMV-M45HA or MCMV-ΔM45 and 15 hours post infection were treated with a molecular rotor dye, which labels protein aggregates (ProteoStat-Red-dye aggresome detection assay). In fibroblasts infected with MCMV-M45HA, the ProteoStat dye stained numerous intracytoplasmic aggregates, similar to those seen in MEFs treated with the proteasomal inhibitor MG-132 (positive control). In contrast, ProteoStat-positive aggregates were not detected in fibroblasts infected with MCMV-ΔM45 (Figure 14).

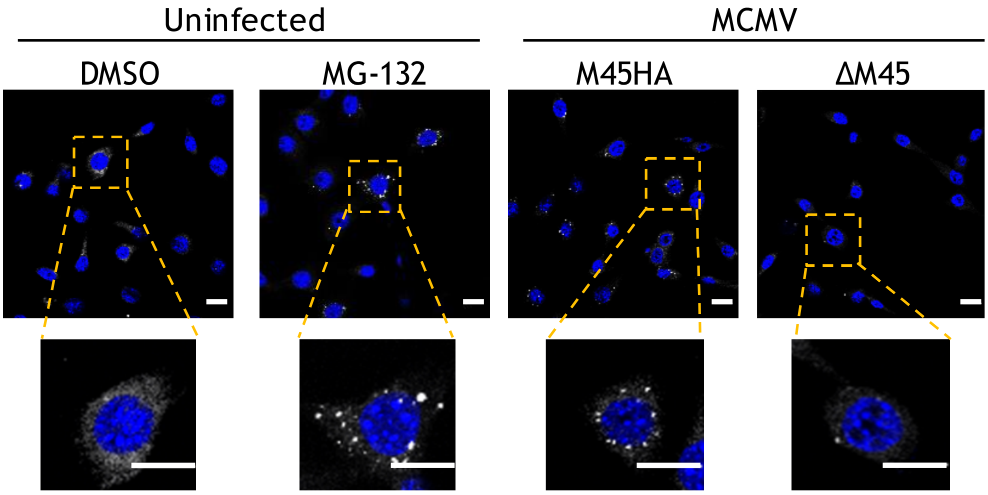

Figure 14. Aggregates staining upon MCMV-M45 infection.
NIH-3T3 cells infected with MCMV-M45HA or MCMV-ΔM45 (MOI 3 $TCID_{50}$). Aggregates were stained using ProteoStat dye (grey).
Nuclei were stained with Hoechst 33342 (blue). Scale bar, 10 µm.

To confirm that M45 expression was sufficient for aggregate formation, NIH-3T3 were transfected with plasmids expressing full-length M45-HA or Ct3-HA, an inactive and C-terminally truncated M45 protein, previously described [148, 155]. 24 h post transfection, cells were fixed and stained with the ProteoStat Red-dye. Indeed, ProteoStat-positive aggregates colocalizing with M45 were detected in cells expressing the full-length M45 but not in those expressing the truncated protein (Figure 15).

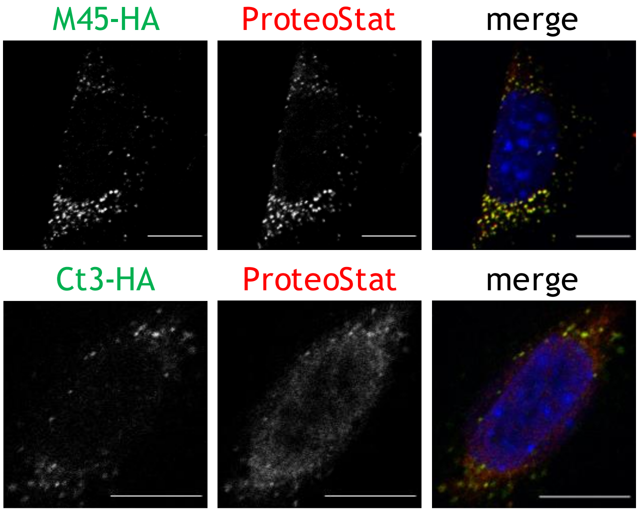

Figure 15. Aggregates staining upon M45-HA transfection.
NIH-3T3 cells were transfected with plasmids expressing full length or truncated M45 proteins (M45-HA and M45-Ct3HA, respectively). HA-tagged proteins were detected by immunofluorescence staining (green) and protein aggregates with the ProteoStat dye (red). Nuclei were stained with Hoechst 33342 (blue). Scale bar, 10 µm.

Secondly, the aggregates induced by M45 were further characterized by means of Correlative Light and Electron Microscopy (CLEM), which is a technique that combines fluorescence microscopy with electron microscopy [162]. In order to visualize M45 aggregates by light microscopy, a recombinant MCMV expressing an M45-mCherry fusion protein was constructed by *en passant* BAC mutagenesis.

MCMV-M45mCherry was used to infect WT and *Atg5*$_{-/-}$ MEFs. At 20 hpi, cells were fixed, stained with BODIPY (lipid droplets) and Hoechst 33342 (nuclear DNA), and imaged with fluorescence microscopy (Figure 16). M45 positive dots within cells were subsequently analyzed by transmission electron microscopy (TEM) (Figure 16). BODIPY was used as a fiducial marker in order to enable accurate overlaying of fluorescence and electron microscopy images. Red fluorescent M45 dots colocalized with highly electron dense, irregularly shaped structures in electron photographs. These structures resembled aggregates and had an estimate volume of 500 nm$_3$ in WT MEFs (Figure 16A) and up to 1 µm$_3$ in *Atg5*$_{-/-}$ MEFs (Figure 16B). Considering the entire volume of the cell, WT and *Atg5*$_{-/-}$ MEFs presented several aggregates per cell (the EM images were obtained with the help of Rudolph Reimer and Carola Schneider, TP microscopy and image analysis, [HPI]).

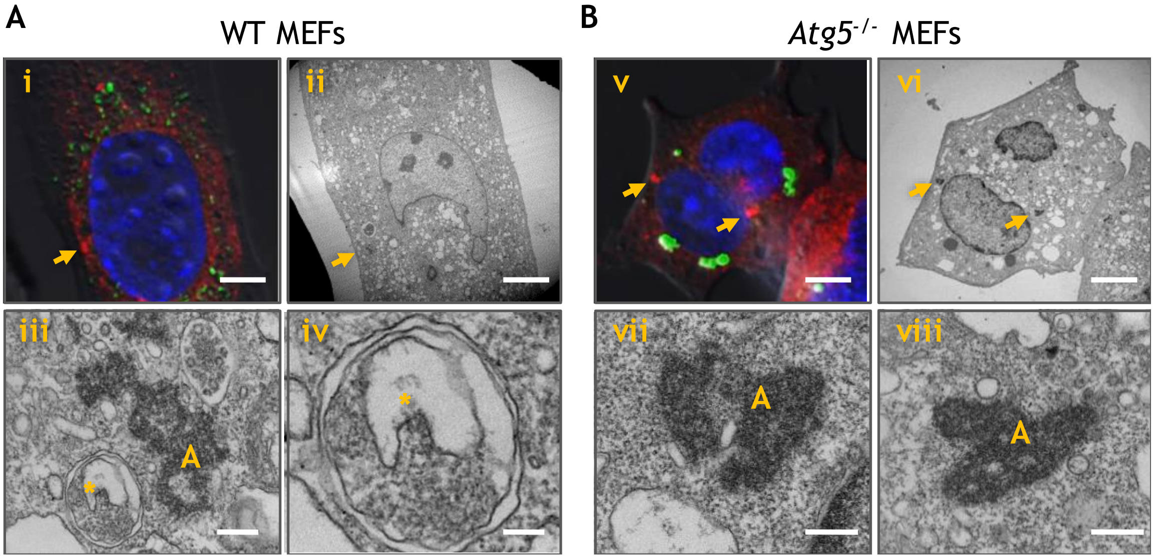

Figure 16. CLEM of WT and *Atg5*$_{-/-}$ MEFs infected with MCMV-M45mCherry.
Confocal images of MCMV infected MEFs (MOI 5 TCID$_{50}$) (i,v): in red M45, in green lipid droplets, in blue nuclei. Scale bars, 5 µm (i, ii, v, vi) or 200 nm (iii, iv, vii, viii). **(A)** Ultrathin (50 nm) section of WT MEFs observed by TEM (ii). Magnification of an area of the same cell containing an aggregate (A), which correlates to an M45mCherry dot (iii) in proximity to an autophagosome (*). Magnification of the autophagosome (iv); **(B)** Ultrathin section of *Atg5*$_{-/-}$ MEFs observed by TEM (vi). Magnification of two aggregates in the same section of an *Atg5*$_{-/-}$ cell (vii - viii).

Notably, in WT MEFs the M45 aggregates were often found in close proximity to autophagosomes or autophagolysosomes (Figure 16A).

Additionally, fluorescence recovery after photobleaching (FRAP) was used to verify whether M45 was immobilized in aggregates and not mobile throughout the cytoplasm (experiment performed with the help of Enrico Caragliano, [HPI]). FRAP is a technique that determines how mobile a fluorescent molecule is. NIH-3T3 cells were transfected with either a plasmid encoding an mCherry-tagged M45 or an mCherry-tagged Nucleolin as positive control for recovery. The accumulation of the M45-mCherry or mCherry-Nucleolin proteins was observed by live cell imaging 48 h post- transfection (Figure 17A).

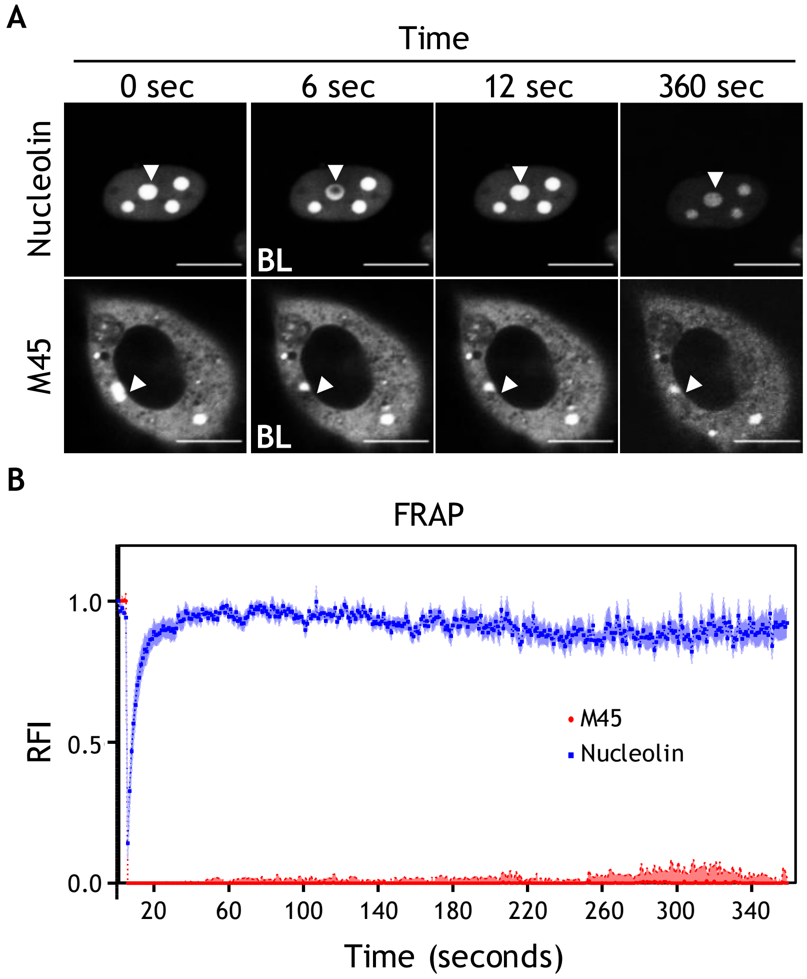

Figure 17. FRAP analysis of M45mCherry upon transfection.
(A) NIH-3T3 cells were transfected with plasmids expressing mCherry-tagged M45 or Nucleolin. Areas of 1 µm diameter within mCherry-positive dots were photobleached for 2 sec, and fluorescence recovery after photobleaching was observed for subsequent 360 sec by live cell microscopy. Scale bar, 10 µm; **(B)** Relative fluorescence intensity (RFI) of FRAP kinetics determined for 10 mCherry-tagged M45 or Nucleolin dots in different cells. Solid dots represent the mean and the colored area denotes 1 standard deviation.

mCherry dots were photobleached by means of a 563 nm laser and the recovery of fluorescence was measured over time. Consistent with the liquid-like nature of nucleoli [163], mCherry-tagged Nucleolin recovered within a few seconds after bleaching. In contrast, M45-mCherry dots did not show any recovery of fluorescence after photobleaching for the entire duration of the experiment, thus confirming its rigidity (Figure 17A and B). Finally, M45-aggregates were observed by live cell imaging. NIH-3T3 cells were transfected with M45-mCherry plasmids and observed with a spinning disk confocal microscope for 36 h (Figure 18). The mCherry-M45 dots initially appeared as small puncta but increased in size and coalesced into larger aggregates over time (Figure 18).

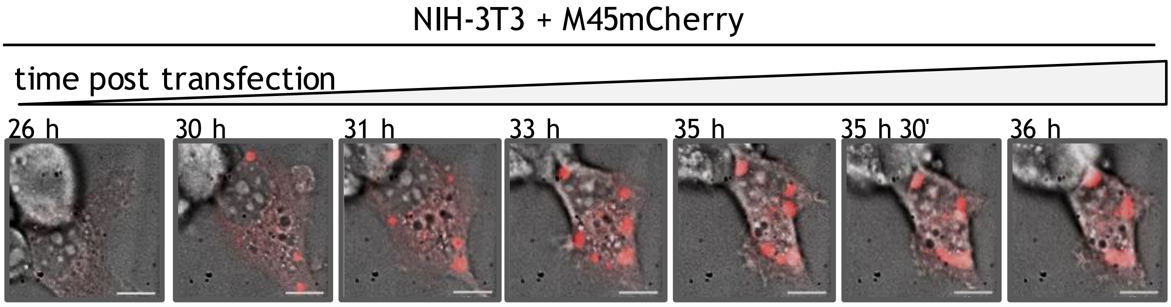

Figure 18. Live cell imaging of transfected M45mCherry.
Maximum intensity projection of a video of NIH-3T3 cell transfected with a plasmid encoding M45-mCherry (red) and observed 6 hours post transfection by live cell imaging for 30 hrs.

Altogether these findings demonstrate that either upon transfection or upon viral infection, M45 is capable of inducing the formation of rigid aggregates that accumulate in the cytoplasm of the cells, often in immediate proximity of autophagosomes.

5.3 A sequence motif within the C-terminal part of M45 mediates NEMO and RIPK1 aggregation

The M45 protein, similar to its homologs in the *Herpesviridae* family, possesses a C-terminal R1 homology domain and a unique N-terminal portion containing a RIP Homotypic Interaction Motif (RHIM) domain [164]. The C-terminal portion is involved in NEMO degradation while the N-terminal portion containing the RHIM domain is required for blocking the RIPK1–RIPK3 interaction and RIPK3-dependent necroptosis [150, 151, 153, 164] but is dispensable for NEMO degradation [148].

In order to investigate whether the C-terminus of M45 is required for NEMO and RIPK1 aggregation, *Atg5*$^{-/-}$ MEFs were infected with recombinant MCMVs expressing progressively C-terminally truncated versions of M45 (Figure 19A). Detergent soluble (S) and insoluble (I) fractions were harvested 24 hours post infection and analyzed by immunoblot (Figure 19B).

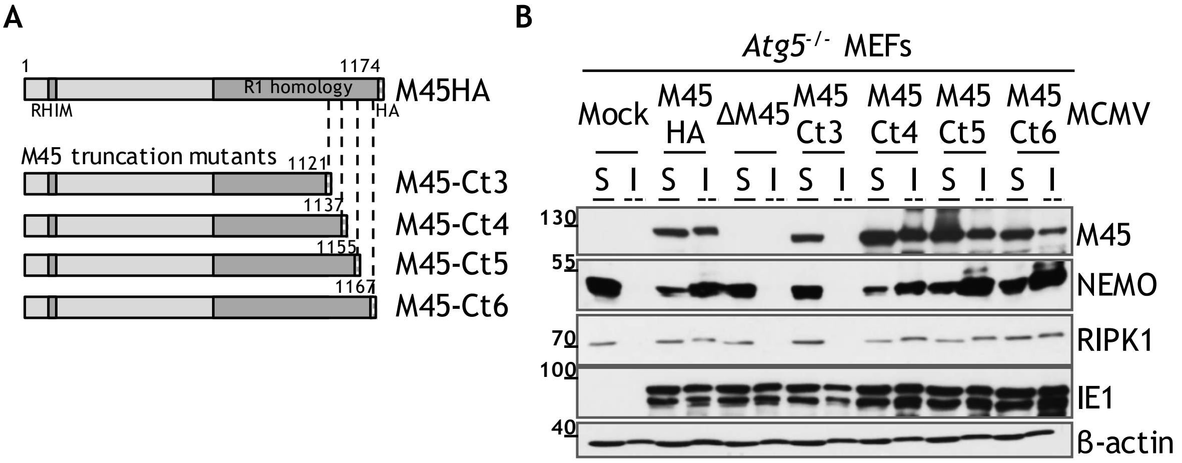
A
1
1174
R1 homology
M45HA
RHIM
HA
M45 truncation mutants
1121
M45-Ct3
1137
M45-Ct4
1155
M45-Ct5
1167
M45-Ct6
B
Atg5-/- MEFs
Mock
M45 HA
ΔM45
M45 Ct3
M45 Ct4
M45 Ct5
M45 Ct6
MCMV
S I S I S I S I S I S I S I
130
55
70
100
40
M45
NEMO
RIPK1
IE1
ß-actin

Figure 19. NEMO and RIPK1 accumulation in the insoluble fraction upon MCMV M45 C-terminus mutants infection.

(A) Schematic representation of HA tagged M45 C-terminal truncation mutants (M45-Ct); **(B)** *Atg5*$^{-/-}$ MEFs were infected with WT and mutant MCMVs (MOI 5 TCID$_{50}$). At 24 hpi, NEMO, RIPK1, and M45 levels were detected in the detergent-soluble (S) and insoluble (I) fractions.

While expression of full-length M45 or the truncated M45 proteins Ct4, Ct5, and Ct6 resulted in the accumulation of NEMO and RIPK1 in the detergent-insoluble fraction, the expression of M45-Ct3 did not. This suggests that the M45 amino acid residues 1122 to 1137 are required for the aggregation and accumulation in the insoluble fraction of NEMO, RIPK1 and M45 itself (Figure 19B).

It has been demonstrated that fusion to a fluorescent protein can be used as a visualization tool for the detection of aggregation-prone proteins and peptides [165]. To test whether the M45 amino acid residues 1122 to 1137 contains an aggregation-inducing functional domain, fragments derived from the M45 C-terminal truncation mutants Ct3 and Ct6 were fused to a plasmid expressing mCherry (Figure 20A). The plasmids were transfected into NIH-3T3 cells, and mCherry distribution was analyzed by confocal microscopy 48 hours post transfection. Indeed, co-expression of mCherry with M45-derived fragments containing the 1122-1137 region caused mCherry aggregation (Figure 20B).

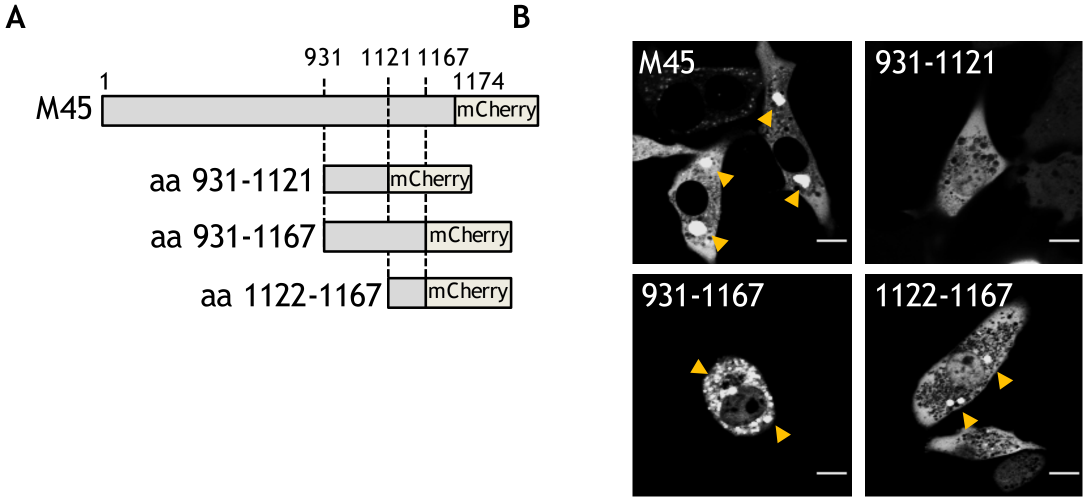
A
B
931
1121
1167
1
1174
M45
mCherry
aa 931-1121
mCherry
aa 931-1167
mCherry
aa 1122-1167
mCherry
M45
931-1121
931-1167
1122-1167

Figure 20. M45 aggregation-inducing domain.
(A) Schematic representation of M45 peptides mCherry-tagged; **(B)** NIH-3T3 cells were transfected with plasmids expressing full-length M45 or M45 fragments fused to mCherry. The distribution of mCherry was visualized by confocal microscopy. Scale bar 10 µm.

To further narrow down the amino acids required for protein aggregation, four MCMV M45 alanine substitution mutants covering the 1122-1134 regions were generated. The mutants were named M45-mut1-HA through mut4-HA (Figure 21A).

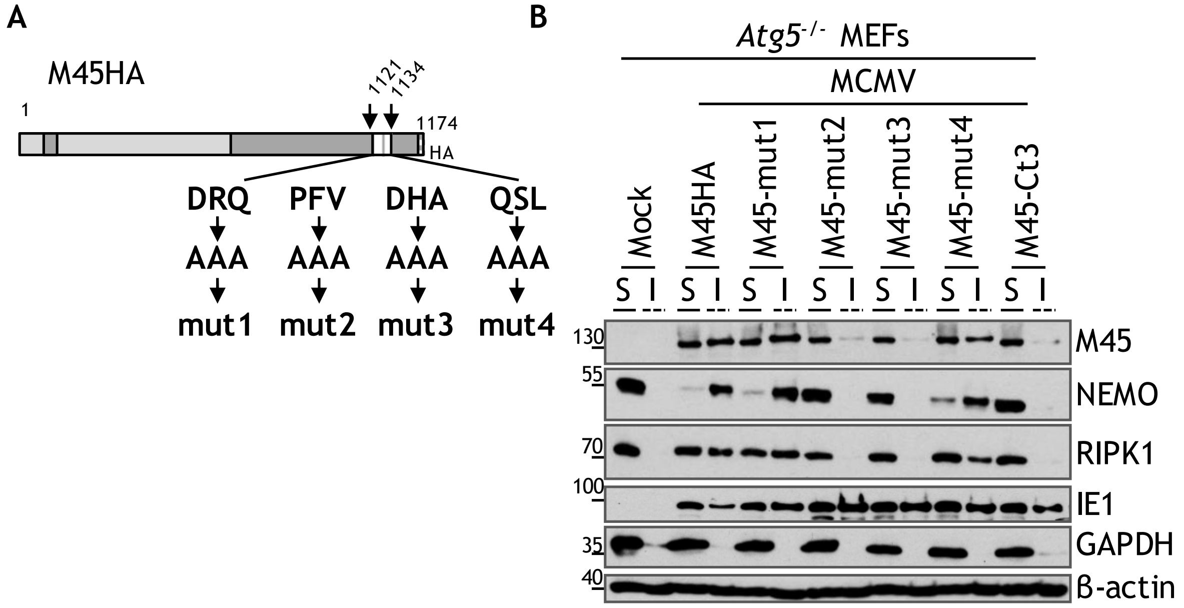
A
B
M45HA
1
1121
1134
1174
HA
DRQ
PFV
DHA
QSL
AAA
AAA
AAA
AAA
mut1
mut2
mut3
mut4
Atg5-/- MEFs
MCMV
Mock
M45HA
M45-mut1
M45-mut2
M45-mut3
M45-mut4
M45-Ct3
S I S I S I S I S I S I S I
130
55
70
100
35
40
M45
NEMO
RIPK1
IE1
GAPDH
β-actin

Figure 21. NEMO and RIPK1 accumulation in the insoluble fraction upon MCMV M45 alanine mutants infection.
(A) Four recombinant MCMVs carrying M45 triple-alanine substitution mutations (M45mut1 to 4), HA tagged; **(B)** *Atg5*-/- MEFs infected with WT and mutant MCMVs (MOI 5 TCID$_{50}$). At

24 hpi, NEMO, RIPK1, and M45 levels were detected in the detergent-soluble (S) and insoluble (I) fractions.

Recombinant viruses expressing M45 variants were used to infect *Atg5*$^{-/-}$ MEFs and then M45, RIPK1 and NEMO protein levels were analyzed by immunoblot in the detergent soluble (S) and insoluble (I) fractions (Figure 21B) at 24 hpi. While MCMV M45-mut1-HA and mut4-HA phenocopied wildtype M45 with respect to NEMO, RIPK1, and M45 accumulation in the insoluble fraction, MCMV M45-mut2-HA and mut3-HA were incapable of rendering NEMO, RIPK1, and M45 insoluble.

The importance of the amino acid motif PFVDH located from 1125 to 1129 was also confirmed with ProteoStat staining. NIH-3T3 cells were transfected with either M45-HA or M45-mut3-HA plasmids. 24 hours post infection cells were fixed, stained with HA and the ProteoStat Red dye and the number of HA and ProteoStat co-localizing dots was counted by observing the cells at a confocal microscope. Indeed, M45-mut3-HA showed a significant less number of aggregates as compared to the wildtype M45HA (Figure 22A and B).

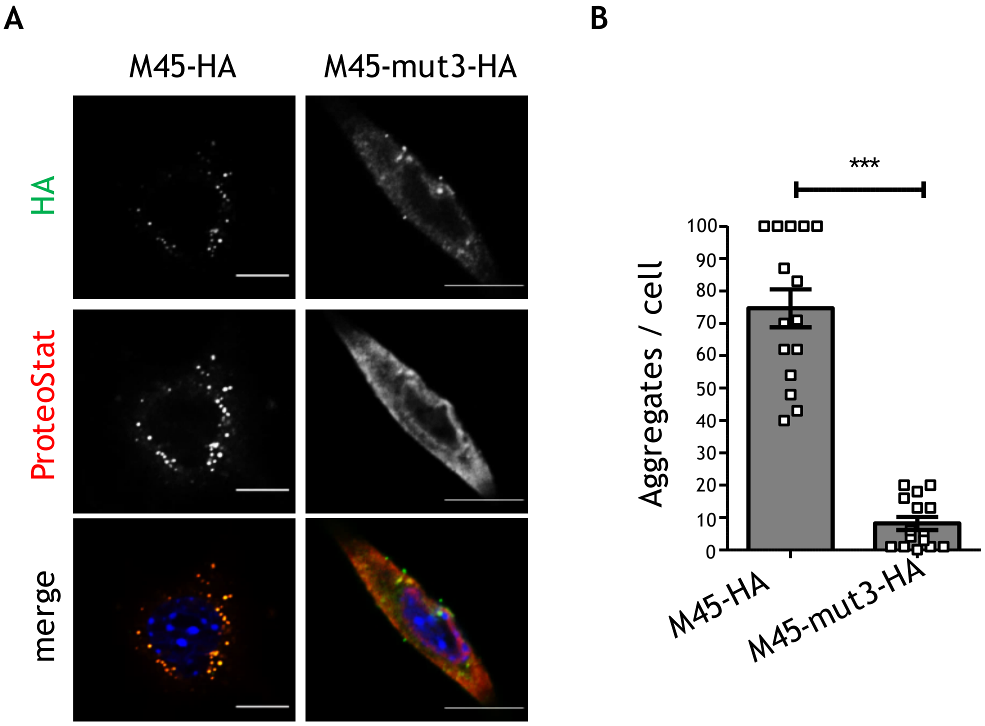

Figure 22. Aggregates staining upon transfection of MCMV WT and IPAM mutant.
(A) NIH-3T3 cells were transfected with HA tagged WT M45 or M45-mut3 plasmids. 24 h post transfection HA-tagged M45 was detected by immunofluorescence (green) and protein aggregates were stained using the ProteoStat dye (red). Scale bar, 10 µm; **(B)** M45 and ProteoStat-positive dots (up to 100 per cell) were counted in 15 cells each using z-stacks and maximum intensity projection. Significance was determined using a two-tailed unpaired *t*-test. Means ± SEM are shown. ***, $P<0.001$

Altogether these data reveal that the amino acid motif 1125 PFVDH 1129 within the C-terminus of M45 is required for rendering NEMO and RIPK1 (as well as M45 itself) insoluble. This motif was therefore named "induced protein aggregation motif" (IPAM).

5.4 M45 aggregates co-localize with LC3BII but not with HSP70 or Caveolin-1

In order to verify whether the aggregates co-localize with autophagosomes, NIH-3T3 cells were infected for 24 hrs with MCMV-M45HA or MCMV M45-mut2-HA prior to fixation and staining for HA and the autophagosome marker LC3BII (Figure 23A). As expected considering that the IPAM motif is required for the accumulation of M45 in aggregates, only the MCMV-M45HA virus showed M45 dots which co-localized with LC3BII. By contrast, the mutant M45 remained dispersed in the cytoplasm when cells were infected with MCMV-M45mut2-HA (Figure 23A).

It is known that chaperones are involved in the protein quality control machinery of the cells and can target aggregates to autophagosomes in a process called aggrephagy (Chapter 3.3.3). In order to check whether the aggregates co-localize with chaperones, fibroblast were infected with MCMV-M45HA or MCMV-M45mut2-HA and 24 hpi were stained for endogenous HSP70, a key component of the protein quality control machinery, either by fluorescence microscopy or by immunoblot of the soluble and insoluble fractions (Figure 23B and C). M45-positive dots did not co-localize with HSP70 nor was HSP70 found in the detergent-insoluble fraction of MCMV-infected cells (Figure 23B and C), suggesting that HSP70 either is not present in M45 aggregates or associates transiently.

Moreover, the aggregates did not co-localize with Caveolin-1, a recently described marker of necrosomes [166], indicating that the M45-induced aggregates are different from necrosomes (Figure 23D).

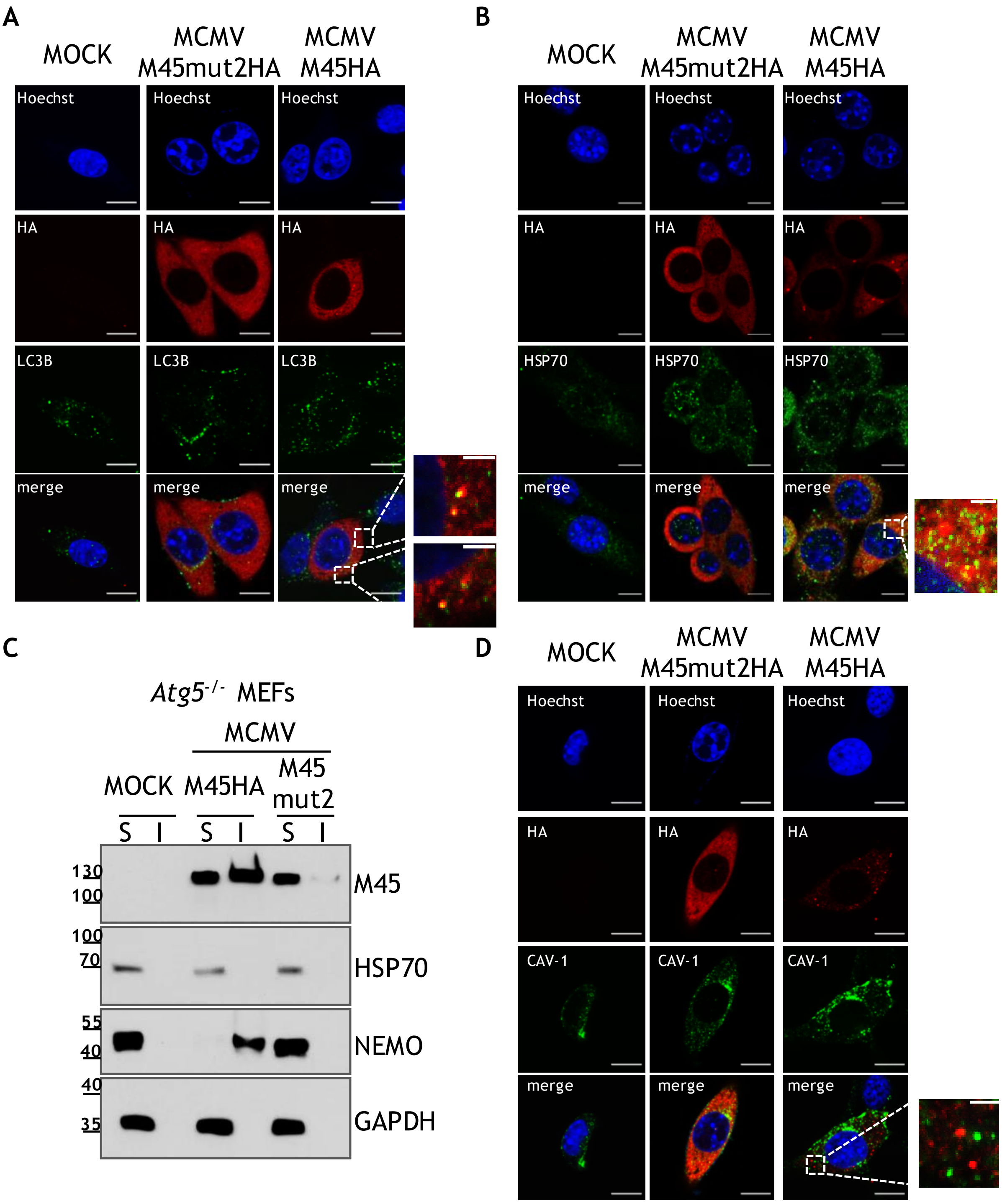
A
MOCK
MCMV M45mut2HA
MCMV M45HA
Hoechst
HA
LC3B
merge
B
MOCK
MCMV M45mut2HA
MCMV M45HA
Hoechst
HA
HSP70
merge
C
Atg5-/- MEFs
MCMV
MOCK
M45HA
M45 mut2
S
I
S
I
S
I
130
100
M45
100
70
HSP70
55
40
NEMO
40
35
GAPDH
D
MOCK
MCMV M45mut2HA
MCMV M45HA
Hoechst
HA
CAV-1
merge

Figure 23. Localization of aggregates relative to cellular markers.
(A) NIH-3T3 cells were infected with MCMV-M45HA or MCMV-M45mut2-HA (MOI 3 $TCID_{50}$). 24 hpi cells were fixed and stained for HA (red) and LC3BII (green); **(B)** Same experimental conditions as A, but cells were stained for HA (red) and HSP70 (green); **(C)** Immunoblot analysis of the S and I fractions of MCMV-M45HA and M45-mut2-HA infected *Atg5*$_{-/-}$ MEFs (MOI 5 $TCID_{50}$) at 24hpi; **(D)** NIH-3T3 infected with MCMV-M45HA or MCMV-M45mut2-HA (MOI 3 $TCID_{50}$). 24 hpi cells were fixed and stained for HA (red) and Caveolin-1 (green).
Nuclei were stained with Hoechst 33342. Scale bar, 10 µm or 2 µm (zoomed image).

5.5 The IPAM is required for M45 interactions with RIPK1, NEMO, and itself

The C-terminal part of M45 is necessary for its interactions with RIPK1 and NEMO [148, 155]. In order to test whether the IPAM is required for these interactions, NIH-3T3 fibroblasts were infected with MCMVs expressing HA-tagged full-length M45, the Ct3 truncation mutant, or a mutant of the IPAM (mut2), and 24 hpi cell lysates were used for immunoprecipitation of M45 using an anti-HA antibody. Consistent with previous results [148, 155], RIPK1 and NEMO co-precipitated with full-length M45, but not with M45-Ct3. Similarly, RIPK1 and NEMO did not co-precipitate with M45mut2 (Figure 24A), indicating that the PFV-to-AAA mutation was sufficient to abrogate these interactions.

Since it has been shown that M45, similar to its homolog in HSV-1, ICP6, can interact with itself [158], I tested whether M45 requires the IPAM for self-interaction. HEK-293A cells were co-transfected with plasmids expressing either Flag-tagged wildtype or mutant (mut3) M45 and HA-tagged wildtype M45. Cell lysates were subjected to immunoprecipitation 24 hours post transfection using an anti-HA antibody. As shown in Figure 24B, HA-tagged M45 co-precipitated with Flag-tagged WT M45, but not with Flag-tagged M45-mut3, suggesting that the IPAM is also required for M45 self-interaction.

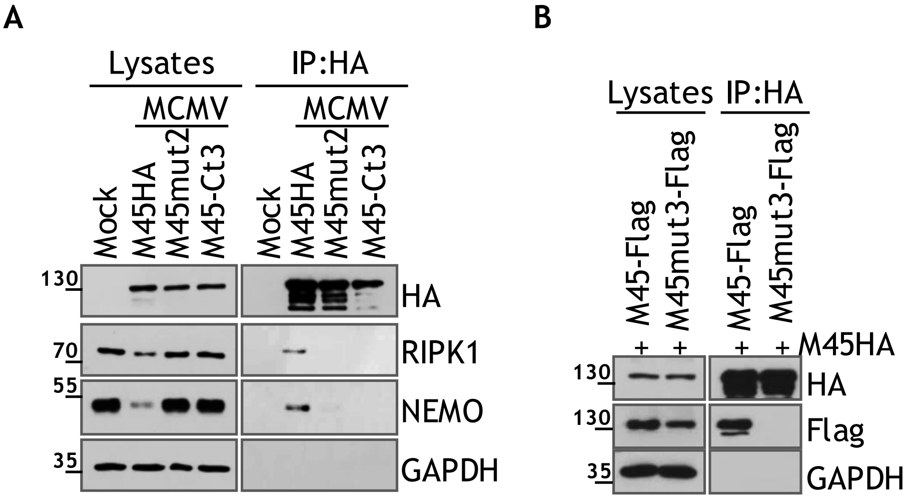
A
Lysates
IP:HA
MCMV
MCMV
Mock
M45HA
M45mut2
M45-Ct3
Mock
M45HA
M45mut2
M45-Ct3
130
HA
70
RIPK1
55
NEMO
35
GAPDH
B
Lysates
IP:HA
M45-Flag
M45mut3-Flag
M45-Flag
M45mut3-Flag
+
+
+
+
M45HA
130
HA
130
Flag
35
GAPDH

Figure 24. M45 IPAM mutant does not co-precipitates with M45, NEMO, or RIPK1
(A) NIH-3T3 cells were infected with MCMV (MOI 3 $TCID_{50}$), and HA-tagged M45 was immunoprecipitated from whole cell lysates; **(B)** HEK-293A cells were co-transfected with plasmids expressing wild type M45HA and wild type or mutant M45-Flag. HA-tagged M45 was immunoprecipitated.

5.6 The IPAM is required for inhibition of necroptosis and viral dissemination *in vivo*

To test whether the IPAM is also required for the inhibition of necroptosis by M45, SVEC4-10 endothelial cells, which are highly sensitive to viral-induced necroptosis [151-153], were infected with wild type as well as M45 mutants (Figure 19A and 25A). Cell viability was measured 24 hpi by quantifying the ATP levels, which indicates the presence of metabolically active, and indeed alive, cells.

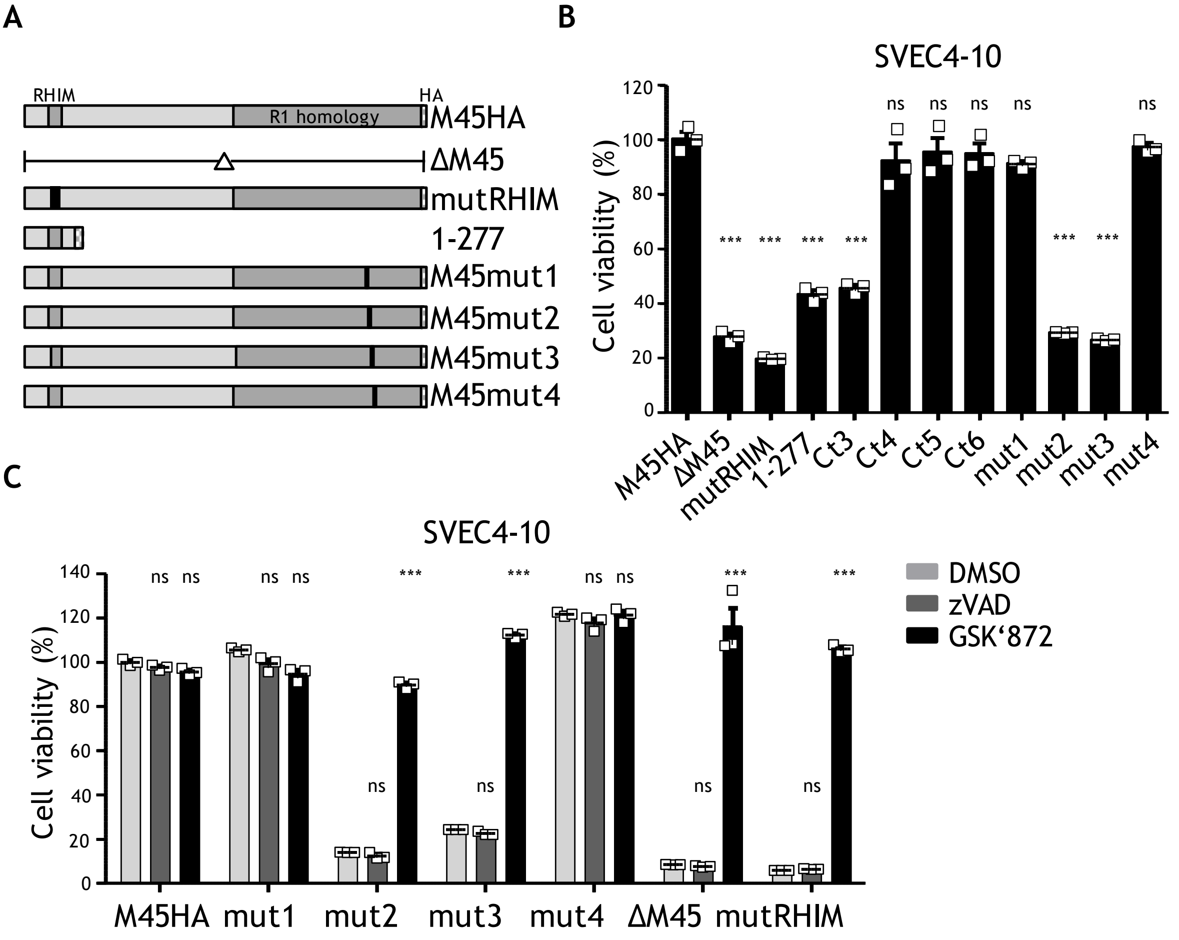

Figure 25. Cell viability assays upon MCMV WT and mutants infection.
(A) Schematic representation of M45 mutants used in B and C; **(B)** SVEC4-10 cells were infected with MCMV expressing WT or mutant M45 (MOI 5 $TCID_{50}$). 24 hpi cell viability was measured with an ATP assay. Data were normalized to the viability of MCMV-M45HA infected cells. Significant differences relative to MCMV-M45HA are indicated. Significance was calculated by one-way ANOVA with Bonferroni post hoc test. Means±SEM of triplicates are shown. ns, not significant, $P>0.05$; ***, $P<0.001$; **(C)** SVEC4-10 cells were infected as in B and treated with a caspase inhibitor (Z-VAD-FMK, 50 µM), a RIPK3 inhibitor (GSK'872, 5 µM), or carrier (DMSO, 0.1%). Cell viability was determined as in B. Significant differences of inhibitor-treated relative to DMSO-treated cells are indicated. Significance was calculated by one-way ANOVA with Bonferroni post hoc test. ns, not significant, $P>0.05$;

***, P<0.001.

As shown in figure 25B, the viability of MCMV-infected cells was significant reduced when M45 was deleted (ΔM45), when the RHIM domain was mutated (mutRHIM), as well as when only the N-terminus was expressed (1-227). However, the C-terminal part of M45 (aa 1122-1137) and particularly an intact IPAM domain (mutated in M45mut2 and mut3) was necessary to preserve the viability of infected cells (Figure 25B). In contrast, SVEC4-10 infection with MCMV mutants carrying variations outside the RHIM or IPAM domains of M45 (e.g. MCMV-M45Ct4HA, MCMV-M45Ct5HA, MCMV-M45Ct6HA, MCMV-M45mut1-HA and MCMV-M45mut4-HA) did not lead to reduced cell viability. In order to confirm that the observed cell death occurred by necroptosis rather than apoptosis, the same assay was performed in the presence of the pan-caspase inhibitor zVAD-fmk or the RIPK3 inhibitor GSK'872, selective inhibitors of apoptosis or necroptosis, respectively. As shown in Figure 25C, cell death induced by MCMV infection in the absence of M45 or in the presence of RHIM and IPAM domain mutants (MCMV-ΔM45, MCMV-M45mut2-HA, MCMV-M45mut3-HA and MCMV-M45mutRHIM) was rescued by the addition of a RIPK3 inhibitor but not of a pan-caspase inhibitor, thus confirming that the mechanism of SVEC4-10 cell death was necroptosis. In summary, inhibition of necroptosis by M45 requires both the RHIM and the IPAM motifs.

Since necroptosis plays a crucial role in restraining MCMV replication in mice when M45 is not expressed or the RHIM domain is mutated [150, 153], the role of IPAM was also tested *in vivo*. C57BL/6 WT mice were infected intraperitoneally with MCMV-M45HA, MCMV-M45mut2-HA, and MCMV-M45mutRHIM, and viral titers in the spleen were measured three days post infection (Figure 26) (*in vivo* experiment performed in collaboration with Eleonore Ostermann [HPI]). To prevent Ly49H-mediated NK cell activation in C57BL/6 mice, as previously described, all viruses used for in vivo experiments were also deleted for m157 [167, 168]. As expected, MCMV-M45HA replicated to high titers in the spleen while MCMV-M45mut2-HA and MCMV-M45mutRHIM titers remained below the detection limit. In infected RIPK3 kinase-dead C57BL/6 *Rip3*$_{K51A/K51A}$ mice, which cannot activate necroptosis [169], MCMV-M45mutRHIM replicated to similar titers as MCMV-M45HA, but the replication defect of MCMV-M45mut2-HA was only partially rescued (Figure 26). These data suggest that the IPAM domain has a similar biological relevance as the RHIM domain in the context of necroptosis. Moreover the replication defect of the IPAM mutant observed in the RIPK3 kinase-dead mice might be explained by the fact that this virus is unable to interact with NEMO and thus can no longer block NEMO-dependent NF-kB activation (Figure 24A).

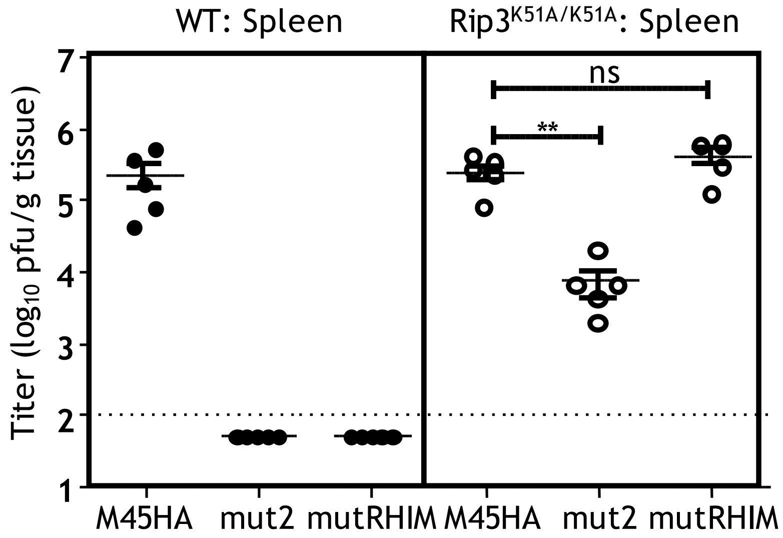

Figure 26. Viral dissemination upon MCMV WT and mutant infection.
C57BL/6 WT and Rip3 kinase-dead (K51A) mice were infected intraperitoneally with 10^5 PFU of MCMV-M45HA, MCMV-M45mut2-HA, and MCMV-M45mutRHIM. Sample size n: WT = 5; K51A = 5. Viral titers in the spleen were determined 3 days post infection. Significance was calculated by two-tailed Mann-Whitney test. ns, not significant, $P>0.05$; **, $P<0.01$

5.7 M45 interacts with the retromer component VPS26B

M45 induces the accumulation of NEMO and RIPK1 as insoluble aggregates in autophagy-deficient but not in autophagy-competent cells (Figure 11), thus suggesting that M45 aggregates might be rapidly degraded by autophagy. As M45 does not contain a canonical LC3-interacting region (LIR), one hypothesis is that the interaction of M45 with the autophagosomes is indirect and requires the recruitment of LIR-containing adaptor proteins.

In an attempt to identify additional M45-interacting proteins, an affinity purification and mass spectrometry (AP-MS) analysis combined with stable isotope labelling of amino acid in cell culture (SILAC) was performed in NIH-3T3 fibroblasts infected with MCMV-M45HA or an untagged control virus (in collaboration with Eva Krause [HPI] and Stefan Loroch [Leibniz-Institut für Analytische Wissenschaften (ISAS), Dortmund]). As shown in Table 1, the already known M45-interacting proteins RIPK1 and NEMO were among the top hits of the AP-MS screen. Interestingly, the vacuolar protein sorting proteins (VPS) 26B and 35 co-purified with M45. Moreover, another VPS protein, VPS29, was identified only in the labeled sample.

Table 1. Proteins co-purifying with M45 detected by IP-MS.
SILAC IP-MS analysis of NIH-3T3 cells infected with MCMV WT or with MCMV HA tagged M45 (15 hpi).

Protein Name	Uniprot	Unique peptides	Normalization	Log_2 enrichment
M45	Q06A28	56	14,8	3,8
VPS26B	Q8C0E2	3	14,7	3,8
VPS35	Q9EQH3	6	12,8	3,6
RIPK1	Q60855	4	10,0	3,3
NEMO	O88522	3	8,5	3,1
Ipo9	Q91YE6	6	8,3	3,0
m141	A8E1Q6	2	6,9	2,7
m139	A8E1Q4	6	5,2	2,3
m138	A8E1Q3	1	4,4	2,1
M83	A8E1K1	3	4,1	2,0
m140	A8E1Q5	2	3,6	1,8
LIMA1	Q9ERG0	4	2,8	1,5
14-3-3γ	P61982	2	2,3	1,2
HNRPF	Q9Z2X1	3	2,2	1,1
NUP93	Q8BJ71	2	2,1	1,0
ADT2	P51881	3	2,0	1,0
VPS29	Q9QZ88	3	n.a.	n.a.

The interaction between M45 and retromer components VPS26B, VPS35 and VPS29 was then verified by co-immunoprecipitation in NIH-3T3 fibroblasts infected with MCMV expressing either HA-tagged full-length M45 or the truncated M45-Ct3 proteins. VPS26A, the paralog of VPS26B, was used as negative control. Indeed, 15 hpi VPS35, VPS29, and VPS26B (but not VPS26A) co-precipitated with M45 (Figure 27A), thus confirming the results of the AP-MS screen.

To test whether M45 interacts with each of the three retromer components upon transfection, HA-tagged M45 and myc-tagged versions of VPS26B, VPS29, VPS35, or RIPK1 were co-transfected into HEK-293A cells for 24 hours. Under these conditions, RIPK1 (positive control) and VPS26B co-precipitated with M45, but VPS29 and VPS35 did not, suggesting that M45 binds to VPS26B and interacts indirectly with VPS35 and VPS29 via VPS26B (Figure 27B).

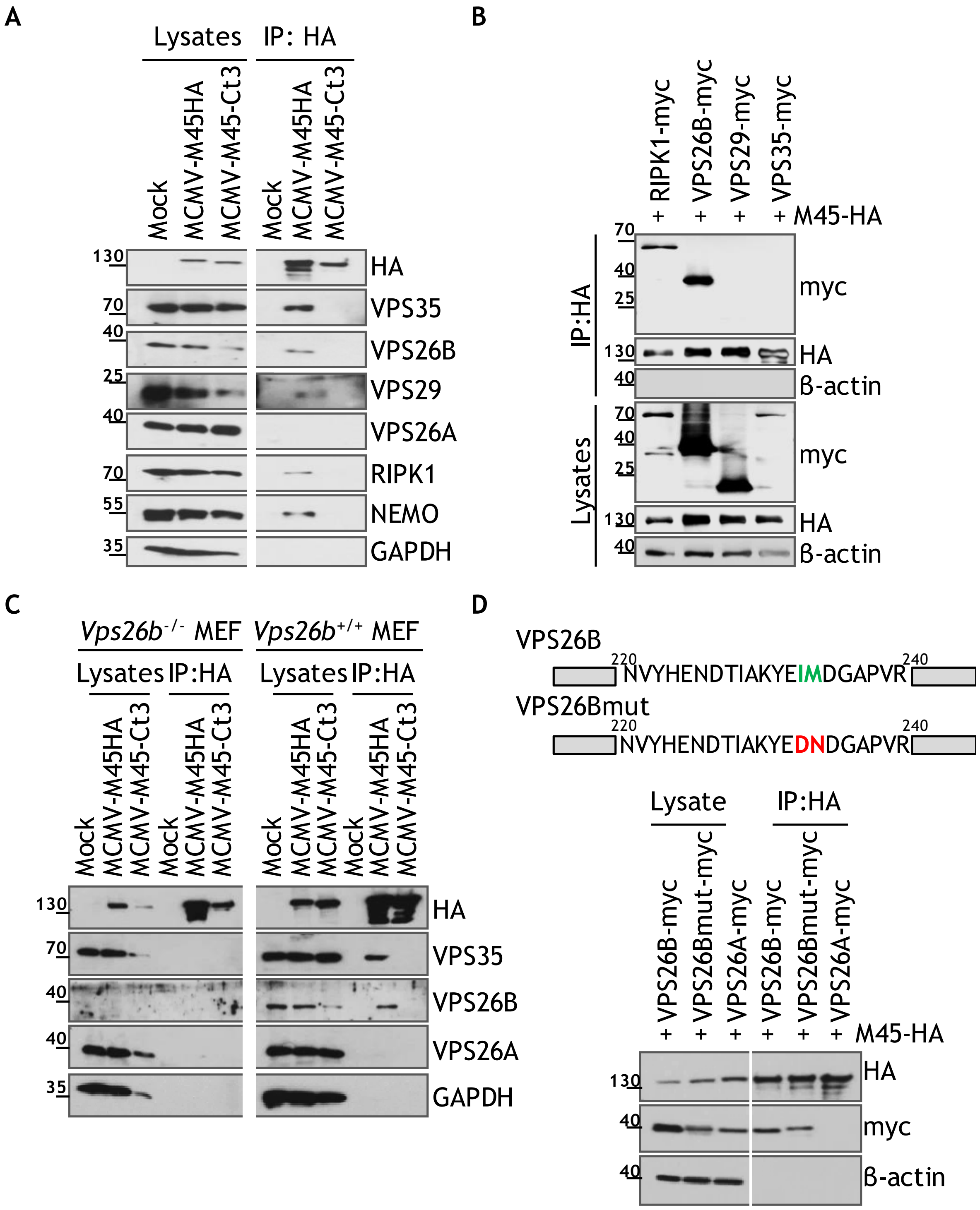
A
Lysates
IP: HA
Mock
MCMV-M45HA
MCMV-M45-Ct3
Mock
MCMV-M45HA
MCMV-M45-Ct3
130
HA
70
VPS35
40
VPS26B
25
VPS29
40
VPS26A
70
RIPK1
55
NEMO
35
GAPDH
B
+ RIPK1-myc
+ VPS26B-myc
+ VPS29-myc
+ VPS35-myc
+ M45-HA
IP:HA
Lysates
70
40
25
myc
130
HA
40
ß-actin
70
40
25
myc
130
HA
40
ß-actin
C
Vps26b-/- MEF
Vps26b+/+ MEF
Lysates
IP:HA
Lysates
IP:HA
Mock
MCMV-M45HA
MCMV-M45-Ct3
Mock
MCMV-M45HA
MCMV-M45-Ct3
Mock
MCMV-M45HA
MCMV-M45-Ct3
Mock
MCMV-M45HA
MCMV-M45-Ct3
130
HA
70
VPS35
40
VPS26B
40
VPS26A
35
GAPDH
D
VPS26B
220
NVYHENDTIAKYEIMDGAPVR
240
VPS26Bmut
220
NVYHENDTIAKYEDNDGAPVR
240
Lysate
IP:HA
+ VPS26B-myc
+ VPS26Bmut-myc
+ VPS26A-myc
+ VPS26B-myc
+ VPS26Bmut-myc
+ VPS26A-myc
+ M45-HA
130
HA
40
myc
40
ß-actin

Figure 27. M45 binding with the retromer component VPS26B.
(A) NIH-3T3 cells were infected with MCMV-M45HA or MCMV-M45Ct3HA (MOI 3 $TCID_{50}$). At 15 hpi, levels of the proteins of interest were analyzed in total cell lysates as well as in HA- immunoprecipitates; **(B)** HEK-293A cells were co-transfected with plasmids expressing M45-HA and either myc-tagged retromer components or myc-tagged RIPK1. At 24 hours post transfection, HA-tagged M45 was immunoprecipitated and the presence of the indicated proteins was assessed by immunoblot; **(C)** *Vps26b*$_{+/+}$ and *Vps26b*$_{-/-}$ MEFs were infected with MCMV-M45HA and MCMV-M45Ct3. At 15 hpi, levels of the proteins of interest were analyzed in total cell lysates as well as in HA-immunoprecipitates obtained from the two cell types; **(D)** HEK-293A cells were co-transfected with plasmids expressing M45-HA and myc-tagged VPS26B wildtype or VPS26B mutant or VPS26A. M45-HA was

immunoprecipitated. This data **(B)** was generated by Rebekka Schmitz, HPI.

To confirm this observation, WT and *Vps26b*-/- fibroblasts were infected for 15 hrs with MCMV-M45HA or MCMV-M45Ct3HA and tested again by immunoprecipitation combined with immunoblot analysis. As shown in Figure 27C, VPS35 co-precipitated with M45 only in the presence of VPS26B.

To test whether M45 binding to VPS26B was dependent on its recruitment to the retromer-complex, a previously described mutant VPS26B protein, which fails to form this complex due to a mutated VPS35 binding site [170] (Figure 27D), was co-transfected with M45 (HA-tagged) in HEK-293A cells. Immunoprecipitation and immunoblot analyses performed 24 hrs post transfection confirmed that M45 interacts with both WT and mutant VPS26B but not with VPS26A (negative control), indicating that the M45–VPS26B interaction is independent of retromer assembly.

5.8 M45 benefits from VPS26B to promote NEMO degradation

As extensively shown, M45 downregulates NEMO and RIPK1 protein levels in MCMV-infected cells. In order to test whether VPS26B was affected in a similar way, NIH-3T3 stably expressing a myc-tagged VPS26B were infected with MCMV-M45HA or MCMV-ΔM45, and VPS26B expression over time was investigated by immunoblot. As shown in Figure 28A, indeed M45 expression led to a downregulation of VPS26B levels (Figure 28A). In contrast to VPS26B, the levels of other retromer components (VPS35, VPS29, and VPS26A) were not reduced upon MCMV infection (Figure 28B).

Since NEMO and RIPK1 are degraded by M45 in an autophagy-dependent manner, I tested whether autophagy also plays a role in VPS26B degradation. To do this, *Atg5*-/- MEFs were infected with MCMV-M45HA, the whole cell lysates were harvested at different times post infection and analyzed by immunoblot. Indeed, VPS26B was not downregulated in *Atg5*-/- MEFs (Figure 28C), suggesting that the progressive loss of VPS26B is due to its autophagic degradation in the presence of M45.

To test whether VPS26B has a role in the degradation of NEMO, WT and *Vps26b*-/- MEFs were MCMV infected prior to analysis of NEMO levels at different times post infection. In order to detect both soluble as well as insoluble NEMO, cells were lysed and boiled in 2x SDS-PAGE sample buffer. This lysis buffer is a stronger denaturing condition than 1% NP-40 lysis buffer used in the first part of the results section. Indeed, NEMO degradation was impaired in the absence of VPS26B (Figure 28D), suggesting that VPS26B contributes to NEMO degradation.

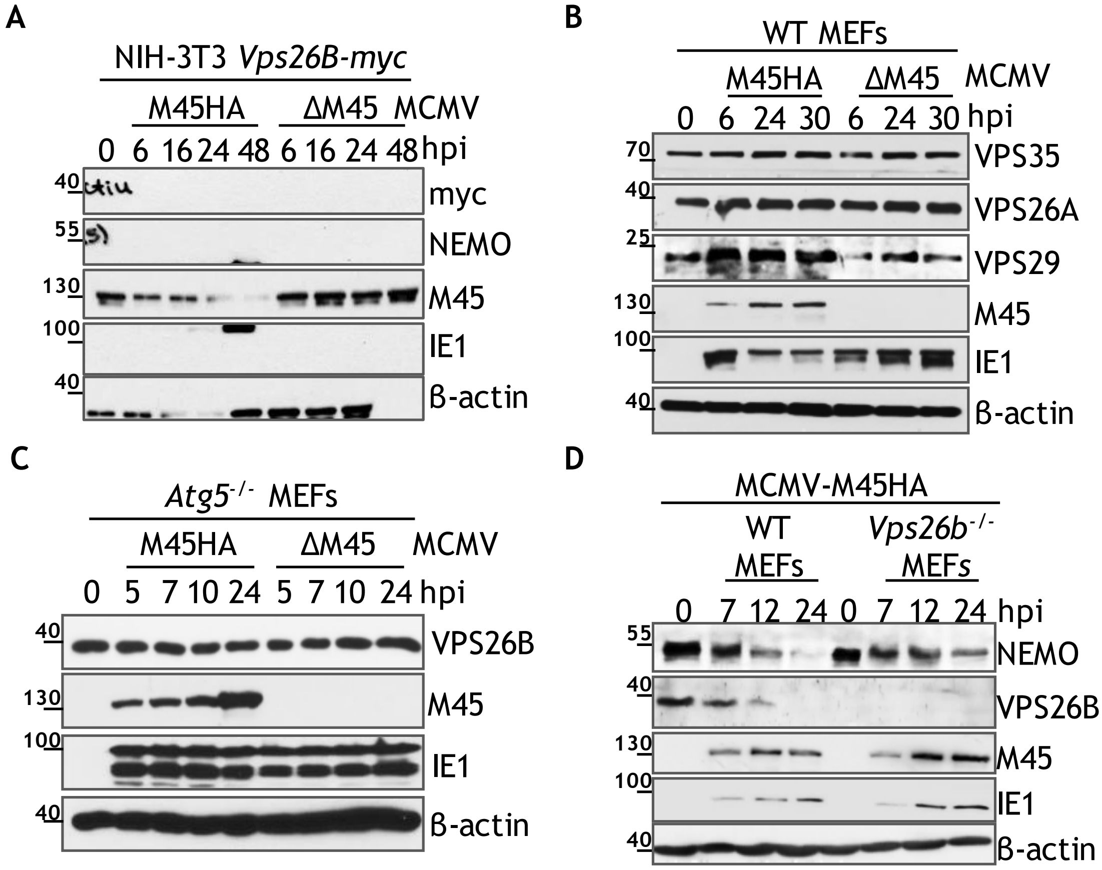
A
NIH-3T3 Vps26B-myc
M45HA
ΔM45
MCMV
0 6 16 24 48 6 16 24 48 hpi
40
55
130
100
40
myc
NEMO
M45
IE1
ß-actin
B
WT MEFs
M45HA
ΔM45
MCMV
0 6 24 30 6 24 30 hpi
70
40
25
130
100
40
VPS35
VPS26A
VPS29
M45
IE1
ß-actin
C
Atg5-/- MEFs
M45HA
ΔM45
MCMV
0 5 7 10 24 5 7 10 24 hpi
40
130
100
40
VPS26B
M45
IE1
ß-actin
D
MCMV-M45HA
WT MEFs
Vps26b-/- MEFs
0 7 12 24 0 7 12 24 hpi
55
40
130
100
40
NEMO
VPS26B
M45
IE1
ß-actin

Figure 28. VPS26B role in NEMO degradation upon MCMV infection.
(A) NIH-3T3 cells stably expressing myc-tagged VPS26B infected with MCMV-M45HA or MCMVΔM45 (MOI 5 $TCID_{50}$). VPS26B, NEMO, and MCMV M45 and IE1 levels were determined between 0 and 48 hpi by immunoblot. **(B)** MEFs infected with MCMV-M45HA or MCMV-ΔM45 (MOI 3 $TCID_{50}$). VPS35, VPS26A, VPS29, and viral protein levels were determined by immunoblot at the indicated times post infection. **(C)** *Atg5*-/- MEFs infected with MCMV-M45HA or MCMVΔM45 (MOI 5 $TCID_{50}$). Whole cell lysates were collected over the indicated time period and analyzed by immunoblot. **(D)** WT and *Vps26b*-/- MEFs infected with MCMV-M45HA (MOI 5 $TCID_{50}$). NEMO and VPS26B levels were detected at different times post infection by immunoblot.

5.9 TBC1D5 is required as an autophagy adaptor to redirect NEMO to autophagosomes

VPS26B does not possess a LIR motif, which is important for the binding to LC3 and other ATG8-family proteins [171]. However, it might use an adaptor protein to tether M45 and associated proteins to the autophagosomes. The most likely candidate was the Rab GTPase-activating protein TBC1D5 as it interacts with

VPS26B [116] and contains two LIR motifs [113]. In order to verify a possible role of TBC1D5 in M45-mediated NEMO degradation, TBC1D5-deficient MEFs were generated by CRISPR/Cas9 gene editing. The success of the technique was verified by immunoblot. Four cell clones showed either incomplete (g1 and g2) or complete (g3 and g4) loss of TBC1D5 expression (Figure 29A). Two of these clones, g2 and g4, were used to test whether TBC1D5 is involved in NEMO degradation. Cells were infected with MCMV-M45HA and NEMO levels in whole cell lysates were analyzed at different times post infection.

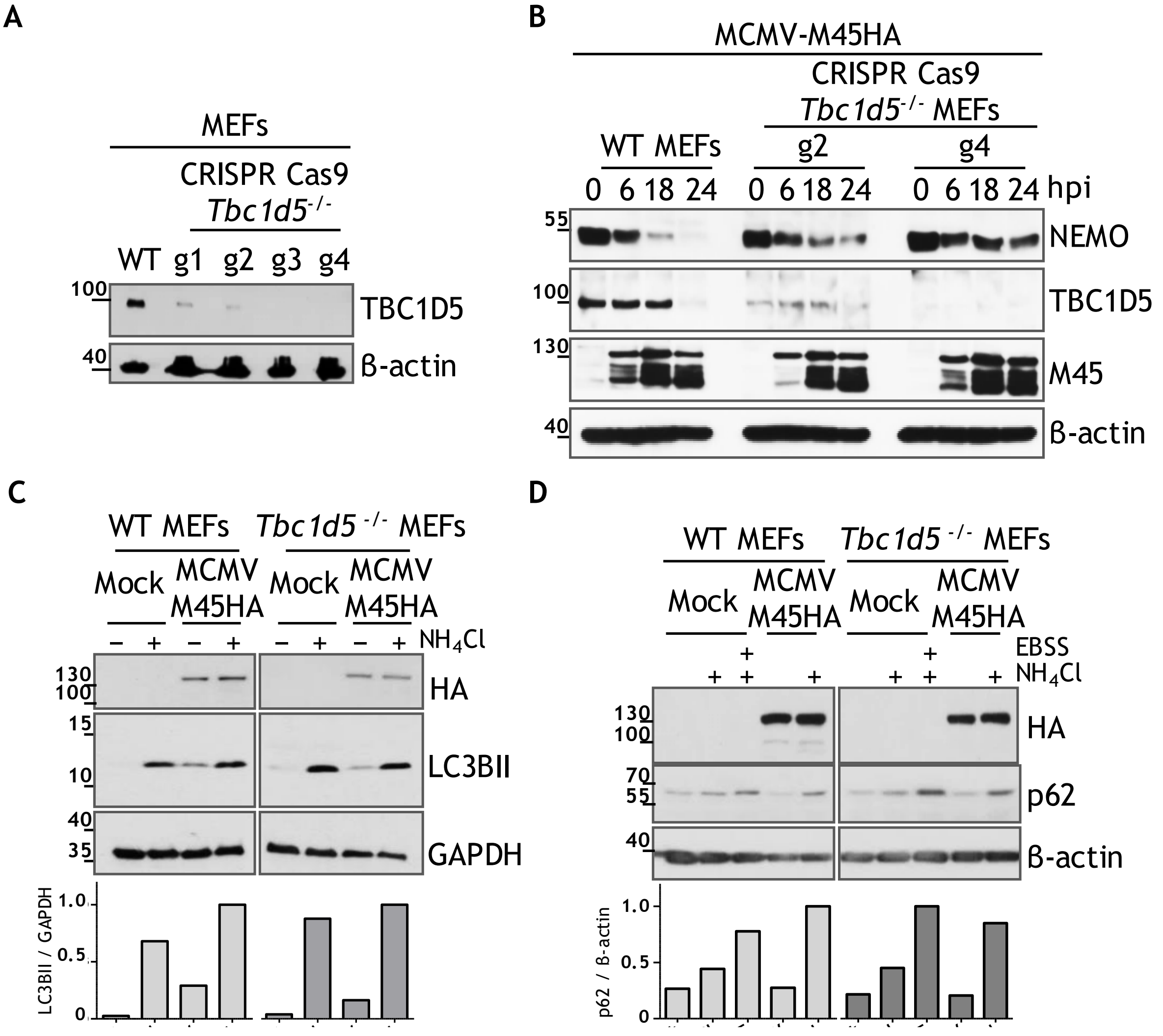

Figure 29. TBC1D5 role in NEMO degradation upon MCMV infection.
TBC1D5-deficient MEF clones generated by CRISPR/Cas9 gene editing using four different gRNAs; **(B)** WT and TBC1D5-deficient MEFs (g2, incomplete knockout; g4, complete knockout) infected with MCMV-M45HA. NEMO and TBC1D5 levels were detected at different times post infection; **(C)** Immunoblot of WT and Tbc1d5-/- MEFs infected with MCMV-M45HA (MOI 5 $TCID_{50}$) for 24 hrs. Cells were treated for 3 h with 10 mM of NH4Cl or left untreated. LC3BII levels were normalized to GAPDH; **(D)** Immunoblot of WT and Tbc1d5-/- MEFs infected with MCMV-M45HA (MOI 5 $TCID_{50}$). Cells were treated for 3 h with 10 mM of NH_4Cl and EBSS or left untreated. p62 levels were normalized to ß-actin. These

data (**A, B**) were generated by Matteo Rizzato as described in his master thesis.

As shown in Figure 29B, MCMV-induced NEMO degradation was strongly attenuated in TBC1D5-deficient MEFs, indicating that TBC1D5 is indeed involved in the degradation of NEMO. It was also observed that in WT MEFs, TBC1D5 levels were reduced at late times post infection (Figure 29B), suggesting that TBC1D5 is degraded as is known to occur with other autophagy adaptor proteins [172].

As TBC1D5 plays a role in ATG9 trafficking [97], I tested whether the reduced NEMO degradation observed in the *Tbc1d5*$_{-/-}$ MEFs might be caused by an impaired autophagic flux. The levels of the autophagy markers p62/SQSTM1 and LC3BII were therefore monitored in MCMV-infected WT and *Tbc1d5*$_{-/-}$ MEFs in the presence or in the absence of NH_4Cl treatment (Figures 29C) at 24 hpi. Moreover, p62 flux was monitored in both cell lines by incubating the cells for 3 hrs with a starvation inducing media (EBSS) in combination with NH_4Cl (Figures 29D). LC3BII and p62 levels were similar in both cell types in the stimulated samples, indicating that autophagic flux is preserved.

M45-dependent NEMO degradation was more attenuated in *Tbc1d5*$_{-/-}$ MEFs than in *Vps26B*$_{-/-}$ MEFs suggesting that M45 could uses both VPS26B-TBC1D5 complex and TBC1D5 alone. In order to test whether M45 interacts with TBC1D5, HEK-293A were co-transfected with plasmids encoding HA tagged M45 and either Flag tagged TBC1D5, Flag tagged NEMO (positive control) or Flag tagged IFI16 (negative control). 24 hours post transfection, HA was immunoprecipitated and samples were analyzed by immunoblot. Indeed, TBC1D5 co-precipitated with M45 (Figure 30A).

The same experiment was repeated by using the M45 mutants described in Figure 19, and the immunoblots showed that a short C-terminal sequence of M45 is required for the interaction with TBC1D5 (Figure 30B). Moreover, WT and *Vps26b*$_{-/-}$ MEFs were infected with MCMV-M45HA, and 20 hpi HA was immunoprecipitated to test whether VPS26B is required for this interaction. As shown in figure 30C, the interaction between M45 and TBC1D5 occurred even in the absence of VPS26B.

Collectively, these data (Figures 28, 29 and 30) show that M45 recruits VPS26B and TBC1D5 to promote the degradation of aggregates by selective autophagy.

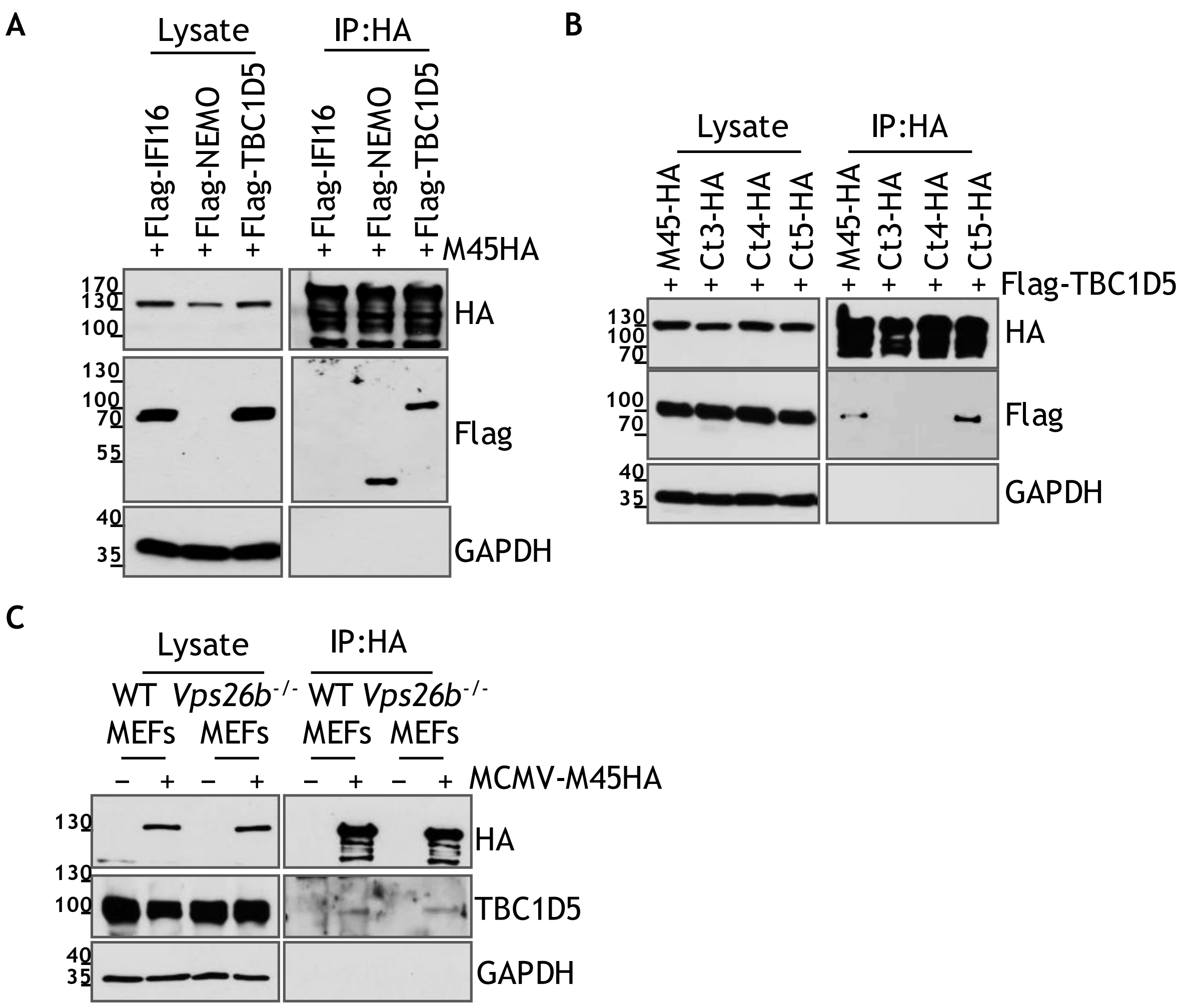
A
Lysate
IP:HA
+Flag-IFI16
+Flag-NEMO
+Flag-TBC1D5
+Flag-IFI16
+Flag-NEMO
+Flag-TBC1D5
+M45HA
170
130
100
HA
130
100
70
55
Flag
40
35
GAPDH
B
Lysate
IP:HA
+M45-HA
+Ct3-HA
+Ct4-HA
+Ct5-HA
+M45-HA
+Ct3-HA
+Ct4-HA
+Ct5-HA
+ + + + + + + + Flag-TBC1D5
130
100
70
HA
100
70
Flag
40
35
GAPDH
C
Lysate
IP:HA
WT MEFs
Vps26b-/- MEFs
WT MEFs
Vps26b-/- MEFs
– + – + – + – + MCMV-M45HA
130
HA
130
100
TBC1D5
40
35
GAPDH

Figure 30. M45 binding to TBC1D5.
(A) HEK-293A cells co-transfected with plasmids expressing M45-HA and either Flag-mTBC1D5 or Flag-IFI16 or Flag-mNEMO. HA was immunoprecipitated; **(B)** HEK-293A cells were co-transfected with plasmids expressing M45-HA full length or C-terminus truncation mutants (HA tagged) and Flag-mTBC1D5. HA was immunoprecipitated; **(C)** WT and Vps26b-/- MEFs infected with MCMV-M45HA (MOI 3). HA was immunoprecipitated 20 hpi.

5.10 Induced protein aggregation and selective autophagy are conserved in HSV-1 ICP6

Since M45 has homologs in all herpesviruses [173], the amino acid sequences of the C-terminal parts of M45 and its homologs were aligned in order to determine whether the M45 IPAM is conserved. Indeed, highly similar motifs were found not only in MCMV's closest relatives (two rat CMV species), but also in other human pathogenic herpesviruses: Herpes Simplex Virus type 1 (HSV-1), HSV-2, Epstein-Barr virus (EBV), and Kaposi Sarcoma-associated Herpesvirus (KSHV). The IPAM consensus sequence is P-F/Y-V-D-H/Q (Figure 31A).

HSV-1 ICP6 shares many functional similarities with MCMV M45. It carries a RHIM in its N-terminus [173], interacts with RIPK1, and inhibits necroptosis [159, 174, 175]. However, ICP6 differs from M45 in that it does not interact with NEMO, as proven by co-expressing Flag tagged NEMO and HA tagged ICP6 plasmids in HEK-293A cells and performing immunoprecipitation of HA 24 hours post transfection (Figure 31B). Thus, in order to test whether HSV-1 infection induces the accumulation of RIPK1 in the detergent-insoluble fraction, Human Foreskin Fibroblasts (HFF) were infected with HSV-1. The detergent soluble (S) and insoluble (I) fractions were collected at 30 hours post infection and analyzed by immunoblot (Figure 31C). Indeed, insoluble RIPK1, but not insoluble NEMO, was detected in HSV-1-infected fibroblasts.

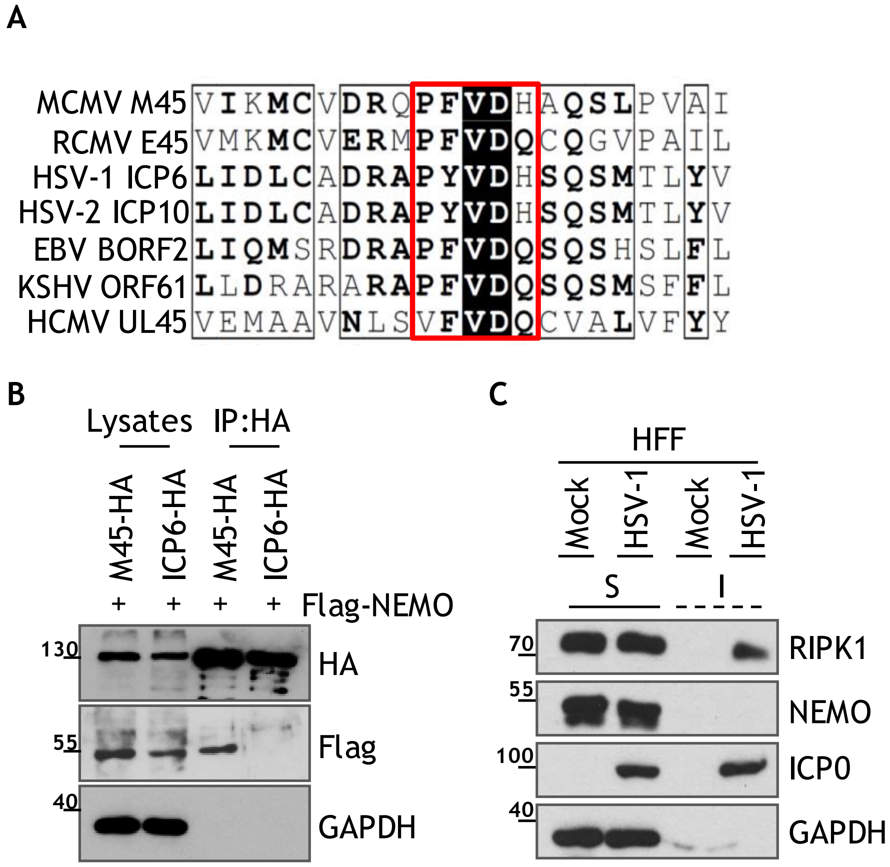
A
MCMV M45 VIKMCVDRQPFVDHAQSLPVAI
RCMV E45 VMKMCVERMPFVDQCQGVPAIL
HSV-1 ICP6 LIDLCADRAPYVDHSQSMTLYV
HSV-2 ICP10 LIDLCADRAPYVDHSQSMTLYV
EBV BORF2 LIQMSRDRAPFVDQSQSHSLFL
KSHV ORF61 LLDRARARAPFVDQSQSMSFFL
HCMV UL45 VEMAAVNLSVFVDQCVALVFYY
B
Lysates
IP:HA
M45-HA
ICP6-HA
M45-HA
ICP6-HA
+ + + + Flag-NEMO
130
HA
55
Flag
40
GAPDH
C
HFF
Mock
HSV-1
Mock
HSV-1
S
I
70
RIPK1
55
NEMO
100
ICP0
40
GAPDH

Figure 31. Conservation of the IPAM.
(A) Conservation of the IPAM (red box) in M45 homologs of selected herpesviruses; **(B)** HEK-293A cells co-transfected with Flag-NEMO and M45-HA or ICP6-HA plasmids. HA-tagged proteins were immunoprecipitated; **(C)** HFF cells mock-infected or infected with HSV-1 (MOI 1). Proteins were detected at 30 hpi in the detergent-soluble (S) and insoluble (I) fractions.

To confirm that the ICP6 IPAM was responsible for the observed accumulation of RIPK1 in the insoluble fraction and also for aggregate formation, a PYVDH-to-PAAAA mutation was introduced into an ICP6 expression plasmid HA tagged (Figure 32A). Wildtype and mutant ICP6 (ICP6mut) expression plasmids were transfected into NIH-3T3 cells. 24 hours post transfection cells were fixed and then stained with HA, for ICP6 WT and mutant, and with ProteoStat Red dye for aggregates (Figure 32B). Cells were then observed by a confocal microscope and HA and ProteoStat-positive dots were quantified (Figure 32C).

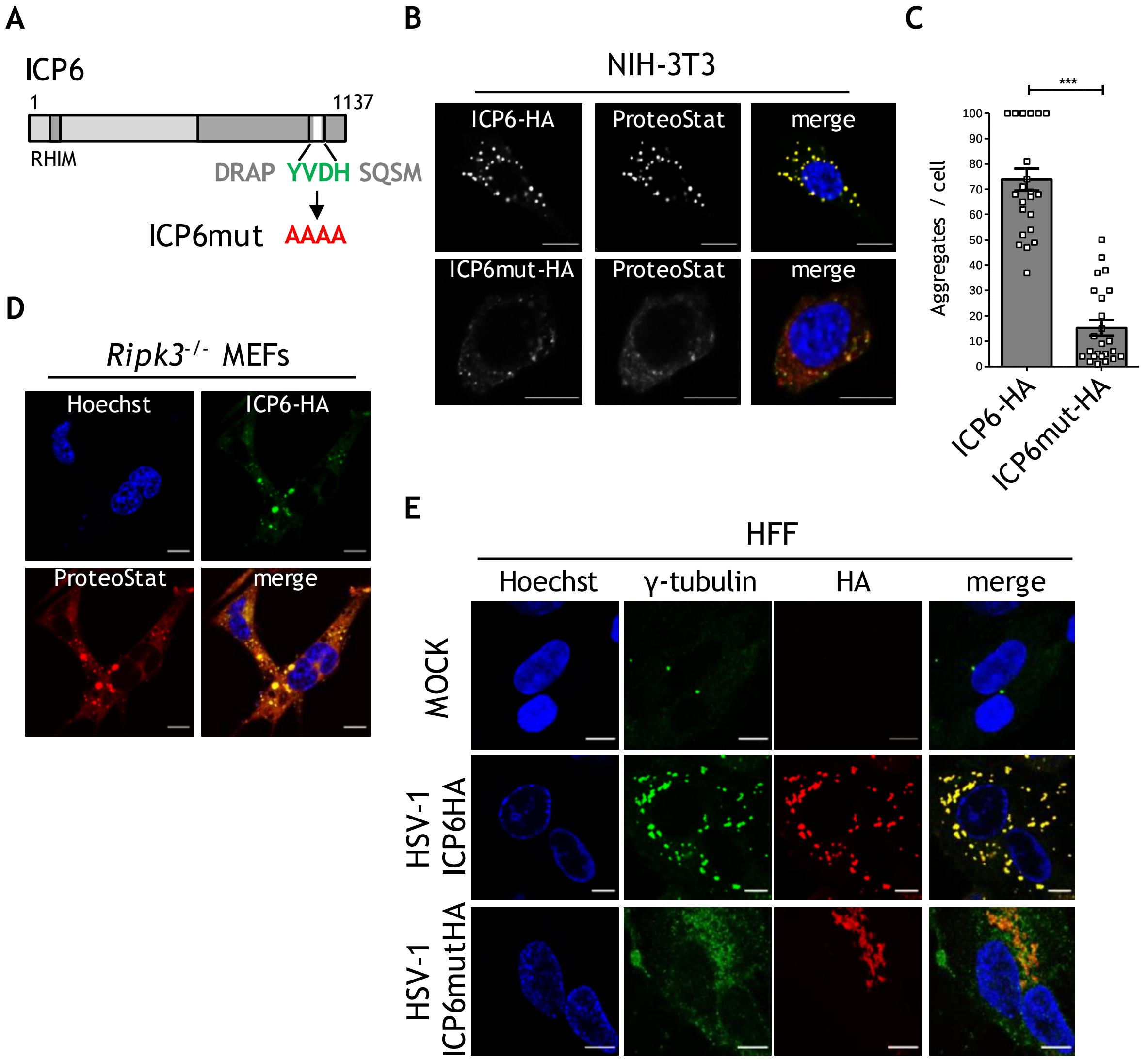
A
ICP6
1
1137
RHIM
DRAP YVDH SQSM
ICP6mut AAAA
B
NIH-3T3
ICP6-HA
ProteoStat
merge
ICP6mut-HA
ProteoStat
merge
C
***
Aggregates / cell
100
90
80
70
60
50
40
30
20
10
0
ICP6-HA
ICP6mut-HA
D
Ripk3-/- MEFs
Hoechst
ICP6-HA
ProteoStat
merge
E
HFF
Hoechst
γ-tubulin
HA
merge
MOCK
HSV-1 ICP6HA
HSV-1 ICP6mutHA

Figure 32. Conserved aggregate function of the IPAM in HSV-1 ICP6.
(A) Schematic representation of the ICP6 alanine substitution mutant (ICP6mut); **(B)** NIH-3T3 transfected with plasmids expressing HA-tagged WT or mutant ICP6. 24 h post transfection aggregates were stained with the ProteoStat dye (red) and ICP6 with HA (green); **(C)** ICP6 and ProteoStat-positive dots (up to 100 per cell) were counted in 24 cells each using z-stacks and maximum intensity projection. Significance was calculated by two-tailed t-test. Means ± SEM are shown. ***, P<0.001; **(D)** *Ripk3*$_{-/-}$ fibroblasts transfected with plasmids expressing WT or mutant ICP6. 24 h post transfection protein aggregates were detected by using the ProteoStat dye (red) and HA-tagged ICP6 by immunofluorescence (green); **(E)** HFF infected with HSV-1 ICP6HA or ICP6mutHA (MOI 1). 24 hpi, cells were fixed and stained for gamma-tubulin (green) and HA (red).

Nuclei were stained with Hoechst 33342. Scale bar, 10 µm.

Since the expression of WT ICP6 in fibroblasts caused the formation of more aggregates than the expression of ICP6mut (Figure 32B and 32C), I could confirm that the IPAM of ICP6 plays a similar role as the IPAM of M45 in the formation of protein aggregates.

Next, I tested whether necroptosis was involved in the ICP6-driven accumulation of ProteoStat positive aggregates. Indeed, while it has been previously reported that HSV-1 ICP6 protects human cells from necroptosis, in murine cells the opposite effect has been detected [159, 174, 175]. When the assay of Figure 32B was repeated in necroptosis incompetent *Ripk3*$_{-/-}$ cells (Figure 32D), expression of ICP6 led to the formation of aggregates thus ruling out any contribution of necroptosis to the formation of ICP6 aggregates.

To confirm the results obtained in transfected murine cells in infected human cells, recombinant HSV-1 carrying a mutation in the IPAM motif of ICP6 with or without a HA-tag (Figure 32A) were constructed by *en passant* BAC mutagenesis.

The HA-tagged virus was used to infect HFF and to investigate the localization of ICP6 by immunofluorescence. 24 hpi, the cells were fixed and stained for HA and for γ-tubulin, a known marker for aggregates [176]. As shown in Figure 32E, ICP6 wildtype appeared as puncta in the cytoplasm and co-localized with γ-tubulin while the IPAM mutant did not. On the other hand, the untagged virus was used to infect HFF and analyze the distribution of RIPK1 in the detergent soluble (S) or insoluble (I) fractions by immunoblot. As shown in Figure 33A, RIPK1 was detected in the insoluble fraction of HFF when the IPAM motif was intact but not in cells infected with the mutant virus. Moreover, the treatment of infected fibroblasts with the lysosomal acidification inhibitor ammonium chloride (NH_4Cl) increased the levels of insoluble RIPK1 in WT HSV-1-infected cells (Figure 33B), indicating that insoluble RIPK1 is degraded in lysosomes.

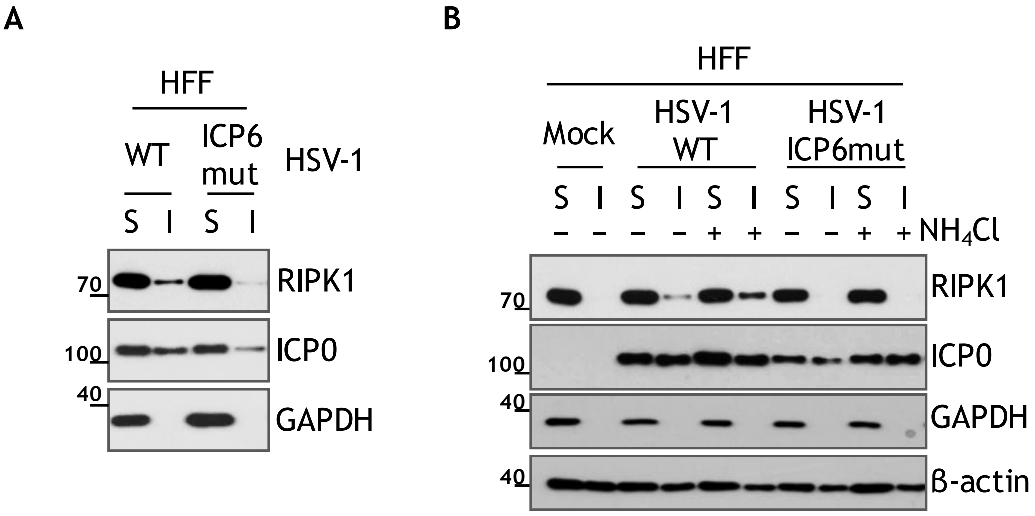

Figure 33. Accumulation of RIPK1 in the insoluble fraction upon HSV-1 infection. **(A)** Immunoblot analysis of the S and I fractions (30 hpi) of HSV-1 WT and ICP6mut-infected HFFs (MOI 1); **(B)** HFF cells infected with WT and ICP6mut HSV-1 (MOI 3). 24 hpi, cells were treated for 6 h with NH_4Cl (10 mM) or left untreated. Proteins in the soluble (S) and insoluble (I) fractions were detected by immunoblot.

To further assess the functional similarities between M45 and ICP6, after testing the formation of RIPK1 aggregates we investigated the roles played by the retromer complex protein VPS26B. HEK-293A cells were co-transfected with a plasmid encoding HA-tagged ICP6 (ICP6-HA) and either myc-tagged VPS26B or VPS26A as control. 24 hours post transfection, HA was immunoprecipitated and the samples were analyzed by immunoblot (M45 was used as a positive control). Indeed, ICP6 co-precipitated with VPS26B but not VPS26A (Figure 34A), suggesting that ICP6 redirects insoluble RIPK1 to autophagosomes in a similar way as M45.

Next, I tested whether the ICP6 IPAM is required for ICP6 self-interaction. HEK-293A cells were co-transfected with HA-tagged ICP6 and either Flag-tagged WT ICP6 or Flag-tagged ICP6 mutant. 24 hours post transfection samples were harvested and HA-immunoprecipitated. Immunoblot analysis showed an interaction between ICP6-HA WT and Flag-tagged ICP6 WT, but there was not interaction between ICP6-HA WT and ICP6mutant-Flag (Figure 34B), consistent with a previously reported requirement of the C-terminal part of ICP6 for self-interaction [159].

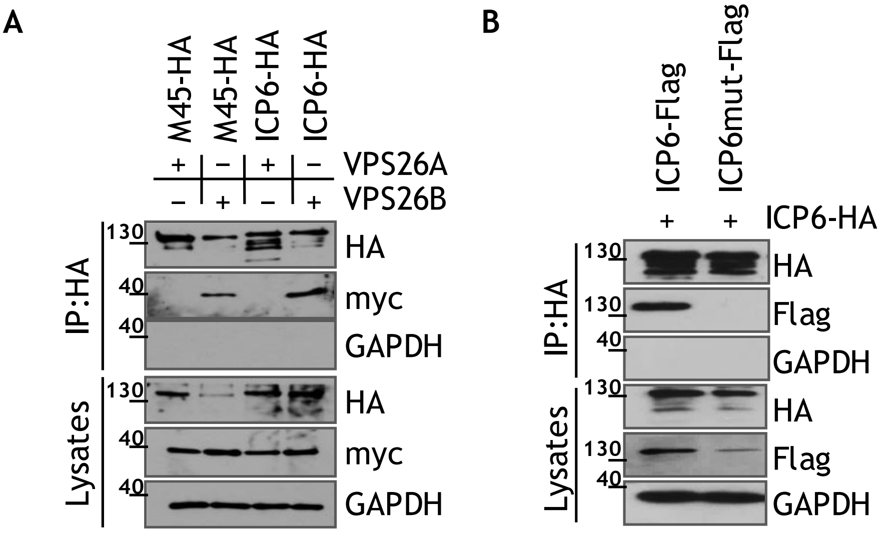

Figure 34. ICP6 interaction with VPS26B and itself.
(A) HEK-293A cells were co-transfected with ICP6-HA or M45-HA and VPS26B-myc or VPS26A-myc expression plasmids. At 24 hpi, levels of the myc-tagged VPS26A and B were analyzed in total cell lysates as well as in HA- immunoprecipitates; **(B)** HEK-293A were cells co-transfected with HA-tagged and Flag-tagged ICP6 expression plasmids. HA-tagged proteins were immunoprecipitated.

Finally, I checked whether the IPAM of ICP6 was necessary for the inhibition of necroptosis. To do this, human colorectal adenocarcinoma cell line HT-29 were infected with WT or mutant HSV-1 and two hours post infection were treated either with necroptosis inducers or necroptosis inhibitors. The combination of TNFα (T), the Smac mimetic BV6 (S), and the pan-caspase inhibitor zVAD-fmk (V) was used to induce necroptosis [159, 174]. Treatment with Necrostatin-1 (RIPK1-Inh), GSK'872 (RIPK3-Inh), or Z-IEDT-FMK (Casp8-Inh) was used to inhibit RIPK1, RIPK3 or Caspase8 dependent cell death, respectively. ATP level within the cells was measured 24 hpi. While HT-29 cells infected with WT HSV-1 were protected from TNFα-induced cell death, mock-infected cells and cells infected with the ICP6mut virus had significantly lower viability (Figure 35). Necroptosis induction was blocked by the addition of a RIPK1 or RIPK3 inhibitor, but not Caspase8 inhibitor, thus confirming that an intact IPAM domain is required for the inhibition of necroptosis. In addition, there was a significant increase in viability in the HSV-1 ICP6mut infected cells when treated with Necrostatin-1 or GSK'872 relative to carrier (DMSO), suggesting that these inhibitors blocked both TNFα-induced and infection-induced necroptosis.

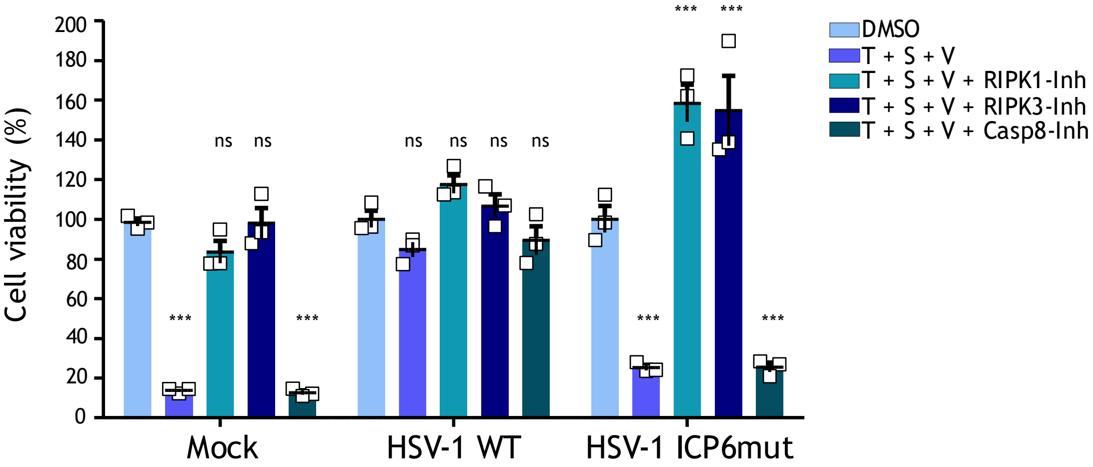

Figure 35. Cells viability assay upon HSV-1 WT and ICP6mutant infection of HT-29 cells.
HT-29 cells were infected with WT or ICP6mut HSV-1 (MOI 5). Cells were treated 2 hpi with a combination of TNFα, Smac Mimetic BV6, and Z-VAD-FMK (T+S+V); (T+S+V) and RIPK1 inhibitor Necrostatin-1 (50 μM); (T+S+V) and RIPK3 inhibitor GSK'872 (5 μM), or finally (T+S+V) and the Caspase-8 inhibitor Z-IEDT-FMK (75 μM). Values were normalized to mock infected DMSO-treated cells. Significance was determined by one-way ANOVA with Bonferroni post hoc test. Means ± SEM of triplicates are shown. ns, not significant, *P>0.05*; ***, *P*<0.001.

Collectively these data showed that HSV-1 ICP6 shares most of the functions described above for MCMV M45: both proteins possess a conserved sequence motif (IPAM) that induces RIPK1 accumulation in the detergent-insoluble fraction, induces the formation of aggregates, mediates self-interaction, and inhibits necroptosis. Moreover, both M45 and ICP6 interact with the retromer component VPS26B to facilitate autophagic degradation of aggregates.

6 Discussion

Herpesviruses escape cellular defenses in order to promote their replication and the establishment of a life-long persistent infection. Several studies have highlighted their ability to escape the host immune response by targeting cellular antiviral factors towards degradation processes. Even though the best characterized pathways of cellular target protein degradation mediated by viral proteins proceed through the proteasome, other pathways of degradation exist [177, 178]. It was previously reported that the MCMV M45 protein, a known viral necroptosis inhibitor, degrades key players of the innate immune response. It induces the degradation of NEMO by autophagy and it promotes the degradation of RIPK1 in an uncharacterized fashion [148, 154].

This study aimed to elucidate the molecular mechanism behind the selective degradation of NEMO and RIPK1 mediated by M45. The results of this study showed that the viral protein induces their loss of function by forming aggregates and then targets them to autophagosomes for degradation.

6.1 Implication aggregate formation and autophagy during MCMV infection

Previous findings of our laboratory showed that overexpression of M45 in transfected fibroblasts induces the formation of aggregates that localize in close proximity to autophagosomes [148]. This observation lead to the hypothesis that M45 mediates aggregates formation.

By comparing the distribution of NEMO and RIPK1 in the detergent soluble or insoluble fractions of MCMV infected wildtype or autophagy deficient fibroblasts (Figure 11 and 13), I observed that the two proteins and M45 itself accumulate in the insoluble fraction when autophagy is prevented. This observation indicated that M45 first renders them insoluble and then exploits autophagy for their degradation. This is consistent with the ability of DNA and RNA viruses to induce the formation of insoluble aggregates or inclusions in order to promote their replication, for instance by using aggregates as a scaffold for anchoring their replication complexes [179]. Strikingly, not only NEMO but also RIPK1 is targeted to autophagosomes for degradation, revealing that aggrephagy is exploited by M45 to dispose of both proteins (Figure 13).

Aggrephagy is the only mechanism described to date that is capable of disposing of large protein aggregates [180]. Immunofluorescence analysis performed during this study showed that M45 and NEMO form aggregate-like structures in an autophagy deficient cell line (Figure 12). The fact that M45 and NEMO co-localize in the absence of ATG5, a gene essential for the maturation of the phagophore, suggests that the formation of M45-NEMO aggregates is not caused by but precedes autophagy. Whether autophagy is then stimulated directly by M45 or instead by the accumulation of aggregates has not yet been clarified. It is tempting to speculate that even though M45 does not directly activate autophagy, the pathway is induced by the presence of aggregates, which if retained would be toxic for the cell. Following this hypothesis, it would be important to assess the impact of autophagy induction on the replication fitness of MCMV.

Unlikely several herpesviruses that contain in their genome specific autophagy inhibitors, no autophagy inhibiting protein has been identified in MCMV so far. On the contrary, when M45 is not expressed or is mutated in essential residues, autophagy is not induced, thus suggesting that MCMV induces autophagy in an M45-dependent manner [148]. Interestingly, human CMV also seems to be capable of activating autophagy early after infection in order to promote the formation of the viral assembly compartment [181]. It remains to be clarified whether autophagy plays a role during MCMV replication. The facts that i) MCMV IE and E proteins are expressed in *Atg5* knockout fibroblasts at levels that are comparable to wildtype cells and ii) both cell types show similar cytopathic effects upon infection might argue against that. However, it remains possible that impairment of autophagy in an *Atg5* knockout cell line would result in apoptotic or necroptotic cell death, which are anyway blocked by other proteins encoded by MCMV and M45 itself [182]. Additionally, ATG5 might have a different impact on cell survival according to the cell type or the time post infection. It is also important to note that an alternative form of macroautophagy has been described in *Atg5* negative cells [183]. These alternative autophagosomes are less well characterized and seem to be LC3-negative. However, M45 aggregates appear to co-localize with LC3BII, as shown in this study (Figure 23) and supported by previous finding that have shown M45 and NEMO co-localizazion with LC3BII [148]. Then, it would be necessary to analyze in detail the contribution of other autophagy essential genes. Nevertheless, it has been reported that depletion of RIPK1 in many cell types leads to increases in basal autophagy. Indeed, autophagy might be activated as a consequence of RIPK1 inhibition [184]. It would therefore be informative to test in several autophagy incompetent cell lines whether the replication of MCMV is compromised and whether cell death increases due to the accumulation of aggregates.

Interestingly, by time-lapse monitoring of the expression of M45 in transfected fibroblasts, I could observe that the viral protein initially appeared in small droplets, which then increased in size and fused together forming large aggregates (Figure 18). This phenomenon resembles a physiological process in which cells generate small cytoplasmic aggregates that afterward coalesce into large aggresomes [123, 185]. It is fascinating that MCMV uses a similar strategy to inactivate cell signaling molecules. At first glance, the movement of the aggregates observed during this study seemed to be associated with microtubules. However further studies would be required to corroborate this hypothesis and to characterize similarities and differences between virally induced and cellular aggregates.

6.2 Characterization of M45 aggresomes

Soluble proteins can interact with other molecules of the same protein and form dimers or oligomers. The intramolecular interaction can induce a conformational change in the protein structure and thus cause the accumulation of insoluble polymers that, if not removed, can trigger downstream events leading to the development of diseases. For instance, extracellular amyloid deposits are characteristic features of Alzheimer's disease [186]. However, the formation of amyloid structures is not always associated with human diseases but can be important for cell signaling. Indeed, it was reported that RIPK1 and RIPK3 associate through their RHIM motif and form a heteromeric amyloid structure that is a functional signaling complex mediating programmed necrosis [80]. In addition to RIPK1 and RIPK3, other RHIM containing proteins, such as DAI, promote the assembly of amyloid signalosomes to prominent mediators of necroptosis [80]. While a recent study showed that *in vitro* expression of the RHIM domain of M45 may lead to the formation of insoluble amyloid fibrils with RIPK1 and RIPK3 [187], studies performed in this laboratory described dot-like structures rather than fibrils in the cytoplasm [148]. Consistent with this previous study, the M45 aggregates I observed by TEM (Figure 16) do not exhibit the amyloid fibrillary structure described for necrosomes. It is possible that whereas ß-amyloid aggregates are required for cell antiviral signaling, M45 aggregates are a strategy adopted by the virus to inhibit this host defense mechanism.

One question that remains to be fully addressed is whether necrosomes are in fact aggresomes and whether the other RHIM containing proteins are recruited into them. The fact that M45 induces the formation of detergent-insoluble aggregates, as shown in this study, while it prevents the formation of necrosomes argues against the fact that they might be the same structure. Moreover, M45-induced aggregates associate with LC3B, consistent with their removal by autophagy, but do not associate with caveolin-1 (Figure 23) a recently described marker for necrosomes [166].

An interesting follow-up would be to determine the aggregate’s volume in autophagy competent of deficient cell lines. In addition, the data obtained so far by EM showed only M45. It would be interesting to know whether NEMO and/or RIPK1 are also in the same structures and/or within the autophagosomes. One way to test this is to generate cell lines expressing either NEMO or RIPK1 tagged with a fluorescent protein and analyzed them by CLEM after MCMV infection.

6.3 Mechanism and implication of aggregate formation

M45 is a multifunctional protein with distinct functional domains: an N-terminal RHIM domain involved in the inhibition of viral induced necroptosis and a C-terminal region involved in a brief and transient activation and then inhibition of NF-κB [148, 154, 155]. Moreover, it was shown that the C-terminus is also required together with the RHIM domain for necroptosis inhibition and that M45 forms dimers or oligomers [151-153, 158]. The data obtained during this study revealed that a small motif at the C-terminus of M45 is also required for aggregate formation. Firstly, by using several MCMV M45 truncation mutants, which were previously described, it was possible to identify a region within the C-terminus of M45 involved in the accumulation of NEMO and RIPK1 in the insoluble fraction (Figure 19). Afterwards, by using several MCMV M45 alanine substitution mutants, it was possible to narrow down a specific sequence motif (P-F-V-D-H), named IPAM, which was crucial to induce this phenotype (Figure 21). The IPAM was required for the interaction with RIPK1 and NEMO, for self-interaction, aggregate formation, and necroptosis inhibition (Figure 22, 24 and 25). The notion that the IPAM is an aggregation-inducing motif is supported by experiments showing that the fusion of short polypeptides containing this motif to mCherry is sufficient to induce the aggregation of the fluorescent protein (Figure 20).

It is remarkable that one small motif is responsible for several functions. The most plausible explanation is that M45 binds RIPK1 and NEMO only as a dimer or oligomer. In this scenario, the motif would catalyze polymerization and aggregation of M45 and its interacting proteins. Indeed several herpesvirus proteins have been described to self-interact in order to elicit their functions. An example is ICP6, the homolog of M45 in HSV-1 [158]. In fact, it has been reported that the ICP6 self-interaction is necessary to impede the induction of necroptosis, consistent with the findings of this thesis.

Importantly, the IPAM is also involved in viral dissemination *in vivo*. Indeed an MCMV mutated in the IPAM does not replicate in wildtype mice (Figure 26). Additionally, the replication defect is only partially rescued in viral-induced necroptosis impaired mice (*Ripk3* knock-in), indicating that the PFVDH sequence and the M45-mediated aggregate formation is not only modulating necroptosis but also other signaling pathways such as the ones leading to NF-κB activation. Indeed, these data confirmed the biological relevance of aggregate formation upon MCMV infection.

6.4 Potential inactivation of RIPK3 and DAI through aggregate formation

Several studies have shown that virally induced necroptosis occurs even in the absence of RIPK1, and its activation is thought to be DAI-RIPK3 dependent [81, 152, 153]. The data presented in this thesis strongly support that the IPAM is involved in the inhibition of necroptosis by targeting RIPK1. It remains to be determined whether RIPK3 and DAI are also present in the aggregates. This is particularly relevant as M45 inhibits viral induced necroptosis by interacting with these two proteins. However, the fibroblast cell lines used in this study do not express significant levels of RIPK3 and DAI. Therefore, it was not possible to verify whether they accumulate in the insoluble fraction. To resolve this question it would be necessary to repeat some experiments in cell lines expressing RIPK3 and DAI. Moreover, the results obtained in this thesis showed that RIPK1 aggregation seems to be necessary to inhibit necroptosis indicating that even though RIPK1 expression might be dispensable for the activation of the signaling pathway, when it is expressed, it certainly plays an important role. Additionally, insoluble RIPK1 showed a slightly different electrophoretic mobility in western blot analysis than the soluble RIPK1 and the same was true in the total fraction of cells treated with NH_4Cl (Figure 13). This different mobility could be caused either by the buffer conditions or by the fact that M45 could sequester an active form of RIPK1.

Indeed, RIPK1 signaling is modulated by post-translational modifications, which includes K63-polyubiquitination, phosphorylation, and N-acetylglucosaminylation (GlcNAcylation) [188]. It would be then plausible that M45 induces the degradation of an active form of RIPK1.

6.5 M45 uses autophagy adaptors to tether aggregates to LC3BII

Selective autophagy is a cellular process by which cytoplasmic components such as protein aggregates or damaged organelles are selected and tagged for sequestration and degradation in autophagosomes. Intracellular bacteria and viruses can also be subjected to selective autophagy, which is called xenophagy [189]. The selectivity is conferred by autophagy receptors such as p62/SQSTM1 or NBR1, and other proteins that connect the tagged structures to nascent autophagosomes through a LIR motif [190-192]. Therefore, it is not surprising that several viruses inhibit autophagy by antagonizing autophagosome formation and/or maturation or manipulate the autophagy machinery in order to promote their replication [193].

Indeed, the findings of this thesis demonstrate that M45 specifically promotes autophagy and targets NEMO and RIPK1 to nascent autophagosomes in a selective manner. Considering the anti-viral roles of NEMO and RIPK1, it is remarkable that MCMV exploits a cellular autophagosome targeting mechanism to dispose of key signaling molecules.

Due to the fact that M45 does not contain a LIR motif, an AP-MS screen was done with the aim of identifying new M45-interacting proteins that could bridge M45 aggregates to nascent autophagosomes (Table 1). Among those hits, VPS26B, VPS35, and VPS29 were particularly interesting due to the fact that they associate with endosomes, which can fuse with autophagosomes. However, not so much is known so far about the relationship between viruses and the retromer complex components. A couple of studies described that the retromer complex is implicated in the entry of human papillomavirus (HPV) as well as in in the late-steps of viral replication and assembly of the Human Immunodeficiency Virus Type-1 (HIV-1) virus [194, 195].

Here I could show that M45 interacts with VPS26B, while the interaction with the other two components turned out to be VPS26B dependent (Figure 27). Since VPS26B does not contain LIR motifs, I investigated whether it might target proteins to the autophagosomes by binding to the LC3-interacting adaptor TBC1D5. Several lines of evidence supported the choice of this target: i) It was reported that TBC1D5 bridges endosomes and autophagosomes via its LIR motifs [113]. ii) Although the majority of studies highlight a direct binding of TBC1D5 and VPS29, it has also been reported that the VPS26B retromer associates with TBC1D5 [97, 113, 116, 117]. Also, M45 binding to VPS26B occurs independently of its recruitment to the complex, but the work performed in this study does not exclude a possible involvement of the other two components. Additionally, preliminary observations of this laboratory have shown that TBC1D5 can be an M45 potential interaction partner (Claudia Mack, unpublished data) as well as interacts with VPS26B (Matteo Rizzato, unpublished data).

The knocking out of either VPS26B or TBC1D5, led to a severe impairment of NEMO degradation in MCMV infected cells (Figure 28 and 29). Indeed, in addition to its already recognized role as regulator of endocytic trafficking, we could for the first time describe TBC1D5 as an autophagic receptor for selective autophagy of virus-induced protein aggregates. Nevertheless, it is plausible that there are also other autophagic receptors involved in the removal of insoluble aggregates. This hypothesis is strongly supported by the fact that NEMO degradation in a VPS26B or TBC1D5 knockout cell line is not completely blocked. An interesting candidate as an additional autophagy adaptor is OPTN1 [196]. OPTN1 plays a crucial role in the delivery of ubiquitinated cargo to autophagophores. What makes this protein extremely interesting for a follow-up study is the fact that OPTN1 originated from a gene duplication of NEMO. A preliminary sequence alignment between the two proteins revealed that multiple conserved motifs are located in the M45 binding site in NEMO (data not shown). This raises the possibility that M45 can also bind to OPTN1 for tethering proteins or aggregates to nascent autophagosomes.

6.6 Possible implication of cellular chaperones in aggregate disposal

The degradation of protein aggregates (aggrephagy) in the cells is a highly regulated process. In fact, cells have evolved an elaborate machinery to preserve protein homeostasis [197], and several cellular markers have been identified as being involved in protein quality control, including cellular chaperones. Chaperones dictate the balance between protein folding, degradation, and aggregation. There are several classes of chaperones, some being involved in protein folding and some assisting in protein degradation [122, 198-200]. For instance, BAG3 together with HSPB8 recognizes misfolded proteins and activates the autophagy machinery to induce cargo degradation [201]. Moreover, it has recently been reported that BAG3 complexes with HSP70 and controls protein aggregation [202]. This is remarkable because a motif search revealed in the co-chaperone BAG3 the presence of a similar PFFVDH motif very similar to the IPAM motif within M45. Here, I verified whether chaperones are recruited to M45 aggregates. Immunofluorescence experiments showed that HSP70 did not co-localize with M45-induced aggregates, nor was HSP70 found in the detergent-insoluble fraction by immunoblot (Figure 23). However, this interaction might be transient or time point dependent. Additionally, the molecular adaptor 14-3-3γ, which couples chaperone associated misfolded proteins with dynein motors and facilitates the formation of aggresomes [203], was identified in the SILAC screen as an M45 potential interaction partner. This interaction was not investigated during the course of this study, but preliminary data revealed that, similar to HSP70, 14-3-3γ does not accumulate in the insoluble fraction of infected cells upon MCMV infection (data not shown). However, further study should be performed to rule out whether the chaperones are recruited to the M45-aggregates. Moreover, the quality control machinery includes a large number of proteins, which requires more extensive analysis. Nevertheless, there remains the intriguing possibility that the viral protein induces misfolding and aggregation of client proteins by mimicking the function of a cellular chaperone. Considering that some viruses encode for their own chaperone-like proteins to enhance their infectivity, one intriguing possibility is that M45 acts as a chaperone-like protein displacing HSP90 from RIPK1 and NEMO and then, by recruiting HSP70 or mimicking its function, targets aggregates to the nascent autophagosomes.

6.7 Aggregate formation is a conserved mechanism among herpesviruses

In this study, I could show that this M45-mediated viral immune evasion strategy is not unique to MCMV but is shared by HSV-1, a human herpesvirus, and probably by other members of the *Herpesvirales* order. HSV-1 ICP6 shares many functions with M45. Both proteins interact with RIPK1 and inhibit viral induced necroptosis. However, HSV-1 ICP6 protects only human cells (i.e., cells of its natural host) from viral induced necroptosis, but it activates necroptosis in murine cells, suggesting that HSV-1 is so highly adapted to its human host that its strategy to escape necroptosis functions only in human cells.

Here I showed that HSV-1 ICP6, similar to M45, contains the IPAM, targets RIPK1 to the insoluble fraction of infected cells, and mediates RIPK1 degradation via autophagy (Figure 31 and 32). Even though HSV-1 prevents autophagy induction after infection [140], basal levels of autophagy are detectable in some cell lines [139, 142]. Indeed, treatment with ammonium chloride, a known lysosome inhibitor, showed a strong increase of RIPK1 in the insoluble fraction of HSV-1 infected cells, indicating an active role of autophagy in aggregate disposal. This was not the case in cells infected with the ICP6 IPAM-mutant, where RIPK1 was found only in the soluble fraction (Figure 33). Moreover, I could show that ICP6 forms aggregates in an IPAM dependent manner and cell viability assays showed that the IPAM motif is also required for necroptosis inhibition (Figure 32). Finally, ICP6 interacts with the retromer component VPS26B, similar to M45, underlining a possible employment of this protein as an autophagic receptor. However, it remains to be investigated whether ICP6 can also interact directly with TBC1D5 as M45 can.

The reason to perform a comparative study on HSV-1 ICP6 rather than the HCMV homolog UL45 was due to the fact that UL45 differs from M45 in that it does not contain a RHIM domain and is dispensable for growth in endothelial cells [160]. It has been recently reported that UL45 can inhibit NF-κB signaling together with UL48 [161]. However, there is no evidence that UL45 plays a role in necroptosis inhibition similar to MCMV. HCMV blocks TNF-induced necroptosis, but it employs a different strategy. HCMV IE1 contributes to the establishment of an environment that prevents necroptosis during viral infection. Omoto and colleagues reported that an early IE1-regulated viral gene inhibits necroptosis after RIPK3 activation and MLKL phosphorylation, but prior to membrane leakage [204].

By comparing M45 with its homologs in related herpesviruses, the IPAM consensus motif P-F/Y-V-D-H/Q was identified in more than 70 viral R1 homologs of herpesviruses, baculoviruses, and giant viruses (e.g. mimivirus and pandoravirus), suggesting that its function might be widely conserved. Thus, it would be worthwhile to test whether M45 homologs in other viral orders are also aggregation-prone.

While the IPAM is conserved in numerous viral R1 homologs, the cellular interacting partners appear to be more diverse. M45 and HSV-1 ICP6 both interact with RIPK1, but while M45 interacts also with NEMO, ICP6 interacts with Caspase-8 [156]. Moreover, a recent study showed that ICP6 can interact with APOBEC3A and to a lower extent also APOBEC3B [205].

The EBV BORF2 protein and the KSHV ORF61 protein have been recently shown to induce the relocalization of APOBEC3B to perinuclear dot-like structures [206], but it is still unknown whether these structures represent protein aggregates. BORF2 and ORF61 interact with APOBEC3B, whereas ICP6 and UL45 do not [205]. In line with this, APOBEC3B was not detected as an M45-interacting protein by AP-MS in this study. Conversely, ORF61 does not interact with RIPK1 [161].

This apparent diversity suggests that the viral R1 proteins have individual binding sites for their respective target proteins. Finally, the IPAM has been found not only in many viral proteins and but also in the co-chaperone BAG3 (data not shown). It is then important to expand this research to other viral homologues and analyze in more detail the interplay between viral aggregates and cellular chaperones.

6.8 Short summary and conclusions

Viruses manipulate cellular signaling by inducing the degradation of crucial signal transducers. After infection, MCMV is sensed by pattern recognition receptors, which in turn activate the innate cellular immune response. However, the MCMV protein M45 is able to interfere with key signaling molecules of the innate immune response, such as NEMO and RIPK1, causing their degradation. In summary, the data of this thesis showed that the MCMV M45 protein induces the degradation of these two cellular proteins by a novel mechanism: it induces their sequestration as insoluble protein aggregates and subsequently facilitates their degradation by autophagy. Aggregation of target proteins requires a newly defined “induced protein aggregation motif” (IPAM) within M45, which is required for aggregation, inhibition of necroptosis, and viral pathogenesis in mice. Autophagy activation by M45 is carried out by recruitment of the retromer component VPS26B and the LC3-interacting adaptor protein TBC1D5 to facilitate degradation of aggregates by selective autophagy. Importantly, the IPAM was found to be present in homologous proteins of more than 70 large DNA viruses (58 herpesviruses, 8 baculoviruses, and 7 giant viruses). Indeed, here I showed that this two-steps mechanism is not unique to MCMV but is shared by ICP6 of HSV-1. These results suggest that induced protein aggregation and selective autophagy might be a widely-used viral strategy making these findings highly significant for defining mechanisms of viral pathogenesis.

6.9 Graphical Summary

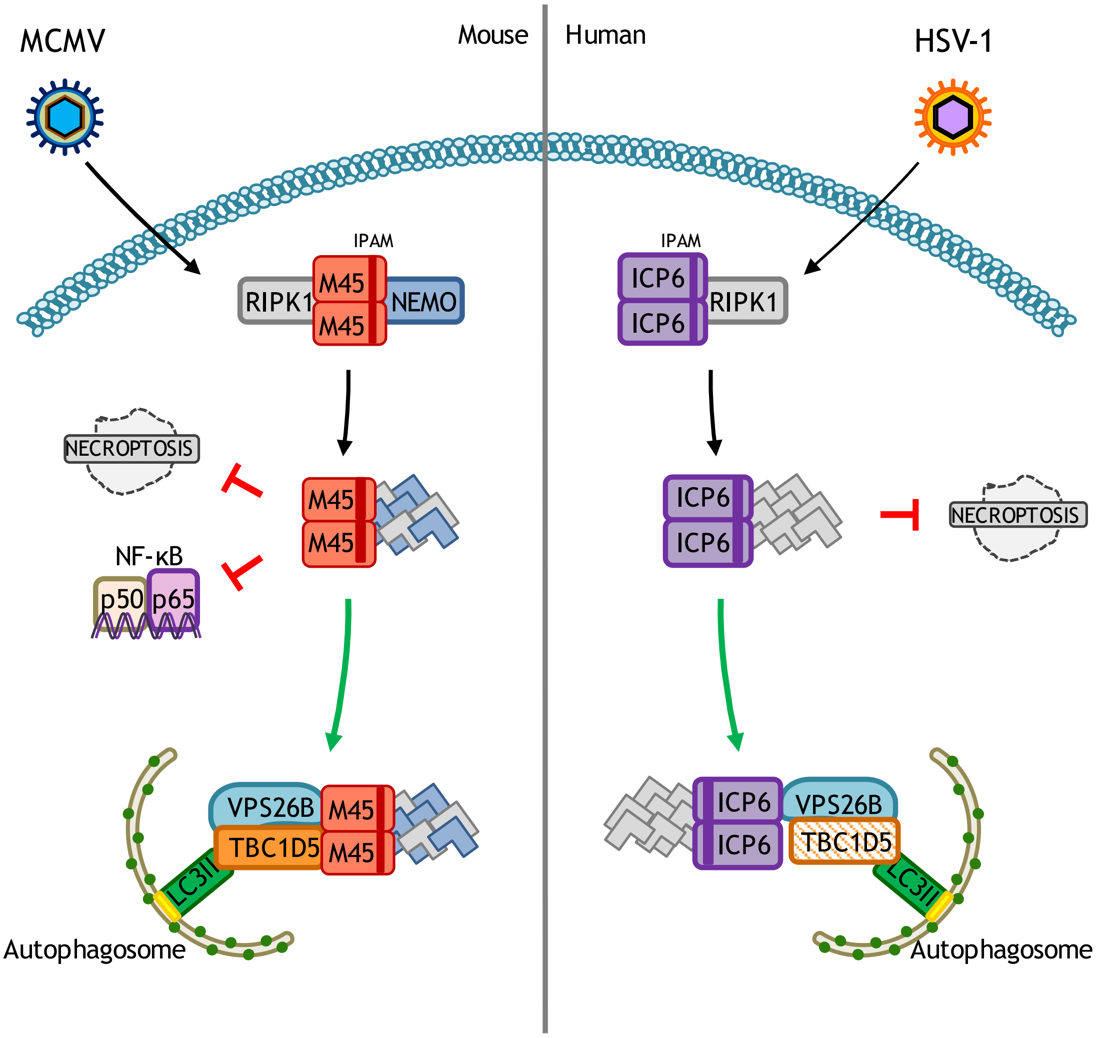
MCMV
Mouse
Human
HSV-1
IPAM
RIPK1
M45
M45
NEMO
IPAM
ICP6
ICP6
RIPK1
NECROPTOSIS
NF-κB
p50
p65
M45
M45
ICP6
ICP6
NECROPTOSIS
VPS26B
M45
TBC1D5
M45
LC3II
Autophagosome
ICP6
ICP6
VPS26B
TBC1D5
LC3II
Autophagosome

Figure 36. Graphical Summary
MCMV M45 and HSV-1 ICP6 induce the aggregation of target proteins, mediated by an induced protein aggregation motif (IPAM). They facilitate selective autophagy of aggregates (aggrephagy) by recruiting VPS26B and TBC1D5, which in turn tethers them to the cellular autophagy marker LC3-II.

7 Material

7.1 Cells

Name	Description	References
NIH-3T3	Murine embryonal fibroblasts from NIH/Swiss, spontaneous immortalized	ATCC CRL-1658
NIH-3T3 *Vps26B*-myc	NIH-3T3 stably transduced with Vps26B-myc expressing pMSCVpuro	Rebekka Schmitz
Tbc1d5-/- MEF	Mouse embryonic fibroblasts lacking tbc1d5 gene expression obtained by CRISPR/Cas9 mutagenesis	Matteo Rizzato
Atg5 -/- MEF	Mouse embryonic fibroblasts lacking Atg5 gene expression, SV40 large T	RIKEN BRC cell bank
HEK-293A	Human embryonal kidney epithelial cells, contains a stably integrated copy of the E1 gene	Thermo Fisher R70507
Primary wild type MEF	Murine embryonal fibroblasts derived from embryos of C57BL/6 WT mice	this study
Primary *Vps26B* -/- MEF	Murine embryonal fibroblasts derived from embryos of C57BL/6 *vps26B* -/- mice	Ekyune Kim
Wild type MEF	Murine embryonal fibroblasts derived from embryos of C57BL/6 WT mice, spontaneous immortalized	this study
Immortalized *Vps26* -/- MEF	Murine embryonal fibroblasts derived from embryos of C57BL/6 *Vps26B* -/- mice, spontaneous immortalized	this study
SVEC4-10	Murine endothelial cells, immortalized using SV40 large T antigen	ATCC (CRL-2181)
HT-29	Human colorectal adenocarcinoma cell line	Udo Schumacher
VERO	African green monkey kidney	ATCC (CCL-81)
HFF	Telomerase-immortalized human foreskin fibroblasts cell line	Thomas Shenk
RIPK3-/- MEFs	Mouse embryonic fibroblasts lacking ripk3 gene	Edward Mocarski
M2-10B4	Bone marrow stromal cells	ATCC (CRL-1972)

7.2 Viruses

Name	Description	References
MCMV wild type	MCMV Smith pSM3fr-MCK-2f	Barbara Adler

MCMV-M45HA	MCMV Smith pSM3fr-MCK-2fl with reinserted M45 full length ORF including an C-terminal HA tag	Eva Krause
MCMV-ΔM45	MCMV Smith pSM3fr-MCK-2fl lacking the entire M45 open reading frame	Eva Krause
MCMV-M45 Ct3HA	MCMV Smith pSM3fr-MCK-2fl with reinserted M45 C-terminus truncation mutant (1 – 1121)	Eva Krause
MCMV-M45 Ct4HA	MCMV Smith pSM3fr-MCK-2fl with reinserted M45 C-terminus truncation mutant (1 – 1137)	Eva Krause
MCMV-M45 Ct5HA	MCMV Smith pSM3fr-MCK-2fl with reinserted M45 C-terminus truncation mutant (1 – 1155)	Eva Krause
MCMV-M45 Ct6HA	MCMV Smith pSM3fr-MCK-2fl with reinserted M45 C-terminus truncation mutant (1 – 1167)	Eva Krause
MCMV-M45mutRHIM	MCMV Smith pSM3fr-MCK-2fl with reinserted M45 full length ORF including an C-terminal HA tag and a mutation in the RHIM domain	Eva Krause
MCMV-M45-1-227	MCMV Smith pSM3fr-MCK-2fl with truncated version of M45 (aa 1-227)	Eva Krause
HSV-1 F strain	HSV-BAC pYEbac102 (from Yasushi Kawaguchi)	Martin Messerle

The following viruses were generated during this study.

Name	Description	References
MCMV-M45 HA – Δm157	MCMV Smith pSM3fr-MCK-2fl with reinserted M45 full length ORF including an C-terminal HA tag lacking m157	this study
MCMV-M45 HA mutant 1 – Δm157	MCMV Smith pSM3fr-MCK-2fl with reinserted M45 full length ORF mutated in the aminoacyl residues 1122, 1123, 1124 to AAA including a C-terminal HA tag, lacking m157	this study
MCMV-M45 HA mutant 2 – Δm157	MCMV Smith pSM3fr-MCK-2fl with reinserted M45 full length ORF mutated in the aminoacyl residues 1125, 1126, 1127 to AAA including a C-terminal HA tag, lacking m157	this study
MCMV-M45 HA mutant 3 – Δm157	MCMV Smith pSM3fr-MCK-2fl with reinserted M45 full length ORF mutated in the aminoacyl residues 1128, 1129, 1130 to AAA including a C-terminal HA tag, lacking m157	this study
MCMV-M45 HA mutant 4 – Δm157	MCMV Smith pSM3fr-MCK-2fl with reinserted M45 full length ORF mutated in the aminoacyl residues 1131, 1132, 1133 to AAA including a C-terminal HA tag, lacking m157	this study
MCMV-M45mutRHIM - Δm157	MCMV Smith pSM3fr-MCK-2fl with reinserted M45 full length ORF including an C-terminal HA tag and a mutation in the RHIM domain, lacking m157	this study
HSV-1 ICP6-HA	HSV-1 F strain pYEbac102 with full length ICP6 ORF including a C-terminal HA tag	this study

HSV-1 ICP6mut	HSV-1 F strain pYEbac102 with full length ICP6 ORF mutated in the aminoacyl residues YVDH in position 1070, 1071, 1072, 1073 to AAAA	this study
HSV-1 ICP6mut-HA	HSV-1 F strain pYEbac102 with full length ICP6 ORF mutated in the aminoacyl residues YVDH in position 1070, 1071, 1072, 1073 to AAAA including a C-terminal HA tag	this study
MCMV-M45mCherry	MCMV Smith pSM3fr-MCK-2fl with reinserted M45 full length ORF including a C-terminally mCherry tag	this study

7.3 Bacteria

Strain	Growth t°	Description	References
E.coli DH10B	37 °C	*F- mcrA Δ(mrr-hsdRMS-mcrBC) Φ80dlacZΔM15 ΔlacX74 endA1 recA1 deoR Δ(ara,leu)7697 araD139 galU GalK nupG rpsL λ-*	Life technologies
E.coli GS1783	30 °C	DH10B l cI857 Δ(cro-bioA)<>araC-PBADI-sceI	Tischer,2010

7.4 Plasmids

Name	Description	References
pcDNA3	expression vector, *amp*$_R$, *neo*$_R$	Life Technologies
pEPkan-S	template plasmid for en passant mutagenesis, contains I-Sce-aphA1 cassette, *kan*$_R$	N.Osterrieder, FU Berlin, Germany
pMSCVpuro	retroviral expression vector to generate retrovirus for transduction of eukaryotic cells, *amp*$_R$, *puro*$_R$	Clontech Laboratories
pcDNA3-M45HA	pcDNA plasmid containing the full length M45 gene C-terminally HA tagged, *amp*$_R$	Patrizia Fliss, Eva Krause
pcDNA3-M45Flag	pcDNA plasmid containing the full length M45 gene C-terminally Flag tagged, , *amp*$_R$	Eva Krause
pcDNA3- Ct3HA	pcDNA plasmid containing C-terminus truncation mutant of M45 (Ct3) c-terminally HA tagged, , *amp*$_R$	Eva Krause
pcDNA3-FlagmNEMO	pcDNA plasmid containing mNEMO amplified from cDNA of NIH-3T3 cells and N-terminally Flag tagged, , *amp*$_R$	Patrizia Fliss
pCMVTAG-NEMO	Expression plasmid of human NEMO with N-terminal Flag tag based on pCMVTAG2B,	Addgene (11970)

	kanR, *neoR*	
pcDNA3-Vps26Bmyc	pcDNA plasmid containing Vps26B C-terminally myc tagged, *ampR*	Rohan Teasdale Queensland, Australia
pcDNA3-Vps26Amyc	pcDNA plasmid containing C-terminally myc tagged Vps26A generated by PCR amplification, *ampR*	Rebekka Schmitz
pcDNA3-Vps35myc	pcDNA plasmid containing C-terminally myc tagged Vps35 generated by PCR amplification, *ampR*	Rebekka Schmitz
pcDNA3-Vps29myc	pcDNA plasmid containing C-terminally myc tagged Vps29 generated by PCR amplification, *ampR*	Rebekka Schmitz
pcDNA-FlagTBC1D5	pcDNA plasmid containing N-terminally Flag tagged Tbc1d5 generated by PCR amplification, *ampR*	Matteo Rizzato
pGFP-LC3B	Expression plasmid of human LC3B based on pEGFP-C3, *kanR*, *neoR*	Addgene (11546)
pmCherry N1	expression vector, *kanR, neoR*	Addgene
Flag-IFI16	pcDNA3-FLAG vector containing the full length human IFI16	Addgene (35064)
pSico-CRISPR/Cas9	Vector containing fusion gRNA-tracrRNA, encoding for *S. pyogenes* Cas9 enzyme, *amp*, *puro* resistance	Robert Jan Lebbink
pMDG	Packaging vector, lentiviral *gag*, *pol*, *rev* encoding vector, *amp* resistance	Robert Jan Lebbink
pCMVR8.91	Envelope vector, encoding VSV-G protein, *amp* resistance	Robert Jan Lebbink

The following plasmids were generated during this study:

Name	Description	References
pcDNA-Vps26MUT-myc	pcDNA plasmid containing C-terminally myc tagged Vps26B carryng a mutation in the residues 233D/ M234N, *ampR*	this study
M45-mCherry	pmCherry N1 vector containing the full length M45 gene, *kanR*	this study
pmCherry M45 aa931-1121	pmCherry N1 vector containing the a C-terminal portion of the M45 gene (aa931-1121), *kanR*	this study
pmCherry M45 aa931-1167	pmCherry N1 vector containing the a C-terminal portion of the M45 gene (aa931-1167), *kanR*	this study
pmCherry M45 aa1122-1167	pmCherry N1 vector containing the a C-terminal portion of the M45 gene (1121-1167), *kanR*	this study

pcDNA M45mut3-HA	pcDNA plasmid containing M45 full length ORF mutated in the aminoacyl residues 1128, 1129, 1130 to AAA including a C-terminal HA, *ampR*. BAC-DNA used as template.	this study
pcDNA- ICP6HA	pcDNA plasmid containing the full length ICP6 gene C-terminally HA tagged, *ampR*. Viral DNA used as template.	this study
pcDNA ICP6mutHA	pcDNA plasmid containing the full length ICP6 gene mutated in the aminoacyl residues 1070, 1071, 1072, 1073 to AAAA including a C-terminal HA tag, *ampR*. Viral DNA used as template.	this study
pcDNA-ICP6Flag	pcDNA plasmid containing the full length ICP6 gene C-terminally Flag tagged, *ampR* Viral DNA used as template.	this study
Nucleolin-pmCherry	plasmid generated by replacing the EGFP sequence in the GFP-Nucleolin plasmid (Addgene) with the sequence of mCherry	this study
M45-mCherry Shuttle plasmid	pcDNA-M45mCherry plasmid generated by Gibson Assembly as shuttle vector for en passant BAC mutagenesis (MCMV-M45mCherry)	this study

7.5 Primers

7.5.1 Molecular cloning primers

Name	Sequence	Description
pcDNA-Vps26MUT-myc (REV-T7)	CCTCGGACTGGTGCCCCGTCGTTGTCCTCATACTTCGCTATTGTGT	PCR-driven overlap extension
pcDNA-Vps26MUT-myc (FW-BGH)	ACACAATAGCGAAGTATGAGGACAACGACGGGGCACCAGTCCGAGG	PCR-driven overlap extension
M45-pmCherry FW	TTAAGGGCCCTGCGATAATTCACGGAAGGGGG	ApaI
M45-pmCherry REV	TTAA GGATCCGCGCGATAATTCACGGAAGGG	BamHI
pmCherry M45 aa931-1121 FW	TATAGAATTCATGAGCGTCGACCTGTGCATGGC	EcoRI
pmCherry M45 aa931-1121 REV	TTAAGGATCCTTGACGCACATCTTGATGACCG	BamHI
pmCherry M45 aa931-1167	TATAGAATTCATGAGCGTCGACCTGTGCATGGC	EcoRI
pmCherry M45 aa931-1167	TTAAGGATCCTTGACGCACATCTTGATGACCG	BamHI
pmCherry M45 aa1122-1167	TATAGAATTCATGTCCGAGACCGGCTGGACC	EcoRI

pmCherry M45 aa1122-1167	TTAAGGATCCTTGACGCACATCTTGATGACCG	BamHI
pcDNA M45mut3-HA FW	TATAGGTACCATGGATCGCCAGCCCAAA	KpnI
pcDNA M45mut3-HA REV	TTTAATCTAGATCACTTGTCGTCATCGTCTTTGTAGTCGCGATAATTCACGGAAGGGG	XbaI
pcDNA- ICP6HA FW	TATAAAGCTTATGGCCAGCCGCCCAGC	HindIII
pcDNA- ICP6HA REV	TTAATCTAGATCAAGCGTAGTCTGGGACGTCGTATGGGTACAGCGCGCAGCTCATGCAGA	XbaI
pcDNA-ICP6mutHA FW	TATAAAGCTTATGGCCAGCCGCCCAGC	HindIII
pcDNA-ICP6mutHA REV	TTAATCTAGATCAAGCGTAGTCTGGGACGTCGTATGGGTACAGCGCGCAGCTCATGCAGA	XbaI
pcDNA-ICP6-Flag REV	TTAATCTAGATCACTTGTCGTCATCGTCTTTGTAGTCCAGCGCGCAGCTCATGCAGA	XbaI
Nucleolin-pmCherry FW	TATAGCTAGCATGGTGAGCAAGGGCGAG	NheI
Nucleolin-pmCherry REV	TTAAAGATCTCCCTTGTACAGCTCGTCCATGC	BglII
Gibson-M45 C-ter FW	CGTGCTCAACAGCCGCCTCA	//
Gibson-M45 C-ter REV	GCGATAATTCACGGAAGGGGGCATA	//
Gibson-Kan FW	TATGCCCCCTTCCGTGAATTATCGCGATCCACCGGTCGCCACCATGGTGAGCAAGGGCGAGGAGGATAACATGGCTAGGGATAACAGGGTAATCGATTT	//
Gibson-Kan REV	GAAGCGCATGAACTCCTTGATGATGGCCATGTTATCCTCCTCGCCCTTGCTCACCATGGTGGCGACCGGTGGATCGCCAGTGTTACAACCAATTAACC	//
Gibson-mCherry FW	CATCATCAAGGAGTTCATGCGCTTC	//
Gibson-mCherry REV	TAGGTGACACTATAGAATAGGGCCCTACTTGTACAGCTCGTCCATGCC	//

7.5.2 *En passant* BAC mutagenesis primers

Name	Sequence
MCMV Δm157 Zeocine FW	CGTGGTCAAGCCGGTCGTGTTGTACCAGAACTCGACTTCGGTCGCGTTCATGTTGACAATTAATCATCGGCAT
MCMV Δm157 Zeocine REV	CCTAGTAAAATTACTCTTGATTGTGTTTATCTCGGAACGTGCTGTAACAATCAGTCCTGCTCCTCGGCCA
MCMV M45HA MUT1 (Kan) FW	CGATGGCGACGGGCAGCGACTGCGCATGGTCGACGAACGGAGCAGCAGCGACGCACATCTTGATGACCGTAGGGATAACAGGGTAATCGATTT
MCMV M45HA MUT1 (Kan) REV	CTGGACCGTGTCGACCGACGCGGTCATCAAGATGTGCGTCGCTGCTGCTCCGTTCGTCGACCATGCGCAGCCAGTGTTACAACCAATTAACC
MCMV M45HA MUT2 (Kan) FW	CCCCGAAGCCGATGGCGACGGGCAGCGACTGCGCATGGTCAGCAGCAGCCTGTCTGTCGACGCACATCTTAGGGATAACAGGGTAATCGATTT

MCMV M45HA MUT2 (Kan) REV	GTCGACCGACGCGGTCATCAAGATGTGCGTCGACAGACAGGCTGCTGCTGACCATGCGCAGTCGCTGCCGCCAGTGTTACAACCAATTAACC
MCMV M45HA MUT3 (Kan) FW	AAGACCCCCCGAAGCCGATGGCGACGGGCAGCGACTGCGCAGCAGCGACGAACGGCTGTCTGTCGATAGGGATAACAGGGTAATCGATTT
MCMV M45HA MUT3 (Kan) REV	CGCGGTCATCAAGATGTGCGTCGACAGACAGCCGTTCGTCGCTGCTGCGCAGTCGCTGCCCGTCGCGCCAGTGTTACAACCAATTAACC
MCMV M45HA MUT4 (Kan) FW	CCAATTCCACCGAAGACCCCCCGAAGCCGATGGCGACGGGAGCAGCAGCCGCATGGTCGACGAACGGCTTAGGGATAACAGGGTAATCGATTT
MCMV M45HA MUT4 (Kan) REV	CAAGATGTGCGTCGACAGACAGCCGTTCGTCGACCATGCGGCTGCTGCTCCCGTCGCCATCGGCTTCGGGCCAGTGTTACAACCAATTAACC
HSV-1 ICP6mutant (Kan) FW	CCAGAAGTTGCTGATCGACCTGTGTGCGGACCGCGCCCCCGCUGCUGCUGCUAGCCAATCCATGACCCTGTATAGGGATAACAGGGTAATCGATTT
HSV-1 ICP6mutant (Kan) REV	CGTCCGCCTTCTCCGTGACATACAGGGTCATGGATTGGCTAGCAGCAGCAGCGGGGGCGCGGTCCGCACACAGCCAGTGTTACAACCAATTAACC
MCMV-M45mCherry (Kan) FW	GAGACGAGGGAACGCTCTGGGAC
MCMV-M45mCherry (Kan) REV	AGAGCAATAGAACTCGTTTTTTGGCGACGAGTTCGCCGGGGCCCTCTAGACTACTTGTACAGCTCGTCCATGC

7.5.3 CRISPR/Cas9 mutagenesis primers

The following primers were designed by Matteo Rizzato under my supervision.

Name	Sequence	Description
Guide RNA 1 FW	CACCGACTTATACATTGCATAGAG	CRISPR/Cas9
Guide RNA1 REV	AAACCTCTATGCAATGTATAAGT	CRISPR/Cas9
Guide RNA2 FW	ACCGATCTAAGTCAAAATGGAAG	CRISPR/Cas9
Guide RNA2 REV	AAACCTTCCATTTTGACTTAGAT	CRISPR/Cas9
Guide RNA3 FW	ACCGGGCATCCCAGACCACCAGC	CRISPR/Cas9
Guide RNA3 REV	AAACGCTGGTGGTCTGGGATGCC	CRISPR/Cas9
Guide RNA4 FW	ACCGATGAAATCTGAAAGCATGC	CRISPR/Cas9
Guide RNA4 REV	AAACGCATGCTTTCAGATTTCAT	CRISPR/Cas9
TBC1D5/gRNA1 FW	GGACATCGAAGATTAGGGTG	Genomic PCR
TBC1D5/gRNA1 REV	GCTACATGCGAAGACTTACAGC	Genomic PCR

TBC1D5/gRNA2 FW	GAGACTGCTGGATAGTGGCATAGC	Genomic PCR
TBC1D5/gRNA2 REV	GATCACGGAGTAAATTTGGTATC	Genomic PCR
TBC1D5/gRNA3 FW	CAGTGAATAACCTTAGAGGCTGTGC	Genomic PCR
TBC1D5/gRNA3 REV	GCATCTCGGATATAGAGTAGCATGGC	Genomic PCR
TBC1D5/gRNA4 FW	CGGTGGCCATGCTAAGTTTGTAC	Genomic PCR
TBC1D5/gRNA4 REV	GAGGTCAAGACTCAAGCGTTTG	Genomic PCR

7.6 Antibodies

7.6.1 Primary antibodies

Antigen	Clone	Species	Dilution	Reference
NEMO	EA2-6	mouse	WB 1:1000	MBL
M45	Kappa IgG2a	mouse	WB 1:50	Stipan Jonjic
HA	16B12	Mouse	WB 1:1000 IF 1:1000 IP 1:300	Covance Research
HA	3F10	Rat	WB 1:500 IF 1:500	Roche
Flag	M2	mouse	WB 1:2500 IF 1:500 IP 1:500	Sigma
RIPK1	38	mouse	WB 1:1000	BD Transduction Laboratories
Vps26B		Rabbit	WB 1:500	Y.H., Kim [207]
Vps26A	ab181352	Rabbit	WB 1:1000	Abcam
Vps29	ab51972	Goat	WB 1:1000	Abcam
Vps35	ab10099	Goat	WB 1:1000	Abcam
ß-actin	Ac-15	mouse	WB 1:10000	Sigma
GAPDH	14C10	rabbit	WB 1:1000	Cell Signaling
LC3B	D11	rabbit	WB 1:1000 IF 1:200	Cell Signaling
TBC1D5	E-9	mouse	WB 1:1000	Santa Cruz
MCMV IE1	Clone 4	mouse	WB 1:1000	Stipan Jonjic
c-myc	4A6	mouse	WB 1:2000 IF 1:500 IP 1:500	Millipore
HSP70	ab181606	rabbit	IF 1:50 WB 1:1000	Abcam
γ-Tubulin	T5326	mouse	IF 1:3000	Sigma
Caveolin-1	3267S	rabbit	IF 1:200	Cell Signaling
P62/SQSTM1	5114S	rabbit	WB 1:1000	Cell Signaling

ICP0	11060	mouse	WB 1:1000	Santa Cruz

7.6.2 Secondary antibodies

Antigen	Conjugate	Host	Dilution	Reference
Mouse Ig	HRP	Goat	WB 1:5000	DakoCytomation
Rabbit Ig	HRP	Goat	WB 1:5000	DakoCytomation
Mouse Ig	HRP	Goat	WB 1:5000	Jackson ImmunoResearch
Rabbit Ig	HRP	Goat	WB 1:5000	Jackson ImmunoResearch
Goat Ig	HRP	Donkey	WB 1:5000	Jackson ImmunoResearch
Mouse light chain Ig	HRP	Goat	WB 1:5000	Jackson ImmunoResearch
Rabbit light chain Ig	HRP	Goat	WB 1:5000	Jackson ImmunoResearch
Mouse IgG	Alexa 485	Goat	IF 1:1000	Invitrogen
Mouse IgG	Alexa 555	Goat	IF 1:1000	Invitrogen
Rabbit IgG	Alexa 485	Goat	IF 1:1000	Invitrogen
Rabbit IgG	Alexa 555	Goat	IF 1:1000	Invitrogen
Rat IgG	Alexa 485	Goat	IF 1:1000	Invitrogen
Rat IgG	Alexa 555	Goat	IF 1:1000	Invitrogen

7.7 Chemical and reagents

7.7.1 Antibiotics

Name	Working Concentration	Used for	Reference
Ampicillin	100 µg/ml	Selection of bacteria	Roth
Kanamycin	50 µg/ml	Selection of bacteria	Roth
Penicillin	100 µg/ml	cell culture supplement	PAA
Streptomycin	100 µg/ml	cell culture supplement	PAA
Chloramphenicol	15 µg/ml	Selection of bacteria	Roth
Zeocine	50 µg/mL	Selection of bacteria	ThermoFisher
Puromycin	5 µg/ml	Selection of transduced cells	Sigma-Aldrich

7.7.2 Enzymes

Name	Reference
Dream Taq Green DNA polymerase and buffer	Thermo Fisher Scientific
Fast alkaline phosphatase	Thermo Fisher Scientific
Fast Digest restriction enzymes and buffer	Thermo Fisher Scientific
PRECISOR DNA polymerase and buffer	BioCat
T4-DNA-ligase and buffer	Thermo Fisher Scientific

7.7.3 Receptor agonists

Name	Working concentration	Reference
Human Tumor Necrosis Factor α (TNF-α)	30 ng/mL	R&D Systems
GSK 872 (Ripk3 inhibitor)	5 µM	BioCat
Necrostatine-1 (Ripk1 inhibitor)	50 µM	Merck Chemicals
M z-VAD-FMK (pan-caspases inhibitor)	25 µM (h), 50 µM (m)	R&D Systems
Z-IETD-FMK (Caspase8 inhibitor)	75 µM	BioVision
BV6 SMAC mimetic (cIAP/XIAP Inhibitor)	1 µM	Selleckchem

7.7.4 Other reagents and chemicals

Name	Reference
Page Ruler Prestained Protein Ladder	Thermo Fisher Scientific
Gene Ruler 1 kb DNA Ladder	Thermo Fisher Scientific
Polyethylenimine (PEI), branched	Sigma Aldrich
PolyFect Transfection reagent	Qiagen
Lipofectamine	Life Technologies GmbH
Polybrene	Millipore
ECL Western Blotting Detection Reagents	GE Healthcare
Lumigen ECL Ultra (TMA-6)	Beckman Coulter
Pierce ECL Western Blotting Substrate	ThermoFisher
Protease Inhibitor Cocktail Complete Mini	Roche
Mounting-Medium	Polysciences

Albumin Fraction V pH 7.0 (BSA)	Applichen Panreac
Anti-HA Affinity Matrix (anti-HA rat, clone 3F10)	Roche
Protein A-Sepharose	GE-Healthcare
Protein G-Sepharose	GE-Healthcare
DMSO (dimethyl sulfoxide)	Roth
Nicodense	PROGEN
Metilcellulose	Sigma
Crystal Violet	Sigma
Bluebromophenole	Roth

7.8 Media

7.8.1 Cell culture media

Name	Reference
Dulbecco's Modified Eagle's Medium (DMEM) with glucose	Sigma - Aldrich
Dulbecco’s Phosphate Buffered Saline	Sigma - Aldrich
Trypsin-EDTA (1x)	Sigma - Aldrich
Fetal calf serum (FCS)	Pan Biotech GmbH
Earle's Balanced Salt Solution (EBSS)	Invitrogen
OptiMEM-I	Thermo Fisher Scientific
Penicillin/streptomycin (100x)	Sigma - Aldrich
Hepes	Life Technologies GmbH

7.8.2 Bacterial media

Name	Components	Reference
Luria Bertani (LB) liquid medium	1 % Bacto-tryptone	Roth
	0.5% YeastExtract	Roth
	0,5% NaCl	Roth
Luria Bertani (LB) agar medium	1 % Bacto-tryptone	Roth
	0.5% YeastExtract	Roth
	0,5% NaCl	Roth
	15 g/L Agar-Agar	

7.9 Buffers

7.9.1 Agarose gel electrophoresis

Name	Components	pH
50 X TAE buffer (used 1 X for pouring agarose gel and running buffer)	2M Tris-HCl 50 mM EDTA 5,7 % (v/v) acetic acid	8.0
10 X TBE buffer (used 0.5 X for pouring agarose gel and running buffer)	990 mM Tris-HCl 40 mM EDTA 990 mM boric acid	8.0

7.9.2 SDS polyacrylamide gel electrophoresis (SDS-Page) and Western Blot

Name	Components	pH
SDS-Resolving Gel (Tricine-System)	3M Tris-HCl 10 % or 15 % Acrylamide 50 % Glycerol 0.3 % SDS	8.45
SDS-Stacking Gel (Tricine System)	3M Tris-HCl 4% Acrylamide 0.3 % SDS	8.45
NP-40 lysis buffer	50 mM Tris-HCl 150 mM NaCl 1 % Nonidet P-40	7.5
2 X Sample Loading Buffer	125 mM Tris-HCl 4 % (v/v) SDS 20 % (v/v) glycerol 10 % ß-mercaptoethanol Bromophenol blue	6.8
5 X sample loading buffer	200 mM Tris-HCl 4 % (v/v) SDS 50 % (v/v) glycerol 10 % ß-mercaptoethanol	6.8

	Bromophenol blue	
10 X Anode Buffer (used 1 X for running polyacrylamide gels – Tricine System)	2 M Tris-HCl	8.9
10 X Cathode Buffer (used 1 X for running polyacrylamide gels – Tricine System)	1 M Tris	//
	1 M Tricin	
	1 % SDS	
10 X TBS-T Buffer (used 1X for antibody dilutions and washing nitrocellulose membranes)	100 mM Tris-HCl	7.5
	1.5 mM NaCl	
	1 % Tween 20	
Western Blot Transfer Buffer	50 mM Tris	//
	40 mM Glycin	
	0,04 % SDS	
	20 % Methanol	

7.9.3 Immunoprecipitation

Name	Components	pH
IP Washing Buffer 1	10 mM Tris-HCl	7.6
	150 mM NaCl	
	0.2 % Nonidet P-40	
	2 mM EDTA	
IP Washing Buffer 2	10 mM Tris-HCl	7.6
	500 mM NaCl	
	0.2 % Nonidet P-40	
	2 mM EDTA	
IP Washing Buffer 3	10 mM Tris-HCl	7.6

7.9.4 Immunofluorescence

Name	Components
Fixation Buffers	4% Paraformaldehyd in PBS or Ice cold Methanol or Ice cold Methanol/Acetone (50:50)

Quenching Buffer	50 mM NH4Cl in PBS
Permeabilization Buffer	0,3 % or 0,5 % Triton X-100 in PBS
Blocking Buffers	0,2 % Gelatine in PBS or TBS-BG buffer (Tris buffered saline with 5% glycine, 5% bsa. 0.05% Tween20 and 0.05% NaN3)

7.9.5 DNA preparation from bacteria ("Mini Scale")

Name	Components	pH
S1 Buffer	50 mM Tris-HCl	8.0
	100 µg/mL RNAse A	
	10 mM EDTA	
S2 Buffer	200 mM NaOH	//
	1 % (v/v) SDS	
S3 Buffer	2.8 M calcium acetate	5.2

7.10 Kits

Name	Reference
BCA Protein Assay Kit	Thermo Fisher Scientific
innuPREP DNA mini kit	Analytik Jena
mi-Plasmid Miniprep Kit	Metabion
NucleoBond Gel and PCR Clean-up	Macherey-Nagel
NucleoBond Xtra Midi	Macherey-Nagel
ProteoStat aggresome detecting reagent	Enzo
Cell Titer-Glo Luminescent Cell Viability Assay kit	Promega
Gibson Assembly Ultra Master Mix A and Mix B	Synthetic Genomics Inc.

7.11 Devices and equipment

Name	Reference
Fusion SL-4 3500 WL Molecular Imaging	Peqlab
NanoDrop ND-2000 Spectrophotometer	Peqlab
Confocal Nikon C1 Microscope	Nikon

Nikon A1 confocal laser scanning microscope (cLSM)	Nikon
Spinning Disk Nikon (Yokogawa W2 and Andor iXON888 cameras)	Nikon
Zeiss CLSM 510	Zeiss
Centrifuge 5414R	Eppendorf
Centrifuge 5810R	Eppendorf
Thermomixer comfort 5355	Eppendorf
Shaking incubator HT	Infors
Gene Pulser XCell	Bio-Rad
GelDoc XR	BioRad
Automatic Cell Counter TC10	Bio-Rad
Trans Blot Turbo Transfer System	Bio-Rad
Sterile Bench HeraSafe	Heraeus
Hera Cell CO2 incubator	Heraeus
Sorvall RC 6+ Centrifuge	Thermo Fisher Scientific

7.12 Bioinformatics tools

Name	Reference
CLC Main Workbench 7.7	QIAGEN Bioinformatics
Image Lab Software 5.2.1	Bio-Rad
Microsoft Office 2010	Microsoft
Adobe Photoshop CS5.1	Adobe Group
Nikon NIS software v4.51	Nikon
GraphPad Prism 5.03	GraphPad
NIH-ImageJ (Fiji) 1.52i	National Institutes of Health (NIH), (LOCI, University of Wisconsin)
MultAlin	F. Corpet. [208]
ENDscript	X. Robert,P. Gouet [209]
MOTIF	https://www.genome.jp/tools/motif/MOTIF2.html
E-CRISP design tool	http://www.e-crisp.org/E-CRISP

8 Methods

8.1 Molecular biology methods

8.1.1 Production of electrocompetent bacteria

E.coli strains DH10B and GS1783 have been used to produce electro-competent bacteria. For both, 2 to 5 ml of 10 ml overnight cultures were inoculated into 200 ml of warm LB medium and grown in an HT shaking incubator (Infors) stirring at 180 rpm and 30 ^{0}C (GS1783) or 37 ^{0}C (DH10B). When the exponential growth phase reached an OD_{600} between 0.5 and 0.6, the DH10B strain cultures were immediately cooled on ice for 20 minutes, while the cultures of the GS1783 strain were incubated at 42 ^{0}C for 15 minutes in order to induce recombinase expression, and then cooled down as well as the DH10B. The bacteria were pelleted by centrifugation at 4^0 C and 6000 *x g* for 10 minutes in an RC-6 centrifuge (Sorvall). The pellets were then washed twice with 100 ml of cold autoclaved and deionized water and once with 10 % cold and sterile glycerol. The pellet was then resuspended in 1.2 ml of 10 % cold and sterile glycerol and 120 µL aliquots were stored at -80^{0}C.

8.1.2 Bacterial transformation

The competent bacteria were transformed by electroporation. 60 µL of bacteria were thawed on ice and then mixed with either 150-200 ng of linear PCR amplified DNA or 1-10 ng of supercoiled plasmids or 2-4 µL of ligation products. After 15 minutes of incubation on ice the bacteria with the DNA suspension were transferred into 2 mm electroporation cuvettes and pulsed using the Gene Pulser XCell (BioRad) with the following settings: 2500 V, 25 µF and 200 Ω. Immediately after the pulse, 900 µL of warm medium was added to the bacteria and incubated on a Thermomixer comfort 5355 (Eppendorf) for 1 hour before being plated on LB agar for night incubation in a bacterial incubator. The DH10B bacteria were incubated at 37 ^{0}C while the GS1783 were incubated at 30 ^{0}C.

8.1.3 DNA isolation from bacteria

8.1.3.1 Small scale plasmid DNA and BAC-DNA preparation ("Mini Prep")

Plasmid DNA was isolated from a 3 ml overnight culture using the Mi-Plasmid MiniPrep Kit according to the manufacturing protocol.

BAC DNA was isolated from 5 ml of overnight culture using alkaline lysis and isopropanol precipitation as described [210]. 4 ml of the cultures were pelleted at 16,000 *x g* for 1 minute using a benchtop centrifuge 5415R (Eppendorf). The supernatant was discarded and the pellets were resuspended in 300 µL of S1 buffer. The lysis was performed by adding 300 µL of S2 buffer and was stopped after 5 minutes by adding 300 µL of S3 neutralisation buffer. The samples were incubated on ice for 7 minutes. The neutralization step leads to the formation of precipitates containing bacterial chromosomal DNA and proteins. In order to remove those to avoid contamination, samples were centrifuged for 20 minutes at 16,000 *x g* and 4 ^{0}C. The supernatant containing BAC-DNA was transferred to new tubes and precipitated using 640 µL (v/v) isopropanol and centrifuged at 15,000 *x g* for 30 minutes. The supernatants were then discarded and the pellets were washed with 500 µL of 70% ethanol. The ethanol was then removed and the samples dried at room temperature until they changed colour from white to transparent. BAC-DNA was finally resuspended in 50 µL of TE buffer.

8.1.3.2 *Medium scale plasmid DNA and BAC-DNA ("Midi-Prep")*

Plasmid DNA or BAC-DNA were prepared using 200 ml of bacterial cultures. The DNA was isolated using the NucleoBond Midi Xtra Kit according to the manufacturing protocol. For Plasmid DNA the high-copy protocol was used while for BAC-DNA the low-copy protocol was used. Plasmid DNA was eluted in 250-500 µL TE buffer, BAC-DNA was eluted in 150 µL TE buffer.

8.1.4 Polymerase chain reaction (PCR)

PCRs were performed by using either DreamTaq or Precisor Polymerases according to the manufacture protocol. DreamTaq polymerase was used for colony PCR while Precisor polymerase was used for cloning purposes.

8.1.5 Restiction digestion of DNA

DNA was digested using 1 µL FastDigest (FD) restriction enzymes in Fast Digest buffer for 45 min - 1h at 37 ºC according to the manufacturer's instructions. Plasmid vectors which were used in ligation reactions were additionally treated with Fast Akaline Phosphatase (AP) according to the manufacturer's protocol. For analytical plasmid and BAC-DNA digestion was used a concentration between 1 µg and 2 µg of DNA.

8.1.6 Agarose gel electrophoresis

PCR products and plasmid fragments were analyzed on agarose TAE gels for 1 hour at 120 V. The agarose percentage used was between 0.8 and 1.5 (w/v) according to the DNA fragment size. Digested BACs DNA were analyzed on 0.6 % (w/v) agarose TBE gels after overnight continuous run at 60 V. In both cases gels contained 0.5 µg/ml ethidium bromide and O'GeneRuler (ThermoFisher) was used as a size ladder. DNA bands were visualized by UV light using a GelDoc XR + (BioRad).

8.1.7 Purification of DNA fragments

DNA bands of interest were cut out from agarose gels while visualized on an UV transilluminator (Vilber) using a scalpel. DNA was then purified from the agar gel using a NucleoSpin Gel and PCR clean up kit according to the manufacturer's protocol. Concentration (OD_{260}) and purity (OD_{260}/OD_{280}) of DNA was measured using a NanoDrop-1000 (Peqlab) photometer. DNA was stored at 4 ºC for short-term periods or at – 80 ºC for long-term periods.

8.1.8 DNA ligation

Ligations were performed using T4-DNA-Ligase. Vector and insert were mixed in a molar ratio of 1:5 in a final volume of 20 µl. Ligation reactions contained T4 ligases, T4 Buffer 1X, vector and insert. The reaction was carried out for 1h at 22 ºC or overnight at 16 ºC.

8.1.9 DNA sequencing

All Plasmid DNA and PCR products were sequenced by Microsynth SeqLab (Maschmühlenweg 36, 37081, Göttingen, Germany) using the Barcode Economy Run service. MCMV or HSV-1 BACs were sequenced by the HPI's Technology Platform facility.

8.1.10 *En Passant* BAC mutagenesis

Mutation of BACs using en passant was performed as previously described by Tischer and colleagues [211]. Shortly, a linear DNA fragment containing the I-SceI-aphAI-cassette and a duplicate of the region of interest containing the wanted mutation was generated by PCR using as a template the pEP-Kan-S plasmid or Zeocin plasmid. Alternatively a shuttle plasmid was used.

After purification 150 ng of the PCR products were used to transform in GS1783 carrying either the MCMV-M45HA BAC or HSV-1 F strain BAC. Transformed bacteria were then spread on LB agar plates containing chloramphenicol and either kanamycin or zeocin and incubated overnight at 30 °C. Resulting bacterial clones were checked via enzymes restriction digestion, analytical PCR, colony PCR and sequencing. Positive clones were then used for the second recombination procedure. Second recombination requires expression of recombinases such as I-SceI, which was induced by the addition of 2 % (w/v) L-arabinose and by incubation at 42 °C. Recombination bacteria were then plated on LB agar containing 1 % L-arabinose and chloramphenicol. Resulting bacterial clones were checked for loss of kanamycin resistance as well by enzyme restriction digestion, analytical PCR and sequencing. Positive clones were outgrown in 200 ml liquid culture for BAC Midi Prep. For the construction of MCMV Δm157 no second recombination was used.

8.1.11 Gibson assembly

The shuttle plasmid used for the BAC mutagenesis of MCVM-M45mCherry was generated by Gibson assembly. For this purpose, a pcDNA carrying the M45HA sequence was digested with Eco8lI and ApaI restriction enzymes in order to cut the C-terminus portion of M45 containing the HA tag and the STOP codon. Then, three different DNA fragments containing ~20 bp overlapping sequence with the adjacent DNA fragments were amplified by PCR amplified: i) fragment containing the remaining C-terminal part of M45 without HA tag and STOP; ii) fragment containing the selection marker (kan) and the homology sequence for the second recombination of BAC mutagenesis; iii) fragment containing mCherry. After gel purification, the fragments were ligated following the Gibson Assembly Ultra Master Mix A and Mix B manufacturing instructions.

8.2 Cell biology and virology methods

8.2.1 Cell culture

Human and murine cell lines were maintained in 10 or 15 cm_2 culture dishes in DMEM supplemented with 5 or 10 % FCS and 1 % penicillin/streptomycin. All cells were incubated in a Hera Cell CO2 incubator (Heraeus) at 37 °C, 80 % relative humidity and 5 % CO_2. All work was done using a sterile bench (HeraSafe, Heraeus). Cells were passaged at 80 or 90% of confluence by removing the media, washing 1X with PBS and by adding 3 mL of trypsin. The trypsin was then neutralized with double the volume of FCS supplemented medium and split 1:3 to 1:10.

For freezing the cells, they were transferred into a 15 mL tube and centrifuge for 10 min using 500 *x g*, 37 °C. The supernatant was removed and the cells was re-suspended in freezing media containing 90 % FCS and 10 % DMSO in order to prevents mechanical damage to the cells due to the freezing process. The tube were stored at -80 °C for a couple of weeks and then transferred to liquid nitrogen.

For thawing the cells, they were kept shortly at 37 °C in the water bath and then suspended gently in 6 mL of complete media. After a centrifugation at 37 °C for 10 min using 500 *x g* and they were transferred in a 10 cm_2 dish containing 10 mL of fresh media.

Cells number was determined by counting 10 µL of cell suspension using an automated cell counter (TC10, Bio-Rad).

8.2.2 Transfection of plasmid DNA

Cells were transfected with exogenous DNA using different approaches according their susceptibility to transfection. HEK-293A and T and Phoenix cells were transfected using PEI. 3x10^{6} cells were seeded on 10 cm^{2} dishes and transfected using 8 µg of plasmid DNA (pcDNA3). The plasmid and PEI (32µL considering a ration with the DNA of 1:4) were first re-suspended in separate tubes in 100 µL of DMEM without supplements. After 5 min they were mixed together and delivered to the cells after a pre-incubation of 20 minutes. NIH-3T3 fibroblasts or MEFs were transfected by using Lipofectamine. 0.5 or 1 x 10^{5} cells were seeded in a 12-wells plate and transfected using 1.5 µg DNA. The DNA and the lipofectamine were first re-suspended in separates tubes in 50 µL OptiMem media and then mixed together and incubated 10 minutes at RT. Afterwards 500 µL of complete media was added to the mix and the DNA with the transfection reagent was delivered to the cells.

8.2.3 Transfection of BAC DNA

MCMV or HSV-1 BACs DNA were transfected into eukaryotic cells in order to reconstitute the viruses. For MCMV the reconstitution was performed in NIH-3T3 or RIPK3$^{-/-}$ MEFs while for HSV-1 was performed in VERO cells. 1x10^{5} cells were seeded in a 6-well plate and after overnight incubation they were transfected using 3 µg DNA and 10 µL Polyfectamine. The DNA and the polyfectamine were re-suspended separatelly in 100 µL DMEM without supplements and after 5 minutes of incubation at RT were mixed together by using a pipette and incubated for 15 minutes at RT. Afterwards 500 µL of complete media was added to the mix and the DNA with the transfection reagent was delivered to the cells. When the cells reached 90% of confluence were transferred into a 15 cm^{2} dish and the reconstitution of MCMV and HSV-1 was monitored and documented by detection of CPEs.

8.2.4 MCMV stock production and titration

MCMV WT and mutants were grown and titrated on NIH-3T3, RIPK3$^{-/-}$or M2-10B4 cells. 2x10^{6} cells were infected at a MOI of 0.025 and the supernatant was collected 3 days and 5 days post infection. Cell debris were removed after 15 min centrifugation at 6000 *x g* and the viral supernatant was pelleted again by centrifugation at 13000 *rpm* and 4°C for 4h. The viral pellet was resuspended overnight by adding 500 µL of complete media. Optionally a second step of ultracentrifugation was performed using 18 mL of 10% nicodense as cushion and centrifuging the virus at 27,100 *rpm* for 1h. The nicodense was removed and the virus pellet was resuspended in 500 µL of complete media. For *in vivo* experiments the virus pellet was re-suspended in PBS. After overnight re-suspension the virus was aliquoted and stored at -80 °C. Titration was performed in NIH-3T3, RIPK3$^{-/-}$or M2-10B4 cells using two different approaches.

The median tissue culture infective dose (TCID$_{50}$) method represents the virus concentration at which half of the cells show cytopathic effect (CPE). It was performed by seeding 2x10^3 cells per well (100µL of media per well) in a 96 well plate and incubated overnight. For each virus were prepared 6 plates. On the next day serial log$_{10}$ dilutions (from 10^{-3} up to 10^{-10}) of the virus were prepared in 4 mL DMEM containing 10% FCS and antibiotics. All the dilutions were done in triplicates which were in turn spotted in two different plates (100 µL / well). One of the two plates of each replicate was then centrifuged at 2300 *rpm* and 37 °C for 30 min in order to determine the titer after centrifugation enhancement [212]. Five up to six days post titration the virus titer was determined using the formula of Spearman (1908) and Kaerber (1931) [213]:

$$Titer = \frac{TCID50}{ml} = \frac{10^{\frac{1}{2}-lg(x)+\frac{y}{z}}}{V}$$

x= highest dilution wit 100% CPE
y = sum of the wells with CPE from x
z = number of wells per dilution stage
V = volume of infection

The Plaque Assay approach was used in order to determine the titer for *in vivo* experiments [214]. This method determines the number of plaque forming units (pfu) in a virus sample. A virus plaque is formed when a virus infects a cell and spread to adjacent cells. The infected area will create a plaque. The pfu / mL result represents the number of infective particles within the sample and is based on the assumption that each plaque formed is representative of one infective virus particle. 4 x 10^4 M2-10B4 cells were seeded on a 48 well-plate and infected and infected the next day with serial log$_{10}$ dilutions prepared in DMEM supplemented with 3% FCS and antibiotics. 100 µL of each log$_{10}$ dilution was added to one well and after 2-3h of incubation at 37 °C 300 µL of methylcellulose were added to each well in order to prevent the formation of a secondary plaque. After 4 days the titer was calculated according to the formula:

$$Titer = \frac{pfu}{ml} = number\ of\ plaques\ x\ V$$

V = dilution factor

8.2.5 HSV-1 stock production and titration

HSV-1 WT and mutant were grown and titrated in VERO cells. For preparing a virus stock, 15 x 10_6 VERO cells were plated in a T175 cm_2 flask (1 to 3 per virus). The next day the cells were washed 1 X with PBS and infected at a MOI of 0,005 PFU in 10 mL of DMEM containing 1% FCS and 1% antibiotics. After 1 h of incubation on a rotating shaker at 37 ºC, the supernatant was removed and 23 mL of DMEM containing 5% FCS and antibiotics were added. Three days post infection the supernatant and the cells (removed from the flask with the help of a scraper) were transferred in a 50 mL falcon and 3 cycles of freezing (-80ºC) and thawing (4 ºC) were performed. Afterwards, the cell debris were removed by centrifuging at 4000 rpm at 4 ºC for 30 minutes and the virus was pelleted by ultracentrifugation at 20.000 *rpm* and 4 ºC for 1 h and 30 min using 5 mL of 35% sucrose as cushion. Then the supernatant was discarded and the virus re-suspended in DMEM containing 10% FCS and antibiotics. Aliquos were stored at -80 ºC.

The virus was titrated in VERO cells and determined by calculating the pfu according to the formula described above. 1.7 x 10_5 VERO cells were plated in a 12 well-plate and after overnight incubation they were infected with log_{10} serial dilution (10_{-4} up to 10_{-7}) prepare in DMEM containing 1% FCS. Each dilution was done in triplicates and prepared in a final volume of 1 mL. 100 µL of virus dilution was added to the cells and on top 150 µL on DMEM containing 1% FCS were added in order to avoid drying out them. Cells were incubated 1 h at 37 ºC on a shaker, afterwards the inoculum was removed and 1 mL of methylcellulose was added to each well in order to prevent the formation of a secondary plaque. Three days post infection the methylcellulose was removed from the wells and the plaques were visualized by crystal violet staining.

8.2.6 Viral infections

Cells were infected with MCMV using different multiplicities of infection (MOI) based on the TCID$_{50}$/ml of a virus stock. Cells were infected with HSV-1 using MOI based on the pfu/mL of a virus stock. To determine the volume of virus stock needed to infect cells at a given MOI the following equation was used:

$$\frac{number\ of\ cells\ \times MOI}{TC1D50\ or\ pfu\ /\ ml} = volume\ of\ virus\ stock\ in\ ml$$

8.2.7 Viral kinetics

For replication kinetics 2.5 x 10^5 cells were seeded in 6-well dishes. MCMV infection was performed at a MOI of 5 followed by centrifugation enhancement. HSV-1 infection was performed at a MOI of 1 or 3 in minimal volume of DMEM + 1% FCS and shaking for 1 h. After the media was removed and fresh DMEM + 10% FCS was added. Cells were harvested at different time post infection.

8.2.8 Viral DNA extraction

DNA was isolated from virus stocks by using the innuPrep-DNA Mini Kit according to the manufacturing instructions. DNA was stored at 4 ^{0}C for short time or at -20 ^{0}C for long time.

8.2.9 Cell viability assay

5x10^3 murine SVEC4-10 endothelial cells were seeded in 96-well plates and infected with MCMV at a MOI of 5 TCID$_{50}$/cell in 100 µL media. Cell viability was determined at 24 hpi by measuring intracellular ATP levels with a Cell Titer-Glo Luminescent Cell Viability Assay kit (Promega) and a FLUOstar Omega luminometer (BMG Labtech). Cell death inhibitors Z-VAD-FMK (R&D Systems), GSK'872 (Merck), or DMSO (as control) were added 1 h prior to infection and remained on the cells for the duration of the assay. Significance was calculated using one-way ANOVA. Viability of human HT-29 cells was determined essentially as described. 5x10^3 cells were seeded in 96-well plates and infected with HSV-1 at an MOI of 5 PFU/cell in DMEM containing 1% FCS. Two hpi the inoculum was removed and the cells were treated with 30 ng/mL TNF-α (R&D Systems), 1 µM BV6 (Selleckchem), and 25 µM Z-VAD-FMK. Cell death inhibitors Necrostatin-1 (50 µM, BioCat), GSK'872 (5 µM), Z-IEDT-FMK (75 µM, Biovision), or DMSO (as control) were added at the indicated concentrations. Cell viability was determined 24 hpi as described above.

8.2.10 CRISPR/Cas9 mutagenesis

The lentiviral CRISPR/Cas9 vector pSicoR-CRISPR-PuroR was used to generate *Tbc1d5* knockout MEF clones essentially as described [215]. Four guide RNAs were cloned individually in the lentiviral vector: g1, 5'-ACCGACTTATACATTGCATAGAG-3'; g2, 5'-ACCGATCTAAGTCAAAATGGAAG-3'; g3, 5'-ACCGGGCATCCCAGACCACCAGC-3'; g4, 5'-ACCGATGAAATCTGAAAGCATGC-3'. Lentiviruses were generated using standard third-generation packaging vectors in HEK-293T cells. WT MEFs were transduced with *Tbc1d5*-targeting or empty lentiviral CRISPR/Cas9 vectors in the presence of polybrene (Sigma). The cells were selected with 2 µg/mL puromycin (Sigma). Polyclonal cultures were subculture to obtain single cell clones for each gRNA, and TBC1D5 protein expression was evaluated for each clone by immunoblot analysis. This method was performed by Matteo Rizzato under my supervision.

8.3 Biochemistry methods

8.3.1 Cell lysis for immunoblotting and immunoprecipitation

For protein analysis of the whole cell lysates, cells were washed 2X with PBS and lysed in boiling 2x SDS-PAGE sample for 10 minutes. For the separation of detergent-soluble and insoluble fractions, cells were first lysed for 30 min at 4 ºC with NP-40 lysis buffer supplemented with cOmplete Mini Protease Inhibitor Cocktail (Roche). The soluble (supernatant) and insoluble (pellet) factions were then obtained by centrifugation of the lysate for 10 min at 16000 *x g*. Both fractions were then boiled in SDS-PAGE sample buffer (5X for the soluble fraction and 2X for the insoluble fraction). The samples were stored at -20 ºC for maximum two months.

8.3.2 SDS polyacrylamide gel electrophoresis (SDS-Page) and immunoblot

Proteins were separated according their molecular weight by using a lysis buffer containing sodium dodecyl sulfate (SDS) and 2-mercaptoethanol (beta-mercaptoethanol/BME). The protein separation occurred into a polyacrylamide gel formed by two different phases: stacking gel (loading gel) containing 4 % of acrylamide and resolving gel (separation gel) containing 10-15 % of acrylamide. The run was performed at 60-100 V until the samples, visualized by the addition of Bluebromophenole, reached the end of the gel. Two buffers were optionally used for the run according to the setting of the experiment: for the Glycine-system was used the Lämmli running buffer. For the Trycine-system anode and cathode buffers were used. Protein Ruler was used as a size ladder.

After SDS-Page, the gel was equilibrated into the transfer buffer for 10 min. Then the proteins were transferred into a nitrocellulose or polyvinylidenedifluoride (PVDF) membrane by using Trans Blot Turbo Transfer System (BioRad) for 60-90 min at 100 mA per gel. Afterwards, nonspecific antibody binding sites were blocked by incubating the membrane for 1 hour in 5 % milk powder or 5 % BSA powder dissolved in TBS-T buffer. Afterwards, the membrane was incubated with the primary antibody overnight on a shaking platform at 4 °C.

On the next day, the membrane was washed three times for 5 min with TBS-T and incubated with 10 ml of a 1: 5000 dilution of the secondary antibody (anti-mouse-HRP or anti-rabbit-HRP) for one hour. After 3X washing in TBS-T, the chemiluminescent signal was detected by adding the enhanced chemiluminescence solution (GE Healthcare) and imaged using a Fusion Capture Advance FX7 16.15 (Peqlab) device or by X-ray film.

8.3.3 (Co-) Immunoprecipitation

Co-IP was performed after co-transfection in HEK 293A cells. At day 1, $3x10_6$ cells were seeded in 10 cm dishes. On day 2, cells were transfected with the respective constructs by using 32 µg PEI and 8 µg total plasmidic DNA, as previously described. 20-24 hours post transfection, cells were washed twice with PBS and lysed with NP-40 buffer provided with protease inhibitors. Lysates were collected in 1.5 tubes with the help of a cell scraper and incubated on ice for 30 minutes. In parallel, Protein G-sepharose (PGS) or Protein A-sepharose (PAS) were washed three times in the selected lysis buffer (NP-40). Lysates were then centrifuged at full speed for 10 minutes at 4 °C. Supernatant was recollected and the pelleted cell debris discarded. 100 µL of the whole cell lysate (WCL) was collected and mixed with Lämmli buffer 2X in a 1:1 ratio and boiled at 95 °C for 10 minutes. The remaining supernatant was pre-cleared with PGS/PAS beads for at least one hour on a rotating platform. After pre-clearing, PGS/PAS beads were removed by centrifugation, and the supernatant was incubated overnight at 4 °C with the corresponding antibody. On day 3, PGS/PAS beads were added to the protein-antibody containing solution, and incubated for 2 hours at 4 °C on a rotating platform. Alternatively, HA-tagged proteins were pulled-down with anti-HA affinity matrix (Roche). After incubation, samples were spun down and washed three times with IP Washing buffer 1, two times with IP Washing buffer 2 and once with IP Washing buffer 3. After removing all traces of buffers with vacuum pump, beads were treated with Lämmli buffer 2X, boiled at 95 °C for 10 minutes, spun down and the supernatant was recollected, representing the IP sample. Samples were analyzed by Western Blot.

8.4 Microscopy methods

8.4.1 Live cell imaging and fluorescence recovery after photo bleaching (FRAP)

For live imaging of aggregate, $1x10_6$ NIH-3T3 cells were cultured in a µ-Dish 35 mm (ibidi) and transfected with a plasmid encoding M45-mCherry. 6 h post transfection the medium was removed and the cells were placed in a Nikon spinning disc system consisting of Yokogawa W2 and Andor iXON888 cameras. A Nikon 100x 1.49 NA Apo-TIRF objective was used resulting in 130 nm pixel size and 11 z-stacks were recorded for 30 hours. For FRAP, NIH-3T3 cells were transfected with plasmids encoding M45 or M45-derived polypeptides fused to mCherry. mCherry-Nucleolin was used as negative control. At least 30 h post transfection mCherry fluorescence was detected by live cell imaging using a Nikon A1 confocal microscope. Red-fluorescent dots with a diameter ≥1 µm were selected for FRAP analysis. FRAP analysis was performed by bleaching an area of 1 µm for 2 sec with a 563 laser. Recovery of fluorescence of at least 10 different cells per sample was recorded at 1 frames/second for 6 minutes. The fluorescence intensity of an unbleached point was also measured under the same conditions. The average of all data sets for each time point was normalized to the background and the relative fluorescence intensity (RFI) was calculated according to the formula: RFI = $(Ae_t/A1_1)/(Ae_0/A1_0)$ as described before [216]. Briefly, Ae_t is the average intensity of the bleached area at various time points after photobleaching. $A1_1$ is the average intensity of the control unbleached area in the same cell at the corresponding time points. Ae_0 is the average intensity of the bleached area before bleaching. $A1_0$ is the average intensity of a control unbleached area in the same cell before bleaching. When $Ae_0/A1_0$ equals $Ae_t/A1_1$ (RFI = 1), the fluorescence recovery is 100%.

8.4.2 Immunofluorescence

Cells were seeded on coverslips (pre-treated with 0.4 % Gelatin for 30 min at 37 °C) or on µ-Slide 8 well chamber slides (ibidi). Next day, cells were infected or transfected with designated viruses or plasmids. Afterwards, cells were washed twice with PBS and fixed with paraformaldehyde (PFA) or ice cold methanol or ice cold methanol/acetone (accordingly to the datasheet of the primary antibody) for 20 minutes.

Then cells were washed twice with PBS, and the free aldehyde groups were neutralized by using 50 mM NH4Cl (in PBS) for 10 min at RT. After two washes with PBS, the cells were permeabilized for 10 min at RT with 1 ml 0.3 – 0.5 % TritonX-100 (in PBS). Blocking of unspecific antibody binding sites was performed for at least 20 min at RT by adding 0.2 % gelatin or TBS-BG blocking buffer. The incubation with primary antibody diluted in PBS was done for 1 h at RT, samples were then washed 2X with PBS, one time with 0.1 % Tween (in PBS), and the Alexa-secondary antibody was added (in PBS) according to its final concentration. After 2X washing with PBS, the nuclei were stained by using DRAQ5 (1:1000 in H2O) for 10 min at RT or Hoechst (1:1000 in PBS) for 30 min at RT. Then samples were washed 3 times with PBS and 3 times with water. For coverslips, one drop of mounting medium was poured on a glass slide and the cover slips were mounted onto them and left overnight.

Intracellular aggregates were stained with ProteoStat fluorescent red dye (Enzo Life Science) as described in the instruction manual. Quantification of aggregates was done by acquiring 0.25 µm z-stacks of at least 20 cells and evaluation using maximum intensity projection. Co-localizating red (ProteoStat) and green (viral protein) fluorescent dots were counted. Cells with >100 dots were considered uncountable and scored as 100. Significance was calculated using the Student's *t*-test.

Fluorescence images were acquired using a Nikon C2 or a Nikon A1 confocal laser scanning microscope (cLSM).

8.4.3 Correlative light and electron microscopy (CLEM)

WT and *Atg5*$_{-/-}$ MEFs were cultured and infected with MCMV-M45mCherry at a MOI of 1.5 in dishes with imprinted grids (Ibidi). Fluorescence signals of M45mCherry, BODIPY 493/503 (4,4-Difluoro-1,3,5,7,8-Pentamethyl-4-Bora-3a,4a-Diaza-s-Indacene; ThermoFisher), and Hoechst 33342 (ThermoFisher) as well as DIC were acquired with a Nikon A1 cLSM, deconvolved with Nikon NIS-Elements v.4.51 and later used for re-localization of morphological features in TEM Images. The samples were processed for TEM as it was previously described [217].

8.5 Animal experiment

Animal experiments were performed according to the recommendations and guidelines of the Federation for Laboratory Animal Science Associations (FELASA) and Society of Laboratory Animals (GV-SOLAS) and approved by the institutional review board and local authorities (Behörde für Gesundheit und Verbraucherschutz, Amt für Verbraucherschutz, Freie und Hansestadt Hamburg, reference number 017/2019). C57BL/6 Rip3K51A/K51A mice were kindly provided by Jannice Connor, John Bertin (GSK, Collegeville, PA), and Edward Mocarski (Emory University, Atlanta, GA). Six to 8 week-old female mice were infected intraperitoneally with 105 PFU MCMV per mouse as described [35]. Spleens were harvested on day 3 post infection, homogenized, and used to determine organ titers by plaque assay on Ripk3-/- MEFs cells. Statistical significance was assessed using the Mann-Whitney test.

9 References

1. Davison, A.J., et al., *The order Herpesvirales*. Arch Virol, 2009. **154**(1): p. 171-7.
2. David M. Knipe, P.M.H., ed. *Fields Virology*. ed. B.R. Philip E. Pellett. Vol. 2 - Chapter 66. 2006, Lippincott Williams & Wilkins.
3. Cannon, M.J., D.S. Schmid, and T.B. Hyde, *Review of cytomegalovirus seroprevalence and demographic characteristics associated with infection*. Rev Med Virol, 2010. **20**(4): p. 202-13.
4. Riley, H.D., Jr., *History of the cytomegalovirus*. South Med J, 1997. **90**(2): p. 184-90.
5. Cannon, M.J., T.B. Hyde, and D.S. Schmid, *Review of cytomegalovirus shedding in bodily fluids and relevance to congenital cytomegalovirus infection*. Rev Med Virol, 2011. **21**(4): p. 240-55.
6. Kenneson, A. and M.J. Cannon, *Review and meta-analysis of the epidemiology of congenital cytomegalovirus (CMV) infection*. Rev Med Virol, 2007. **17**(4): p. 253-76.
7. Britt, W., *Manifestations of human cytomegalovirus infection: proposed mechanisms of acute and chronic disease*. Curr Top Microbiol Immunol, 2008. **325**: p. 417-70.
8. Deayton, J.R., et al., *Importance of cytomegalovirus viraemia in risk of disease progression and death in HIV-infected patients receiving highly active antiretroviral therapy*. Lancet, 2004. **363**(9427): p. 2116-21.
9. Lumbreras, C., et al., *Cytomegalovirus infection in solid organ transplant recipients*. Clin Microbiol Infect, 2014. **20 Suppl 7**: p. 19-26.
10. Atabani, S.F., et al., *Cytomegalovirus replication kinetics in solid organ transplant recipients managed by preemptive therapy*. Am J Transplant, 2012. **12**(9): p. 2457-64.
11. Grundy, J.E., et al., *Symptomatic cytomegalovirus infection in seropositive kidney recipients: reinfection with donor virus rather than reactivation of recipient virus*. Lancet, 1988. **2**(8603): p. 132-5.
12. Pass, R.F., et al., *Congenital cytomegalovirus infection following first trimester maternal infection: symptoms at birth and outcome*. J Clin Virol, 2006. **35**(2): p. 216-20.
13. Reynolds, D.W., et al., *Maternal cytomegalovirus excretion and perinatal infection*. N Engl J Med, 1973. **289**(1): p. 1-5.
14. Stagno, S., et al., *Maternal cytomegalovirus infection and perinatal transmission*. Clin Obstet Gynecol, 1982. **25**(3): p. 563-76.
15. Stagno, S., et al., *Congenital cytomegalovirus infection: consecutive occurrence due to viruses with similar antigenic compositions*. Pediatrics, 1973. **52**(6): p. 788-94.
16. Stagno, S., et al., *Breast milk and the risk of cytomegalovirus infection*. N Engl J Med, 1980. **302**(19): p. 1073-6.
17. Carlson, A., E.R. Norwitz, and R.J. Stiller, *Cytomegalovirus infection in pregnancy: should all women be screened?* Rev Obstet Gynecol, 2010. **3**(4): p. 172-9.
18. Ahmed, A., *Antiviral treatment of cytomegalovirus infection*. Infect Disord Drug Targets, 2011. **11**(5): p. 475-503.
19. El Helou, G. and R.R. Razonable, *Letermovir for the prevention of cytomegalovirus infection and disease in transplant recipients: an evidence-based review*. Infect Drug Resist, 2019. **12**: p. 1481-1491.
20. Tan, B.H., *Cytomegalovirus Treatment*. Curr Treat Options Infect Dis, 2014. **6**(3): p. 256-270.
21. Gibson, W., *Structure and formation of the cytomegalovirus virion*. Curr Top Microbiol Immunol, 2008. **325**: p. 187-204.
22. Brocchieri, L., et al., *Predicting coding potential from genome sequence: application to betaherpesviruses infecting rats and mice*. J Virol, 2005. **79**(12): p. 7570-96.

23. Murphy, E. and T. Shenk, *Human cytomegalovirus genome*. Curr Top Microbiol Immunol, 2008. **325**: p. 1-19.
24. Kalejta, R.F., *Tegument proteins of human cytomegalovirus*. Microbiol Mol Biol Rev, 2008. **72**(2): p. 249-65, table of contents.
25. Kalejta, R.F., *Functions of human cytomegalovirus tegument proteins prior to immediate early gene expression*. Curr Top Microbiol Immunol, 2008. **325**: p. 101-15.
26. McCormick, A.L., et al., *The Human Cytomegalovirus UL36 Gene Controls Caspase-Dependent and -Independent Cell Death Programs Activated by Infection of Monocytes Differentiating to Macrophages*. J Virol, 2010. **84**(10): p. 5108-5123.
27. Xuan, B.Q., et al., *Human Cytomegalovirus Protein pUL38 Induces ATF4 Expression, Inhibits Persistent JNK Phosphorylation, and Suppresses Endoplasmic Reticulum Stress-Induced Cell Death*. J Virol, 2009. **83**(8): p. 3463-3474.
28. Fu, Y.Z., et al., *Human Cytomegalovirus Tegument Protein UL82 Inhibits STING-Mediated Signaling to Evade Antiviral Immunity*. Cell Host Microbe, 2017. **21**(2): p. 231-243.
29. Bechtel, J.T. and T. Shenk, *Human cytomegalovirus UL47 tegument protein functions after entry and before immediate-early gene expression*. J Virol, 2002. **76**(3): p. 1043-1050.
30. Isaacson, M.K. and T. Compton, *Human cytomegalovirus glycoprotein B is required for virus entry and cell-to-cell spread but not for virion attachment, assembly, or egress*. J Virol, 2009. **83**(8): p. 3891-903.
31. Vanarsdall, A.L. and D.C. Johnson, *Human cytomegalovirus entry into cells*. Curr Opin Virol, 2012. **2**(1): p. 37-42.
32. Farrar, G.H. and J.D. Oram, *Characterization of the human cytomegalovirus envelope glycoproteins*. J Gen Virol, 1984. **65 (Pt 11)**: p. 1991-2001.
33. Smith, M.G., *Propagation in Tissue Cultures of a Cytopathogenic Virus from Human Salivary Gland Virus (Sgv) Disease*. Proceedings of the Society for Experimental Biology and Medicine, 1956. **92**(2): p. 424-430.
34. Podlech, J., et al., *Animal models: Murine cytomegalovirus*. Immunology of Infection, Second Edition, 2002. **32**: p. 493-525.
35. Brune, W., H. Hengel, and U.H. Koszinowski, *A mouse model for cytomegalovirus infection*. Curr Protoc Immunol, 2001. **Chapter 19**: p. Unit 19 7.
36. Brizic, I., et al., *Cytomegalovirus Infection: Mouse Model*. Curr Protoc Immunol, 2018: p. e51.
37. Sinzger, C., M. Digel, and G. Jahn, *Cytomegalovirus cell tropism*. Curr Top Microbiol Immunol, 2008. **325**: p. 63-83.
38. Sinzger, C. and G. Jahn, *Human cytomegalovirus cell tropism and pathogenesis*. Intervirology, 1996. **39**(5-6): p. 302-19.
39. Sinclair, J., *Human cytomegalovirus: Latency and reactivation in the myeloid lineage*. J Clin Virol, 2008. **41**(3): p. 180-5.
40. Sinclair, J. and P. Sissons, *Latency and reactivation of human cytomegalovirus*. J Gen Virol, 2006. **87**(Pt 7): p. 1763-79.
41. Ryckman, B.J., et al., *Human cytomegalovirus entry into epithelial and endothelial cells depends on genes UL128 to UL150 and occurs by endocytosis and low-pH fusion*. J Virol, 2006. **80**(2): p. 710-22.
42. Zhou, M., J.M. Lanchy, and B.J. Ryckman, *Human Cytomegalovirus gH/gL/gO Promotes the Fusion Step of Entry into All Cell Types, whereas gH/gL/UL128-131 Broadens Virus Tropism through a Distinct Mechanism*. J Virol, 2015. **89**(17): p. 8999-9009.
43. Gibson, W., *Structure and assembly of the virion*. Intervirology, 1996. **39**(5-6): p. 389-400.
44. Irmiere, A. and W. Gibson, *Isolation and characterization of a noninfectious virion-like particle released from cells infected with human strains of cytomegalovirus*. Virology, 1983. **130**(1): p. 118-33.

45. Tandon, R., E.S. Mocarski, and J.F. Conway, *The A, B, Cs of Herpesvirus Capsids*. Viruses-Basel, 2015. **7**(3): p. 899-914.
46. Jean Beltran, P.M. and I.M. Cristea, *The life cycle and pathogenesis of human cytomegalovirus infection: lessons from proteomics*. Expert Rev Proteomics, 2014. **11**(6): p. 697-711.
47. Boo, K.H. and J.S. Yang, *Intrinsic cellular defenses against virus infection by antiviral type I interferon*. Yonsei Med J, 2010. **51**(1): p. 9-17.
48. Akira, S. and H. Hemmi, *Recognition of pathogen-associated molecular patterns by TLR family*. Immunol Lett, 2003. **85**(2): p. 85-95.
49. Gay, N.J., et al., *Assembly and localization of Toll-like receptor signalling complexes*. Nature Reviews Immunology, 2014. **14**(8): p. 546-558.
50. Barton, G.M. and R. Medzhitov, *Toll-like receptors and their ligands*. Toll-Like Receptor Family Members and Their Ligands, 2002. **270**: p. 81-92.
51. Medzhitov, R., *Toll-like receptors and innate immunity*. Nat Rev Immunol, 2001. **1**(2): p. 135-45.
52. Gilmore, T.D., *Introduction to NF-kappaB: players, pathways, perspectives*. Oncogene, 2006. **25**(51): p. 6680-4.
53. Hayden, M.S., A.P. West, and S. Ghosh, *NF-kappaB and the immune response*. Oncogene, 2006. **25**(51): p. 6758-80.
54. West, A.P., A.A. Koblansky, and S. Ghosh, *Recognition and signaling by toll-like receptors*. Annu Rev Cell Dev Biol, 2006. **22**: p. 409-37.
55. Yamamoto, M., et al., *Role of adaptor TRIF in the MyD88-independent toll-like receptor signaling pathway*. Science, 2003. **301**(5633): p. 640-3.
56. Yamamoto, M., et al., *Essential role for TIRAP in activation of the signalling cascade shared by TLR2 and TLR4*. Nature, 2002. **420**(6913): p. 324-9.
57. Yamamoto, M., et al., *TRAM is specifically involved in the Toll-like receptor 4-mediated MyD88-independent signaling pathway*. Nat Immunol, 2003. **4**(11): p. 1144-1150.
58. Rhyasen, G.W. and D.T. Starczynowski, *IRAK signalling in cancer*. Br J Cancer, 2015. **112**(2): p. 232-7.
59. Cusson-Hermance, N., et al., *Rip1 mediates the Trif-dependent toll-like receptor 3- and 4-induced NF-{kappa}B activation but does not contribute to interferon regulatory factor 3 activation*. J Biol Chem, 2005. **280**(44): p. 36560-6.
60. Walsh, M.C., J. Lee, and Y. Choi, *Tumor necrosis factor receptor- associated factor 6 (TRAF6) regulation of development, function, and homeostasis of the immune system*. Immunological Reviews, 2015. **266**(1): p. 72-92.
61. Deguine, J. and G.M. Barton, *MyD88: a central player in innate immune signaling*. F1000Prime Rep, 2014. **6**: p. 97.
62. Keating, S.E., et al., *IRAK-2 participates in multiple toll-like receptor signaling pathways to NF kappa B via activation of TRAF6 ubiquitination*. Journal of Biological Chemistry, 2007. **282**(46): p. 33435-33443.
63. Qian, Y.C., et al., *IRAK-mediated translocation of TRAF6 and TAB2 in the interleukin-1-induced activation of N-F kappa B*. Journal of Biological Chemistry, 2001. **276**(45): p. 41661-41667.
64. Yamamoto, M., et al., *Key function for the Ubc13 E2 ubiquitin-conjugating enzyme in immune receptor signaling*. Nat Immunol, 2006. **7**(9): p. 962-70.
65. Ramos, H.J. and M. Gale, *RIG-I like receptors and their signaling crosstalk in the regulation of antiviral immunity*. Curr Opin Virol, 2011. **1**(3): p. 167-176.
66. Rebsamen, M., et al., *DAI/ZBP1 recruits RIP1 and RIP3 through RIP homotypic interaction motifs to activate NF-kappa B*. EMBO Rep, 2009. **10**(8): p. 916-922.
67. Clark, K., S. Nanda, and P. Cohen, *Molecular control of the NEMO family of ubiquitin-binding proteins*. Nat Rev Mol Cell Biol, 2013. **14**(10): p. 673-85.
68. Jun, J.C., et al., *Innate immune-directed NF-kappaB signaling requires site-specific NEMO ubiquitination*. Cell Rep, 2013. **4**(2): p. 352-61.

69. Chen, Z.J., L. Parent, and T. Maniatis, *Site-specific phosphorylation of I kappa B alpha by a novel ubiquitination-dependent protein kinase activity.* Cell, 1996. **84**(6): p. 853-862.
70. DiDonato, J.A., et al., *A cytokine-responsive I kappa B kinase that activates the transcription factor NF-kappa B.* Nature, 1997. **388**(6642): p. 548-554.
71. Israel, A., *The IKK complex, a central regulator of NF-kappaB activation.* Cold Spring Harb Perspect Biol, 2010. **2**(3): p. a000158.
72. Brune, W. and C.E. Andoniou, *Die Another Day: Inhibition of Cell Death Pathways by Cytomegalovirus.* Viruses-Basel, 2017. **9**(9).
73. Elmore, S., *Apoptosis: A review of programmed cell death.* Toxicologic Pathology, 2007. **35**(4): p. 495-516.
74. Shi, J.J., W.Q. Gao, and F. Shao, *Pyroptosis: Gasdermin-Mediated Programmed Necrotic Cell Death.* Trends in Biochemical Sciences, 2017. **42**(4): p. 245-254.
75. Dhuriya, Y.K. and D. Sharma, *Necroptosis: a regulated inflammatory mode of cell death.* J Neuroinflammation, 2018. **15**(1): p. 199.
76. Grootjans, S., T. Vanden Berghe, and P. Vandenabeele, *Initiation and execution mechanisms of necroptosis: an overview.* Cell Death Differ, 2017. **24**(7): p. 1184-1195.
77. Mompean, M., et al., *The Structure of the Necrosome RIPK1-RIPK3 Core, a Human Hetero-Amyloid Signaling Complex.* Cell, 2018. **173**(5): p. 1244-+.
78. Zhang, X.H., J.P. Dowling, and J.K. Zhang, *RIPK1 can mediate apoptosis in addition to necroptosis during embryonic development.* Cell Death & Disease, 2019. **10**.
79. Newton, K., *RIPK1 and RIPK3: critical regulators of inflammation and cell death.* Trends Cell Biol, 2015. **25**(6): p. 347-353.
80. Li, J.X., et al., *The RIP1/RIP3 Necrosome Forms a Functional Amyloid Signaling Complex Required for Programmed Necrosis.* Cell, 2012. **150**(2): p. 339-350.
81. Upton, J.W. and W.J. Kaiser, *DAI Another Way: Necroptotic Control of Viral Infection.* Cell Host Microbe, 2017. **21**(3): p. 290-293.
82. Moriwaki, K. and F.K. Chan, *RIP3: a molecular switch for necrosis and inflammation.* Genes Dev, 2013. **27**(15): p. 1640-9.
83. Kroemer, G., G. Marino, and B. Levine, *Autophagy and the integrated stress response.* Mol Cell, 2010. **40**(2): p. 280-93.
84. Levine, B., N. Mizushima, and H.W. Virgin, *Autophagy in immunity and inflammation.* Nature, 2011. **469**(7330): p. 323-35.
85. English, L., et al., *Autophagy enhances the presentation of endogenous viral antigens on MHC class I molecules during HSV-1 infection.* Nat Immunol, 2009. **10**(5): p. 480-7.
86. Yang, Z. and D.J. Klionsky, *Eaten alive: a history of macroautophagy.* Nat Cell Biol, 2010. **12**(9): p. 814-22.
87. Li, W.W., J. Li, and J.K. Bao, *Microautophagy: lesser-known self-eating.* Cell Mol Life Sci, 2012. **69**(7): p. 1125-36.
88. Cuervo, A.M. and E. Wong, *Chaperone-mediated autophagy: roles in disease and aging.* Cell Res, 2014. **24**(1): p. 92-104.
89. Suzuki, K., et al., *The pre-autophagosomal structure organized by concerted functions of APG genes is essential for autophagosome formation.* EMBO J, 2001. **20**(21): p. 5971-81.
90. Bar-Peled, L. and D.M. Sabatini, *Regulation of mTORC1 by amino acids.* Trends Cell Biol, 2014. **24**(7): p. 400-6.
91. Hosokawa, N., et al., *Nutrient-dependent mTORC1 association with the ULK1-Atg13-FIP200 complex required for autophagy.* Mol Biol Cell, 2009. **20**(7): p. 1981-91.
92. Jung, C.H., et al., *ULK-Atg13-FIP200 complexes mediate mTOR signaling to the autophagy machinery.* Mol Biol Cell, 2009. **20**(7): p. 1992-2003.
93. Russell, R.C., et al., *ULK1 induces autophagy by phosphorylating Beclin-1 and activating VPS34 lipid kinase.* Nat Cell Biol, 2013. **15**(7): p. 741-50.

94. Liang, C., *Negative regulation of autophagy*. Cell Death Differ, 2010. **17**(12): p. 1807-15.
95. Proikas-Cezanne, T., et al., *WIPI proteins: essential PtdIns3P effectors at the nascent autophagosome*. J Cell Sci, 2015. **128**(2): p. 207-217.
96. Karanasios, E., et al., *Autophagy initiation by ULK complex assembly on ER tubulovesicular regions marked by ATG9 vesicles*. Nat Commun, 2016. **7**: p. 12420.
97. Popovic, D. and I. Dikic, *TBC1D5 and the AP2 complex regulate ATG9 trafficking and initiation of autophagy*. EMBO Rep, 2014. **15**(4): p. 392-401.
98. Kabeya, Y., et al., *LC3, a mammalian homologue of yeast Apg8p, is localized in autophagosome membranes after processing*. EMBO J, 2000. **19**(21): p. 5720-8.
99. Mizushima, N., et al., *Mouse Apg16L, a novel WD-repeat protein, targets to the autophagic isolation membrane with the Apg12-Apg5 conjugate*. J Cell Sci, 2003. **116**(Pt 9): p. 1679-88.
100. Mizushima, N., et al., *A new protein conjugation system in human. The counterpart of the yeast Apg12p conjugation system essential for autophagy*. J Biol Chem, 1998. **273**(51): p. 33889-92.
101. Liou, W., et al., *The autophagic and endocytic pathways converge at the nascent autophagic vacuoles*. J Cell Biol, 1997. **136**(1): p. 61-70.
102. Razi, M., E.Y. Chan, and S.A. Tooze, *Early endosomes and endosomal coatomer are required for autophagy*. J Cell Biol, 2009. **185**(2): p. 305-21.
103. Stromhaug, P.E. and P.O. Seglen, *Evidence for acidity of prelysosomal autophagic/endocytic vacuoles (amphisomes)*. Biochem J, 1993. **291 (Pt 1)**: p. 115-21.
104. Liang, C., et al., *Autophagic and tumour suppressor activity of a novel Beclin1-binding protein UVRAG*. Nat Cell Biol, 2006. **8**(7): p. 688-99.
105. Zhong, Y., et al., *Distinct regulation of autophagic activity by Atg14L and Rubicon associated with Beclin 1-phosphatidylinositol-3-kinase complex*. Nat Cell Biol, 2009. **11**(4): p. 468-76.
106. Matsunaga, K., et al., *Two Beclin 1-binding proteins, Atg14L and Rubicon, reciprocally regulate autophagy at different stages*. Nat Cell Biol, 2009. **11**(4): p. 385-96.
107. Jager, S., et al., *Role for Rab7 in maturation of late autophagic vacuoles*. J Cell Sci, 2004. **117**(Pt 20): p. 4837-48.
108. Raiborg, C. and H. Stenmark, *The ESCRT machinery in endosomal sorting of ubiquitylated membrane proteins*. Nature, 2009. **458**(7237): p. 445-52.
109. Nakamura, S. and T. Yoshimori, *New insights into autophagosome-lysosome fusion*. J Cell Sci, 2017. **130**(7): p. 1209-1216.
110. Wild, P., D.G. McEwan, and I. Dikic, *The LC3 interactome at a glance*. J Cell Sci, 2014. **127**(Pt 1): p. 3-9.
111. Xu, Z., et al., *The receptor proteins: pivotal roles in selective autophagy*. Acta Biochim Biophys Sin (Shanghai), 2015. **47**(8): p. 571-80.
112. Mathew, R., et al., *Autophagy suppresses tumorigenesis through elimination of p62*. Cell, 2009. **137**(6): p. 1062-75.
113. Popovic, D., et al., *Rab GTPase-Activating Proteins in Autophagy: Regulation of Endocytic and Autophagy Pathways by Direct Binding to Human ATG8 Modifiers*. Mol Cell Biol, 2012. **32**(9): p. 1733-1744.
114. Kim, E., et al., *Implication of mouse Vps26b-Vps29-Vps35 retromer complex in sortilin trafficking*. Biochem Biophys Res Commun, 2010. **403**(2): p. 167-171.
115. Seaman, M.N., *The retromer complex - endosomal protein recycling and beyond*. J Cell Sci, 2012. **125**(Pt 20): p. 4693-702.
116. Bugarcic, A., et al., *Vps26A and Vps26B Subunits Define Distinct Retromer Complexes*. Traffic, 2011. **12**(12): p. 1759-1773.
117. Jia, D., et al., *Structural and mechanistic insights into regulation of the retromer coat by TBC1d5*. Nat Commun, 2016. **7**.

118. Overbye, A., M. Fengsrud, and P.O. Seglen, *Proteomic analysis of membrane-associated proteins from rat liver autophagosomes*. Autophagy, 2007. **3**(4): p. 300-22.
119. Barral, J.M., et al., *Roles of molecular chaperones in protein misfolding diseases*. Seminars in Cell & Developmental Biology, 2004. **15**(1): p. 17-29.
120. Arrasate, M., et al., *Inclusion body formation reduces levels of mutant huntingtin and the risk of neuronal death*. Nature, 2004. **431**(7010): p. 805-10.
121. Chiti, F. and C.M. Dobson, *Protein misfolding, functional amyloid, and human disease*. Annu Rev Biochem, 2006. **75**: p. 333-66.
122. Bukau, B., J. Weissman, and A. Horwich, *Molecular chaperones and protein quality control*. Cell, 2006. **125**(3): p. 443-51.
123. Kopito, R.R., *Aggresomes, inclusion bodies and protein aggregation*. Trends Cell Biol, 2000. **10**(12): p. 524-530.
124. Johnston, J.A., C.L. Ward, and R.R. Kopito, *Aggresomes: A cellular response to misfolded proteins*. Faseb Journal, 1999. **13**(7): p. A1520-A1520.
125. Bjorkoy, G., et al., *p62/SQSTM1 forms protein aggregates degraded by autophagy and has a protective effect on huntingtin-induced cell death*. Journal of Cell Biology, 2005. **171**(4): p. 603-614.
126. Clausen, T.H., et al., *p62/SQSTM1 and ALFY interact to facilitate the formation of p62 bodies/ALIS and their degradation by autophagy*. Autophagy, 2010. **6**(3): p. 330-344.
127. Kawaguchi, Y., et al., *The deacetylase HDAC6 regulates aggresome formation and cell viability in response to misfolded protein stress*. Cell, 2003. **115**(6): p. 727-738.
128. Iwata, A., et al., *HDAC6 and microtubules are required for autophagic degradation of aggregated Huntingtin*. Journal of Biological Chemistry, 2005. **280**(48): p. 40282-40292.
129. Yao, T.P., *The role of ubiquitin in autophagy-dependent protein aggregate processing*. Genes Cancer, 2010. **1**(7): p. 779-786.
130. Kaganovich, D., R. Kopito, and J. Frydman, *Misfolded proteins partition between two distinct quality control compartments*. Nature, 2008. **454**(7208): p. 1088-U36.
131. Lussignol, M. and A. Esclatine, *Herpesvirus and Autophagy: "All Right, Everybody Be Cool, This Is a Robbery!"*. Viruses-Basel, 2017. **9**(12).
132. Pattingre, S., et al., *Bcl-2 antiapoptotic proteins inhibit Beclin 1-dependent autophagy*. Cell, 2005. **122**(6): p. 927-39.
133. Lee, D.Y. and B. Sugden, *The latent membrane protein 1 oncogene modifies B-cell physiology by regulating autophagy*. Oncogene, 2008. **27**(20): p. 2833-42.
134. Fotheringham, J.A. and N. Raab-Traub, *Epstein-Barr virus latent membrane protein 2 induces autophagy to promote abnormal acinus formation*. J Virol, 2015. **89**(13): p. 6940-4.
135. Lee, J.S., et al., *FLIP-mediated autophagy regulation in cell death control*. Nat Cell Biol, 2009. **11**(11): p. 1355-U225.
136. Leida, A.M., et al., *Subversion of Autophagy by Kaposi's Sarcoma-Associated Herpesvirus Impairs Oncogene-Induced Senescence*. Cell Host Microbe, 2012. **11**(2): p. 167-180.
137. Liang, Q.M., et al., *Kaposi's Sarcoma-Associated Herpesvirus K7 Modulates Rubicon-Mediated Inhibition of Autophagosome Maturation*. J Virol, 2013. **87**(22): p. 12499-12503.
138. Yakoub, A.M. and D. Shukla, *Basal Autophagy Is Required for Herpes simplex Virus-2 Infection*. Sci Rep, 2015. **5**.
139. Alexander, D.E., et al., *Analysis of the role of autophagy in replication of herpes simplex virus in cell culture*. J Virol, 2007. **81**(22): p. 12128-12134.
140. Orvedahl, A., et al., *HSV-1 ICP34.5 confers neurovirulence by targeting the Beclin 1 autophagy protein*. Cell Host Microbe, 2007. **1**(1): p. 23-35.

141. Gobeil, P.A. and D.A. Leib, *Herpes simplex virus gamma34.5 interferes with autophagosome maturation and antigen presentation in dendritic cells.* MBio, 2012. **3**(5): p. e00267-12.
142. Lussignol, M., et al., *The Herpes Simplex Virus 1 Us11 Protein Inhibits Autophagy through Its Interaction with the Protein Kinase PKR.* J Virol, 2013. **87**(2): p. 859-871.
143. Yin, H.C., et al., *Autophagy activated by duck enteritis virus infection positively affects its replication.* Journal of General Virology, 2017. **98**(3): p. 486-495.
144. Buckingham, E.M., et al., *Autophagy and the Effects of Its Inhibition on Varicella-Zoster Virus Glycoprotein Biosynthesis and Infectivity.* J Virol, 2014. **88**(2): p. 890-902.
145. Chaumorcel, M., et al., *The Human Cytomegalovirus Protein TRS1 Inhibits Autophagy via Its Interaction with Beclin 1.* J Virol, 2012. **86**(5): p. 2571-2584.
146. Mouna, L., et al., *Analysis of the role of autophagy inhibition by two complementary human cytomegalovirus BECN1/Beclin 1-binding proteins.* Autophagy, 2016. **12**(2): p. 327-342.
147. Braggin, J.E., S.J. Child, and A.P. Geballe, *Essential role of protein kinase R antagonism by TRS1 in human cytomegalovirus replication.* Virology, 2016. **489**: p. 75-85.
148. Fliss, P.M., et al., *Viral Mediated Redirection of NEMO/IKK gamma to Autophagosomes Curtails the Inflammatory Cascade.* PLoS Pathog, 2012. **8**(2).
149. Brune, W., et al., *A ribonucleotide reductase homolog of cytomegalovirus and endothelial cell tropism.* Science, 2001. **291**(5502): p. 303-305.
150. Lembo, D., et al., *The ribonucleotide reductase R1 homolog of murine cytomegalovirus is not a functional enzyme subunit but is required for pathogenesis.* J Virol, 2004. **78**(8): p. 4278-4288.
151. Upton, J.W., W.J. Kaiser, and E.S. Mocarski, *Cytomegalovirus m45 cell death suppression requires receptor-interacting protein (RIP) homotypic interaction motif (RHIM)-dependent interaction with RIP1.* Journal of Biological Chemistry, 2008. **283**(25): p. 16966-16970.
152. Upton, J.W., W.J. Kaiser, and E.S. Mocarski, *DAI/ZBP1/DLM-1 Complexes with RIP3 to Mediate Virus-Induced Programmed Necrosis that Is Targeted by Murine Cytomegalovirus vIRA.* Cell Host Microbe, 2012. **11**(3): p. 290-297.
153. Upton, J.W., W.J. Kaiser, and E.S. Mocarski, *Virus inhibition of RIP3-dependent necrosis.* Cell Host Microbe, 2010. **7**(4): p. 302-13.
154. Mack, C., et al., *Inhibition of proinflammatory and innate immune signaling pathways by a cytomegalovirus RIP1-interacting protein.* Proc Natl Acad Sci U S A, 2008. **105**(8): p. 3094-9.
155. Krause, E., et al., *Murine Cytomegalovirus Virion-Associated Protein M45 Mediates Rapid NF-kappa B Activation after Infection.* J Virol, 2014. **88**(17): p. 9963-9975.
156. Chabaud, S., et al., *The ribonucleotide reductase domain of the R1 subunit of herpes simplex virus type 2 ribonucleotide reductase is essential for R1 antiapoptotic function.* Journal of General Virology, 2007. **88**: p. 384-394.
157. Guo, H.Y., et al., *Herpes Simplex Virus Suppresses Necroptosis in Human Cells.* Cell Host Microbe, 2015. **17**(2): p. 243-251.
158. Huang, Z., et al., *RIP1/RIP3 Binding to HSV-1 ICP6 Initiates Necroptosis to Restrict Virus Propagation in Mice.* Cell Host Microbe, 2015. **17**(2): p. 229-242.
159. Huang, Z., et al., *RIP1/RIP3 binding to HSV-1 ICP6 initiates necroptosis to restrict virus propagation in mice.* Cell Host Microbe, 2015. **17**(2): p. 229-42.
160. Hahn, G., et al., *The human cytomegalovirus ribonucleotide reductase homolog UL45 is dispensable for growth in endothelial cells, as determined by a BAC-cloned clinical isolate of human cytomegalovirus with preserved wild-type characteristics.* J Virol, 2002. **76**(18): p. 9551-9555.

161. Kwon, K.M., et al., *Cooperative inhibition of RIP1-mediated NF-kappaB signaling by cytomegalovirus-encoded deubiquitinase and inactive homolog of cellular ribonucleotide reductase large subunit*. PLoS Pathog, 2017. **13**(6): p. e1006423.
162. de Boer, P., J.P. Hoogenboom, and B.N. Giepmans, *Correlated light and electron microscopy: ultrastructure lights up!* Nat Methods, 2015. **12**(6): p. 503-13.
163. Brangwynne, C.P., T.J. Mitchison, and A.A. Hyman, *Active liquid-like behavior of nucleoli determines their size and shape in Xenopus laevis oocytes*. Proc Natl Acad Sci U S A, 2011. **108**(11): p. 4334-4339.
164. Lembo, D. and W. Brune, *Tinkering with a viral ribonucleotide reductase*. Trends in Biochemical Sciences, 2009. **34**(1): p. 25-32.
165. Link, C.D., et al., *Conversion of green fluorescent protein into a toxic, aggregation-prone protein by C-terminal addition of a short peptide*. Journal of Biological Chemistry, 2006. **281**(3): p. 1808-1816.
166. Ali, M., L. Roback, and E.S. Mocarski, *Herpes simplex virus 1 ICP6 impedes TNF receptor 1-induced necrosome assembly during compartmentalization to detergent-resistant membrane vesicles*. Journal of Biological Chemistry, 2019. **294**(3): p. 991-1004.
167. Arase, H., et al., *Direct recognition of cytomegalovirus by activating and inhibitory NK cell receptors*. Science, 2002. **296**(5571): p. 1323-6.
168. Handke, W., et al., *Viral inhibition of BAK promotes murine cytomegalovirus dissemination to salivary glands*. J Virol, 2013. **87**(6): p. 3592-6.
169. Mandal, P., et al., *RIP3 Induces Apoptosis Independent of Pronecrotic Kinase Activity*. Mol Cell, 2014. **56**(4): p. 481-495.
170. Collins, B.M., et al., *Structure of Vps26B and mapping of its interaction with the retromer protein complex*. Traffic, 2008. **9**(3): p. 366-79.
171. Birgisdottir, A.B., T. Lamark, and T. Johansen, *The LIR motif - crucial for selective autophagy*. J Cell Sci, 2013. **126**(Pt 15): p. 3237-47.
172. Johansen, T. and T. Lamark, *Selective autophagy mediated by autophagic adapter proteins*. Autophagy, 2011. **7**(3): p. 279-96.
173. Lembo, D. and W. Brune, *Tinkering with a viral ribonucleotide reductase*. Trends Biochem Sci, 2009. **34**(1): p. 25-32.
174. Guo, H., et al., *Herpes simplex virus suppresses necroptosis in human cells*. Cell Host Microbe, 2015. **17**(2): p. 243-51.
175. Yu, X., et al., *Herpes Simplex Virus 1 (HSV-1) and HSV-2 Mediate Species-Specific Modulations of Programmed Necrosis through the Viral Ribonucleotide Reductase Large Subunit R1*. J Virol, 2016. **90**(2): p. 1088-95.
176. Guo, Z.J., et al., *Characterization of aggregate/aggresome structures formed by polyhedrin of Bombyx mori nucleopolyhedrovirus*. Sci Rep, 2015. **5**: p. 14601.
177. Boutell, C. and R.D. Everett, *Regulation of alphaherpesvirus infections by the ICP0 family of proteins*. J Gen Virol, 2013. **94**(Pt 3): p. 465-81.
178. Lanfranca, M.P., H.H. Mostafa, and D.J. Davido, *HSV-1 ICP0: An E3 Ubiquitin Ligase That Counteracts Host Intrinsic and Innate Immunity*. Cells, 2014. **3**(2): p. 438-454.
179. Moshe, A. and R. Gorovits, *Virus-induced aggregates in infected cells*. Viruses, 2012. **4**(10): p. 2218-32.
180. Lamark, T. and T. Johansen, *Aggrephagy: selective disposal of protein aggregates by macroautophagy*. Int J Cell Biol, 2012. **2012**: p. 736905.
181. Taisne, C., et al., *Human cytomegalovirus hijacks the autophagic machinery and LC3 homologs in order to optimize cytoplasmic envelopment of mature infectious particles*. Sci Rep, 2019. **9**(1): p. 4560.
182. Liao, Z., et al., *Knockout of Atg5 inhibits proliferation and promotes apoptosis of DF-1 cells*. In Vitro Cell Dev Biol Anim, 2019. **55**(5): p. 341-348.
183. Nishida, Y., et al., *Discovery of Atg5/Atg7-independent alternative macroautophagy*. Nature, 2009. **461**(7264): p. 654-8.
184. Yonekawa, T., et al., *RIP1 negatively regulates basal autophagic flux through TFEB to control sensitivity to apoptosis*. EMBO Rep, 2015. **16**(6): p. 700-708.

185. Lu, M., C. Boschetti, and A. Tunnacliffe, *Long Term Aggresome Accumulation Leads to DNA Damage, p53-dependent Cell Cycle Arrest, and Steric Interference in Mitosis*. Journal of Biological Chemistry, 2015. **290**(46): p. 27986-28000.
186. Lee, V.M., M. Goedert, and J.Q. Trojanowski, *Neurodegenerative tauopathies*. Annu Rev Neurosci, 2001. **24**: p. 1121-59.
187. Pham, C.L.L., et al., *Viral M45 and necroptosis-associated proteins form heteromeric amyloid assemblies*. EMBO Rep, 2019. **20**(2).
188. Liu, X., et al., *Post-translational modifications as key regulators of TNF-induced necroptosis*. Cell Death & Disease, 2016. **7**.
189. Mao, K. and D.J. Klionsky, *Xenophagy: A battlefield between host and microbe, and a possible avenue for cancer treatment*. Autophagy, 2017. **13**(2): p. 223-224.
190. Zaffagnini, G. and S. Martens, *Mechanisms of Selective Autophagy*. J Mol Biol, 2016. **428**(9): p. 1714-1724.
191. Levine, B. and G. Kroemer, *Biological Functions of Autophagy Genes: A Disease Perspective*. Cell, 2019. **176**(1-2): p. 11-42.
192. Deretic, V. and B. Levine, *Autophagy balances inflammation in innate immunity*. Autophagy, 2018. **14**(2): p. 243-251.
193. Choi, Y., J.W. Bowman, and J.U. Jung, *Autophagy during viral infection - a double-edged sword*. Nature Reviews Microbiology, 2018. **16**(6): p. 340-353.
194. Lipovsky, A., et al., *Genome-wide siRNA screen identifies the retromer as a cellular entry factor for human papillomavirus*. Proc Natl Acad Sci U S A, 2013. **110**(18): p. 7452-7457.
195. Groppelli, E., et al., *Retromer Regulates HIV-1 Envelope Glycoprotein Trafficking and Incorporation into Virions*. PLoS Pathog, 2014. **10**(11).
196. Korac, J., et al., *Ubiquitin-independent function of optineurin in autophagic clearance of protein aggregates*. J Cell Sci, 2013. **126**(2): p. 580-592.
197. Balchin, D., M. Hayer-Hartl, and F.U. Hartl, *In vivo aspects of protein folding and quality control*. Science, 2016. **353**(6294).
198. Buchner, J., *Molecular chaperones and protein quality control: an introduction to the JBC Reviews thematic series*. Journal of Biological Chemistry, 2019. **294**(6): p. 2074-2075.
199. Hartl, U., *Role of molecular chaperones in de novo protein folding and in misfolding disease*. Protein Science, 2004. **13**: p. 67-67.
200. Papsdorf, K. and K. Richter, *Protein folding, misfolding and quality control: the role of molecular chaperones*. Essays Biochem, 2014. **56**: p. 53-68.
201. Behl, C., *BAG3 and friends Co-chaperones in selective autophagy during aging and disease*. Autophagy, 2011. **7**(7): p. 795-798.
202. Meriin, A.B., et al., *Hsp70-Bag3 complex is a hub for proteotoxicity-induced signaling that controls protein aggregation*. Proc Natl Acad Sci U S A, 2018. **115**(30): p. E7043-E7052.
203. Jia, B.H., Y.Y. Wu, and Y. Zhou, *14-3-3 and aggresome formation Implications in neurodegenerative diseases*. Prion, 2014. **8**(2): p. 173-177.
204. Omoto, S., et al., *Suppression of RIP3-dependent Necroptosis by Human Cytomegalovirus*. Journal of Biological Chemistry, 2015. **290**(18): p. 11635-11648.
205. Cheng, A.Z., et al., *A Conserved Mechanism of APOBEC3 Relocalization by Herpesviral Ribonucleotide Reductase Large Subunits*. J Virol, 2019. **93**(23).
206. Cheng, A.Z., et al., *Epstein-Barr virus BORF2 inhibits cellular APOBEC3B to preserve viral genome integrity*. Nature Microbiology, 2019. **4**(1): p. 78-+.
207. Kim, E., et al., *Identification of novel retromer complexes in the mouse testis*. Biochem Biophys Res Commun, 2008. **375**(1): p. 16-21.
208. Corpet, F., *Multiple sequence alignment with hierarchical clustering*. Nucleic Acids Res, 1988. **16**(22): p. 10881-90.
209. Robert, X. and P. Gouet, *Deciphering key features in protein structures with the new ENDscript server*. Nucleic Acids Res, 2014. **42**(Web Server issue): p. W320-4.

210. Birnboim, H.C., *Citation Classic - a Rapid Alkaline Extraction Procedure for Screening Recombinant Plasmid DNA*. Current Contents/Life Sciences, 1988(45): p. 12-12.
211. Tischer, B.K., G.A. Smith, and N. Osterrieder, *En passant mutagenesis: a two step markerless red recombination system*. Methods Mol Biol, 2010. **634**: p. 421-30.
212. Osborn, J.E. and D.L. Walker, *Enhancement of infectivity of murine cytomegalovirus in vitro by centrifugal inoculation*. J Virol, 1968. **2**(9): p. 853-8.
213. Ramakrishnan, M.A., *Determination of 50% endpoint titer using a simple formula*. World J Virol, 2016. **5**(2): p. 85-6.
214. Baer, A. and K. Kehn-Hall, *Viral Concentration Determination Through Plaque Assays: Using Traditional and Novel Overlay Systems*. Jove-Journal of Visualized Experiments, 2014(93).
215. van de Weijer, M.L., et al., *A high-coverage shRNA screen identifies TMEM129 as an E3 ligase involved in ER-associated protein degradation*. Nat Commun, 2014. **5**: p. 3832.
216. Chen, D.Y. and S. Huang, *Nucleolar components involved in ribosome biogenesis cycle between the nucleolus and nucleoplasm in interphase cells*. Journal of Cell Biology, 2001. **153**(1): p. 169-176.
217. Montespan, C., et al., *Multi-layered control of Galectin-8 mediated autophagy during adenovirus cell entry through a conserved PPxY motif in the viral capsid*. PLoS Pathog, 2017. **13**(2).

10 Appendix

10.1 Curriculum Vitae

Lebenslauf entfällt aus datenschutzrechtlichen Gründen.

10.2 List of abbreviation

ALFY: autophagy-linked FYVE protein
Amp: ampicillin
AP: adaptor protein
AP-1: activator protein-1
ATG: autophagy related genes
ATP: adenosine triphosphate
BAC: bacterial artificial chromosome
BAG: Bcl-2 associated athanogene
Bcl-2: B-cell lymphoma 2
BECN1: Beclin1
CARD: Caspase activation and recruitment domains
CDV: cidofovir
CHIP: Carboxyl terminus of HSC70-interacting protein
CIMPR: cation independent mannose 6 phosphate receptor
CMA: chaperone-mediated autophagy
CMV: cytomegalovirus
CpG: Cytosine-phosphate-guanine
DAI/ZBP1: IRFs/Z-DNA binding protein-1
DBs: dense bodies
DC: dendritic cells
DD: death domain
DEV: Duck Enteritis virus
DFCP1: zinc-finger FYVE domain-containing protein 1
DNA: Deoxyribonucleic acid
dNTPs: Deoxynucleotide
dsDNA: double stranded DNA
dsRNA: double stranded RNA
E: early
EBV: Epstein-Barr virus
EIF2AK2: eukaryotic translation initiation factor 2-kinase 2
ER: Endoplasmic Reticulum
ESCRT: endosomal sorting complexes required for transport
FADD: FAS-associated death domain-containing protein
FLIP: Fas-associated death domain-like interleukin-1ß (IL-1ß)-converting enzyme-like inhibitory protein
FOS: foscarnet
g: gravitational acceleration
GCV: ganciclovir
GFP: green fluorescent protein
HA: hemagglutinin
HCMV: Human cytomegalovirus
HDAC: histone deacetylase
HHV: human herpesvirus
HOPS: homotypic fusion and protein sorting
hpi: hours post infection
Hrs: hepatocyte growth factor-regulated tyrosine kinase substrate
HSC: chaperone heat shock cognate
HSP: heat shock chaperone protein
HSV: herpes simplex virus

IE: immediate early
IE1: immediate early 1 protein
IFN: interferon
IKK: IκB kinase complex
IL: interleukin
IL-1R: interleukin receptor
IPAM: Induced Protein Aggregation Motif
IPOD: insoluble protein deposit
IPS-1: IFN-ß promoter stimulator 1
IRAK: interleukin receptor associated kinase
IRF: interferon-regulating factor
IκB: inhibitor kappa B
JUNQ: juxtanuclear quality control
Kan: kanamycin
kDa: kilo Dalton
KSHV: Kaposi associated sarcoma herpesvirus
L: Late
LAMP: Lysosome-associated membrane protein
LC3: microtubule associated protein light chain 3
LIR: LC3 interacting region
LPS: lipopolysaccharide
M45HA: MCMV M45 gene N-terminus HA tagged
MAPK: mitogen-activated protein kinase
MCMV: murine cytomegalovirus
MDA5: melanoma differentiation-associated gene 5
MHC: major histocompatibility complexes
MIEP: Major Immediate Early Promoter
MLKL: mixed lineage kinase domain like pseudokinase
MOI: multiplicity of infection
MTOC: microtubule organizing centre
mTORC1: mammalian target of rapamycin complex 1
MyD88: myeloid differentiation primary response gene 88
NBR1: neighbor of BRCA1 gene 1
NDP52: calcium-binding and coiled coil containing protein 2
NEMO: NF-κB essential modulator
NF-κB: Nuclear factor kappaB
NIEPs: non-infectious enveloped particles
NIX: Bcl2/adenovirus E1B 19kDa protein-interacting preotein-3 like
OPTN: optineurin
ORF: open reading frame
PAMP: pathogen-associated-molecular pattern
PAS: phagophore assembly sites
PCD: programmed cell death
PCR: polymerase chain reaction
PE: phosphatidylethanolamine
PI3K: Phosphatidylinositol 3-kinase
PK: protein kinase
PKR: EIF2AK2/double-stranded RNA-dependent host protein kinase
PRR: Pattern recognition receptor
RAB: Ras-related protein
RHD: Rel-homology domain

RHIM: RIP homotypic interacting motif
RIG-I: retinoic acid-inducible gene-I
RIPK: receptor interacting protein kinase
RNA: Ribonucleic acid
RNR: ribonucleotide reductase
rpm: revolutions per minute
SDS: sodium dodecyl sulfate
SNAP: and synaptosomal-associated protein
SNARE: N-ethylmaleimide-sensitive factor attachment protein receptor
SNX: sorting nexin proteins
SQSTM1: sequestosome 1
STX: syntaxin
TAB: TAK1 binding proteins
TAK: transforming growth factor ß-activated kinase
TBC1D: TBC domain-containing Rab GAP proteins
TBK: TRAF family member-associated NF-κB activator binding kinase
TGN: trans-Golgi network
TIR: toll-IL-1 receptor domain
TLRs: Toll-like receptor
TNF: tumor necrosis factor
TNFR: tumor necrosis factor receptor
TRAF: TNF receptor-associated factor
TRIF: TIR-domain-containing adapter-inducing interferon-ß receptor
Ub: ubiquitin
UBD: ubiquitin-binding domain
ULK: Unc-51 like autophagy activating kinases
UPS: ubiquitin-proteasome system
VAMP: vescicle-associated protein
VGCV: valganciclovir
vIRA: viral inhibitor of RIP activation
Vps: vacuolar protein sorting
VZV: Varicella zoster virus
WIPI: PI3P effector proteins WD repeat domain phosphoinositide-interacting protein
WT: wildtype
Zeo: zeocin
Δ: delta
ΔM45: MCMV M45 deletion mutant

10.3 Toxicity of chemicals

substance	GHS symbol	hazard statements	precautionary statements
2-mercaptoethanol	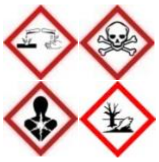	H301 + H331-H310-H315-H317-H318-H373-H410	P261-P280-P301 + P310 + P330-P302 + P352 + P310-P305 + P351 + P338 + P310-P403 + P233
aceton	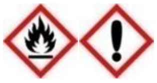	H225-H319-H336	P210-P305+P351+P338-P337+313-P403
acetic acid	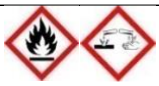	H226-H314	P280-P305 + P351 + P338-P310
acrylamide	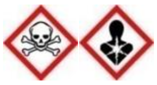	H301-H312 + H332-H315-H317-H319-H340-H350-H361f-H372	P201-P280-P301 + P310-P305 + P351 + P338-P308 + P313
ammonium bicarbonate	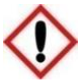	H302	P301 + P312 + P330
ammonium chloride	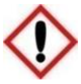	H302	P264-P270-P301+312-P330-P501
ammonium persulfate	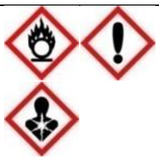	H272-H302-H315-H317-H319-H334-H335	P220-P261-P280-P305 + P351 + P338-P342 + P311
ampicillin	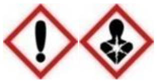	H315-H317-H319-H334-H335	P261-P280-P305 + P351 + P338-P342 + P311
bis-acrylamide	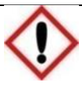	H302 + H332	
bromophenolblue	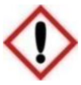	H332-H302-H319	P261-P264-P280-P304+340-P312-P301+312-P330-P305+351+338-P337+313
boric acid	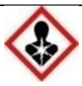	H360FD	P201-P308 + P313
chloramphenicol	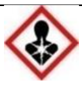	H350	P201-P308 + P313
crystal violet	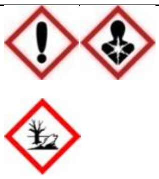	H319-H351-H411	P273-P281-P305 + P351 + P338

dimethyl sulfoxide	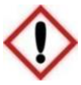	H227	P210-P280-P370+P378-P403+P235-P501
EDTA	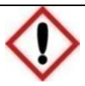	H319	P305 + P351 + P338
ethanol	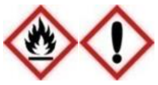	H225-H319	P210-P280-P305 + P351 + P338-P337 + P313-P403 + P235
ethidium bromide	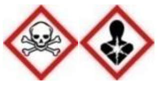	H302-H330-H341	P260-P281-P284-P310
glycerin	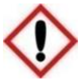	H315-H319-H335	P280-P302+P352-P304+P340-P305+P351+P338
hydrochloric acid	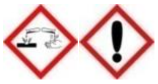	H290-H314-H335	P261-P280-P305 + P351 + P338-P310
isopropanol	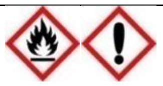	H225-H319-H336	P210-P261-P305 + P351 + P338
kanamycin	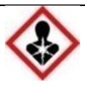	H360	P201-P308 + P313
liquid nitrogen	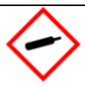	H281	P202-P271 + P403-P282
methanol	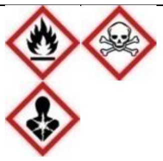	H225-H301 + H311 + H331-H370	P210-P260-P280-P301 + P310-P311
Nonidet-P40	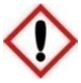	H315-H319-H302	P264-P280-P305+P351+338-P332+313-P337+313-P362+364
paraformaldeide	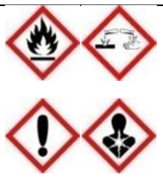	H228-H302+H332-H315-H317-H318-H335-H341-H350	P202-P210-P270-P280-P305+P351+P338-P308+P313
penicillin	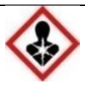	H317-H334	P261-P280-P342 + P311
protein A-agarose	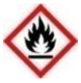	H226	
protein G-agarose	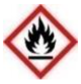	H226	
puromycin	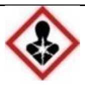	H373	
sodium dodecyl sulfate	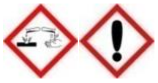	H315-H318-H335	P280-P304 + P340 + P312-P305 + P351 + P338 + P310

sodium hydroxide	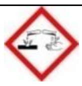	H290-H314	P280-P305 + P351 + P338-P310
streptomycin	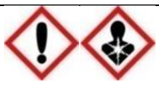	H302-H361	P281
TEMED	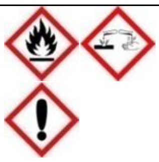	H225-H302-H314-H332	P210-P280-P305 + P351 + P338-P310
Triton X-100	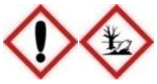	H302-H319-H411	P273-P280-P301 + P312 + P330-P337 + P313-P391-P501

10.4 Acknowledgments

Firstly, I would like to thank my supervisor, Prof. Dr. Wolfram Brune, who gave me the opportunity to work at this exciting and challenging project, to work in freedom and develop my own ideas. Nevertheless, I want to thank him for the guidance and the encouragement advice he has provided throughout my time as his student. Without constructive discussions with him this work would not have been achievable.

I also want to thank my second supervisor Prof. Thomas Dobner who provides me great ideas for the project.

I would like to thank Prof. Dr. Nicole Fischer for agreeing to be an evaluator of my thesis and Prof. Dr. Wolfgang Maison and Dr. Rudolph Reimer who agreed to be the examiners of my oral defense.

Special thanks go to Dr. Giada Frascaroli and Dr. Timothy Soh for critical reading of this manuscript and to Kerstin Pawletko and Renke Brixel for helping me with the german translation. All of you helped to drastically improve the quality of this thesis.

I would like to thank Enrico Caragliano, Eleonore Ostermann, Rudolph Reimer and Carola Schneider, for their collaboration and help to perform experiments that otherwise I would have not been able to perform alone.

Thank you to all present and former lab members of the HPI research unit virus host interaction. Giada, Olha, Kestin, Enrico, Renke, Yingqi, Luis, Tianyu Martina, Xuan, Michaela, Theo, Eleonore, Florian, Antonio, Ana, Leila, Federica, Jiajia, Matteo, Victoria, Umit: you provided good advices, help and lots of fun inside and outside of the lab!

Finally I want to thank my parents, Alfredo and Antonella, my brother, Francesco, and my boyfriend, Angelo, for their support and love.

10.5 Statement of Authorship

I hereby declare on oath, that I have written the present dissertation by my own and have not used other than the acknowledged resources and aids. The submitted written version corresponds to the version on the electronic storage medium. I hereby declare that I have not previously applied or pursued for a doctorate (Ph.D. studies).

Hamburg, 16 December 2019

Elena Muscolino